



Measurements of Higgs boson production by gluon-gluon fusion and vector-boson fusion using $H \rightarrow WW^* \rightarrow e\nu\mu\nu$ decays in pp collisions at $\sqrt{s} = 13$ TeV with the ATLAS detector

The ATLAS Collaboration

Higgs boson production via gluon-gluon fusion and vector-boson fusion in proton-proton collisions is measured in the $H \rightarrow WW^* \rightarrow e\nu\mu\nu$ decay channel. The Large Hadron Collider delivered proton-proton collisions at a center-of-mass energy of 13 TeV between 2015 and 2018, which were recorded by the ATLAS detector, corresponding to an integrated luminosity of 139 fb^{-1} . The total cross sections for Higgs boson production by gluon-gluon fusion and vector-boson fusion times the $H \rightarrow WW^*$ branching ratio are measured to be 12.0 ± 1.4 and $0.75^{+0.19}_{-0.16}$ pb, respectively, in agreement with the Standard Model predictions of 10.4 ± 0.6 and 0.81 ± 0.02 pb. Higgs boson production is further characterized through measurements of Simplified Template Cross Sections in a total of 11 kinematic fiducial regions.

1 Introduction

The Higgs boson is a neutral scalar particle associated with a field whose nonzero vacuum expectation value results in the breaking of electroweak (EW) symmetry in the Standard Model (SM) and gives mass to the W and Z bosons [1–4]. Observation of a new particle consistent with being the Higgs boson was reported by the ATLAS and CMS collaborations in 2012 [5, 6]. The Higgs boson has a rich set of properties that can be verified experimentally. Measurements of these properties are a powerful test of the SM and can be used to constrain theories of physics beyond the SM (BSM). BSM physics can also alter the kinematics of the Higgs boson production and decay. The large data sample delivered by the Large Hadron Collider (LHC) [7] at CERN makes it possible to measure the Higgs boson cross section in different kinematic regions in order to probe for these effects.

This paper describes measurements of Higgs boson production by gluon-gluon fusion (ggF) and vector-boson fusion (VBF) using $H \rightarrow WW^* \rightarrow e\nu\mu\nu$ decays in proton-proton (pp) collisions at a center-of-mass energy of 13 TeV. The data were recorded by the ATLAS detector [8] during Run 2 (2015–2018) of the LHC and correspond to an integrated luminosity of 139 fb^{-1} . The chosen decay channel takes advantage of the large branching ratio for $H \rightarrow WW^*$ decay and the relatively low background from other SM processes due to having two charged leptons of different flavors in the final state. The measured cross section in the ggF production mode probes the Higgs boson couplings to heavy quarks, while the VBF production mode directly probes the couplings to W and Z bosons. Previous studies of the $H \rightarrow WW^* \rightarrow e\nu\mu\nu$ decay channel have been reported by the CMS Collaboration using its 137 fb^{-1} full Run 2 dataset [9] and by the ATLAS Collaboration using a partial Run 2 dataset corresponding to an integrated luminosity of approximately 36 fb^{-1} [10]. Compared to the previous ATLAS Run 2 analysis, several improvements have been made in addition to using the larger dataset—most notably, a measurement of the ggF production mode in the final state with two or more reconstructed jets and measurements of cross sections in kinematic fiducial regions defined in the Simplified Template Cross Section (STXS) framework [11, 12].

The outline of this paper is as follows. Section 2 provides an overview of the signal characteristics and the analysis strategy. Section 3 describes the data and the simulated samples. Section 4 describes the event reconstruction. Section 5 details the various selections used to define the signal and control regions in the analysis. Section 6 discusses how the backgrounds are estimated. Section 7 provides commentary on the systematic uncertainties. Section 8 defines the likelihood fit procedure. Finally, the results of the analysis are presented in Sec. 9 and summarized in Sec. 10.

2 Analysis overview

The $H \rightarrow WW^* \rightarrow e\nu\mu\nu$ decay is characterized by two charged leptons and two undetected neutrinos in the final state. The opening angle between the two charged leptons tends to be small due to the spin-0 nature of the Higgs boson and the chiral structure of the weak force in the decay of the two W bosons [13]. This feature of the decay is exploited to separate the Higgs boson signal from the main backgrounds such as continuum production of WW , where the charged leptons are more likely to have a large opening angle.

In addition to the decay products of the Higgs boson, the final state can be populated by jets either from the quarks participating in the VBF production mode or from initial-state radiation from quarks or gluons (in both the ggF and VBF production modes). The composition of the background processes changes significantly depending on the number of jets (N_{jet}) in the final state. Therefore, the analysis is performed

separately in the $N_{\text{jet}} = 0$, $N_{\text{jet}} = 1$, and $N_{\text{jet}} \geq 2$ channels. The analysis is divided into four categories: one each for the $N_{\text{jet}} = 0$ and $N_{\text{jet}} = 1$ channels, which solely target the ggF signal production mode, and two for the $N_{\text{jet}} \geq 2$ channel, which separately target the VBF and ggF production modes.

For each analysis category, a set of selections are applied in order to enhance the signal contribution in a sample of events referred to as a signal region (SR), and a final fit to these events is performed. For the categories targeting the ggF production mode, the fit variable discriminating between signal and SM background processes is the dilepton transverse mass, defined as $m_T = \sqrt{(E_T^{\ell\ell} + E_T^{\text{miss}})^2 - |\mathbf{p}_T^{\ell\ell} + \mathbf{E}_T^{\text{miss}}|^2}$ with $E_T^{\ell\ell} = \sqrt{|\mathbf{p}_T^{\ell\ell}|^2 + m_{\ell\ell}^2}$, where $m_{\ell\ell}$ is the dilepton invariant mass, $\mathbf{p}_T^{\ell\ell}$ is the vector sum of the lepton transverse momenta, and $\mathbf{E}_T^{\text{miss}}$ (with magnitude E_T^{miss}) is the missing transverse momentum. For the $N_{\text{jet}} \geq 2$ category targeting the VBF production mode, the output of a deep neural network (DNN) trained to identify the VBF topology is used as the discriminating variable in the fit. The analysis likelihood function combines all SRs and determines the best-fit values for a set of parameters of interest (POIs). Cross sections times branching ratios are measured for the ggF and VBF production modes and their combination in the inclusive jet multiplicity.

Cross-section measurements are also conducted in the Stage-1.2 STXS category scheme, which, relative to the 1.1 scheme [14], refines the granularity of bins for ggF events with a Higgs boson produced with large transverse momentum. Selected events are categorized according to the requirements placed on the transverse momentum of the reconstructed Higgs boson candidate (p_T^H) and on potential additional hadronic jets. The ggF STXS template process (referred to subsequently as ggH) is defined to be the Born-level $gg \rightarrow H$ process plus higher-order QCD and EW corrections. This includes real EW radiation, in particular the $gg \rightarrow Z(\rightarrow q\bar{q})H$ process. The VBF STXS template process (referred to subsequently as EW qqH) is defined to include the $V(\rightarrow q\bar{q})H$ topology in addition to the usual VBF topology. After merging certain STXS bins to ensure sensitivity for all the measured POIs, a total of 11 fiducial cross sections corresponding to different STXS-bound kinematic regions are measured: 6 for ggH production and 5 for EW qqH production.

3 Data and simulation samples

3.1 Detector and data samples

The ATLAS detector at the LHC covers nearly the entire solid angle around the collision point.¹ It consists of an inner tracking detector surrounded by a thin superconducting solenoid, electromagnetic and hadronic calorimeters, and a muon spectrometer incorporating three large superconducting toroidal magnets. The inner-detector system (ID) is immersed in a 2 T axial magnetic field and provides charged-particle tracking in the range $|\eta| < 2.5$.

The high-granularity silicon pixel detector covers the vertex region and typically provides four measurements per track, the first hit normally being in the insertable B-layer installed before Run 2 [15, 16]. It is followed by the silicon microstrip tracker, which usually provides eight measurements per track. These silicon

¹ ATLAS uses a right-handed coordinate system with its origin at the nominal interaction point (IP) in the center of the detector and the z axis along the beam pipe. The x axis points from the IP to the center of the LHC ring, and the y axis points upward. Cylindrical coordinates (r, ϕ) are used in the transverse plane, ϕ being the azimuthal angle around the z axis. The pseudorapidity is defined in terms of the polar angle θ as $\eta = -\ln \tan(\theta/2)$. Angular distance is measured in units of $\Delta R \equiv \sqrt{(\Delta\eta)^2 + (\Delta\phi)^2}$.

detectors are complemented by the transition radiation tracker (TRT), which enables radially extended track reconstruction up to $|\eta| = 2.0$. The TRT also provides electron identification information based on the fraction of hits (typically 30 in total) above a higher energy-deposit threshold corresponding to transition radiation.

The calorimeter system covers the pseudorapidity range $|\eta| < 4.9$. Within the region $|\eta| < 3.2$, electromagnetic calorimetry is provided by barrel and end cap high-granularity lead/liquid-argon (LAr) calorimeters, with an additional thin LAr presampler covering $|\eta| < 1.8$ to correct for energy loss in material upstream of the calorimeters. Hadronic calorimetry is provided by the steel/scintillator-tile calorimeter, segmented into three barrel structures within $|\eta| < 1.7$, and two copper/LAr hadronic end cap calorimeters. The solid angle coverage is completed with forward copper/LAr and tungsten/LAr calorimeter modules optimized for electromagnetic and hadronic measurements respectively.

The muon spectrometer comprises separate trigger and high-precision tracking chambers measuring the deflection of muons in a magnetic field generated by the superconducting air-core toroids. The field integral of the toroids ranges between 2.0 and 6.0 T m (Tesla*meter) across most of the detector. A set of precision chambers covers the region $|\eta| < 2.7$ with three layers of monitored drift tubes, complemented by cathode-strip chambers in the forward region, where the background is highest. The muon trigger system covers the range $|\eta| < 2.4$ with resistive-plate chambers in the barrel and thin-gap chambers in the end caps.

Interesting events are selected to be recorded by the first-level trigger system implemented in custom hardware, followed by selections made by algorithms implemented in software in the high-level trigger [17]. The first-level trigger accepts events from the 40 MHz bunch crossings at a rate below 100 kHz, which the high-level trigger reduces in order to record events to disk at about 1 kHz. A combination of unprescaled single-lepton triggers and one $e\text{-}\mu$ dilepton trigger [18, 19] is employed in this analysis so as to maximize the total trigger efficiency. The transverse momentum (p_T) threshold for single-electron(muon) triggers was 24(20) GeV for the first year of data taking and increased to 26 GeV for both lepton flavors during the remainder of Run 2. The $e\text{-}\mu$ trigger had a p_T threshold of 17 GeV for electrons and 14 GeV for muons. The full ATLAS Run 2 dataset is used for this analysis, consisting of pp collision data produced at $\sqrt{s} = 13$ TeV and recorded between 2015 and 2018. The data are subjected to quality requirements [20], including the removal of events recorded when relevant detector components were not operating correctly. The total integrated luminosity after this cleaning of the data corresponds to 139 fb^{-1} [21].

An extensive software suite [22] is used in the reconstruction and analysis of real and simulated data, in detector operations, and in the trigger and data acquisition systems of the experiment.

3.2 Simulated event samples

Higgs boson production and decay into pairs of W bosons or leptonically decaying τ -leptons were simulated for each of the four main production modes: ggF and VBF, as well as WH and ZH (production in association with a vector boson, collectively referred to as VH).

The ggF production was simulated at next-to-next-to-leading-order (NNLO) accuracy in QCD² using the POWHEG NNLOPS program [23–27], interfaced with PYTHIA 8.212 [28] for parton showering and nonperturbative effects. The simulation achieves NNLO accuracy for arbitrary inclusive $gg \rightarrow H$

² When higher orders (NLO and NNLO) are specified, QCD is implied if not explicitly stated.

observables by reweighting the Higgs boson rapidity³ spectrum in Higgs plus one jet (Hj)-MiNLO [29–31] to that of HNNLO [32]. The gluon-gluon fusion prediction from the Monte Carlo (MC) samples is normalized to the next-to-next-to-next-to-leading-order cross section in QCD plus electroweak corrections at next-to-leading order (NLO) [11, 33–42].

VBF events were generated with POWHEG BOX [23–25, 43], interfaced with PYTHIA 8.230 [28] with the dipole recoil option enabled to model the parton shower, hadronization and underlying event. The POWHEG BOX prediction is accurate to NLO in QCD corrections and tuned to match calculations with effects due to finite heavy-quark masses and soft-gluon resummations up to next-to-next-to-leading-logarithm (NNLL) accuracy. The MC prediction is normalized to an approximate-NNLO QCD cross section with NLO electroweak corrections [44–46].

The uncertainties due to the parton shower and hadronization model for the ggF and VBF Higgs boson signal samples are evaluated using the events in the nominal sample generated with POWHEG BOX but interfaced to an alternative showering program HERWIG 7 [47, 48] instead of PYTHIA 8. To estimate the uncertainty related to the matching between the matrix element and the parton shower for ggF and VBF production, MC events produced with the MG5_AMC@NLO [49] generator (where MG5 denotes MADGRAPH5) and interfaced to HERWIG 7 are used. They are accurate to NLO in QCD and utilize the NNPDF30_NLO_AS_0118 [50] parton distribution function (PDF) set. In both cases, the H7UE set of tuned parameters (tune) [48] and the MMHT2014LO PDF set [51] were used for the underlying event.

The VH production was simulated using POWHEG BOX v2 [23–25, 43] and interfaced with PYTHIA 8.212 for parton showering and nonperturbative effects. The POWHEG BOX prediction is accurate to NLO for the production of VH plus one jet. Samples for the loop-induced process $gg \rightarrow ZH$ were generated with POWHEG BOX v2 interfaced to PYTHIA 8.235. The MC prediction is normalized to cross sections calculated at NNLO in QCD (including the $gg \rightarrow ZH$ contribution) and at NLO in electroweak corrections [52–56].

The ggF, VBF, and VH Higgs boson samples use the PDF4LHC15 [57] PDF set and the AZNLO tune [58] of PYTHIA 8. The sample normalizations account for the decay branching ratios calculated with HDECAY [59–61] and PROPHECY4F [62–64] assuming a Higgs boson mass of 125.09 GeV [65]. An uncertainty of 2.16% [11] is assigned to the $H \rightarrow WW^*$ branching ratio, which includes the uncertainty in the Higgs boson mass. All Higgs boson samples are generated with a Higgs boson mass of 125 GeV, with the uncertainty in the Higgs boson mass being negligible for kinematic distributions.

The production of $t\bar{t}H$ events was modeled using the POWHEG BOX v2 [23–25, 66, 67] generator at NLO with the NNPDF3.0NLO [50] PDF set. The events were interfaced to PYTHIA 8.230 using the A14 tune [68]. The prediction is normalized to the cross section computed at NLO QCD and NLO EW accuracy [11]. The sample is inclusive in Higgs decay modes and the cross section is computed assuming a Higgs boson mass of 125.09 GeV.

To model the SM background, quark-initiated production of WW , WZ , $V\gamma^*$, and ZZ involving the strong interaction was simulated with the SHERPA 2.2.2 [69] generator. Fully leptonic final states were generated using matrix elements at NLO accuracy in QCD for up to one additional parton and at leading-order (LO) accuracy for up to three additional parton emissions. For $V\gamma^*$, the γ^* mass was generated with a lower bound of 4 GeV. Samples for the loop-induced processes $gg \rightarrow WW$ and ZZ were generated using LO-accurate matrix elements for up to one additional parton emission.

³ The rapidity is defined in terms of a particle’s energy E and momentum in the direction of the beam pipe p_z as $y = \frac{1}{2} \ln \frac{E+p_z}{E-p_z}$.

For the quark-initiated WW background, systematic uncertainties are evaluated via samples simulated with alternative settings of the SHERPA 2.2.2 generator. The uncertainty in the matching procedure is assessed by varying the parameter Q_{cut} , which determines the transition between the matrix-element and parton-shower domain [70]. Specifically, alternative samples with $Q_{\text{cut}} = 15$ and 30 GeV instead of the nominal value of $Q_{\text{cut}} = 20$ GeV are considered. The uncertainties in the shower model are estimated via samples, in which either the resummation scale, μ_q , is increased or decreased by a factor of 2, or the alternative recoil scheme described in Refs. [71, 72] is used.

The production of $V\gamma$ final states was simulated with the SHERPA 2.2.8 [69] generator. Matrix elements are at NLO QCD accuracy for up to one additional parton and at LO accuracy for up to three additional parton emissions.

Triboson production (VVV) was simulated with the SHERPA 2.2.2 generator using factorized gauge-boson decays. The matrix elements are accurate to NLO for the inclusive process and to LO for up to two additional parton emissions.

For all nominal multiboson samples generated with SHERPA, the matrix-element calculations were matched and merged with the SHERPA parton shower based on Catani-Seymour dipole factorization [71, 73] using the MEPS@NLO prescription [70, 74–76]. The virtual QCD corrections were provided by the OPENLOOPS library [77, 78]. The NNPDF3.0_{NNLO} [50] set of PDFs was used, along with the dedicated set of tuned parton-shower parameters developed by the SHERPA authors.

Electroweak WW production in association with two jets ($WWjj$) was generated by MG5_AMC@NLO with LO matrix elements using the NNPDF3.0_{NLO} PDF set. For the nominal sample, MG5_AMC@NLO was interfaced with PYTHIA 8.244, using the A14 tune to model the parton shower, hadronization, and underlying event. An alternative sample is utilized to evaluate the shower model uncertainty, for which MG5_AMC@NLO was instead interfaced with HERWIG 7.

The quark- or gluon-initiated production of $Z/\gamma^* + \text{jets}$ was simulated with the SHERPA 2.2.1 [69] generator using NLO matrix elements for up to two partons, and LO matrix elements for up to four partons, calculated with the COMIX and OPENLOOPS libraries. They were matched with the SHERPA parton shower [71] using the MEPS@NLO prescription. The NNPDF3.0_{NNLO} set of PDFs was used, and the samples are normalized to a NNLO prediction [79].

An additional sample of $Z/\gamma^* + \text{jets}$ events was made with the MG5_AMC@NLO generator to evaluate the matching uncertainty. The matrix elements are accurate to LO for up to four final-state partons. The NNPDF2.3_{LO} [80] PDF set was used. Events were interfaced to PYTHIA 8.186 [81] with the A14 tune to model the parton shower, hadronization, and underlying event.

Electroweak production of $\ell\ell jj$ final states was simulated with SHERPA 2.2.1, but using LO matrix elements with up to two additional parton emissions.

The production of $t\bar{t}$ events was modeled using the POWHEG BOX v2 generator at NLO with the NNPDF3.0_{NLO} PDF set and the h_{damp} parameter⁴ set to $1.5 \times m_{\text{top}}$ [82]. In order to correct for a known mismodeling of the leading-lepton p_T due to missing higher-order corrections, an NNLO reweighting was applied to the sample [83]. The events were interfaced to PYTHIA 8.230 to model the parton shower, hadronization, and underlying event, with parameters set according to the A14 tune and using the NNPDF2.3_{LO} set of PDFs.

⁴ The h_{damp} parameter is a resummation damping factor and one of the parameters that controls the matching of POWHEG matrix elements to the parton shower and thus effectively regulates the high- p_T radiation against which the $t\bar{t}$ system recoils.

The associated production of top quarks and W bosons (mainly Wt) was modeled using the PowHEG Box v2 generator at NLO in QCD using the five-flavor scheme and the NNPDF3.0NLO set of PDFs. The diagram removal scheme [84] was used to remove interference and overlap with $t\bar{t}$ production. The events were interfaced to PYTHIA 8.230 using the A14 tune and the NNPDF2.3LO set of PDFs. In all samples generated with PowHEG Box v2, the decays of bottom and charm hadrons were performed by EVTGEN 1.6.0 [85].

The W +jets and multijet backgrounds are estimated from data. Generated samples of W +jets and Z +jets events are used to validate the estimate and to determine the flavor composition uncertainties. These MC samples were generated using PowHEG Box interfaced with PYTHIA 8.186, with SHERPA 2.2.1, and with MG5_AMC@NLO [49, 86] interfaced with PYTHIA 8.186.

The MC generators, PDFs, and programs used for the underlying event and parton shower (UEPS) are summarized in Table 1. The alternative generators or UEPS models used to estimate systematic uncertainties are also listed in parentheses. Finally, the orders of the perturbative prediction for each sample are reported.

For all MC samples, the events were processed through the ATLAS detector simulation [87] based on GEANT4 [88]. The effect of pileup was modeled by overlaying the hard-scattering event with simulated inelastic pp events generated with PYTHIA 8.186 using the NNPDF2.3LO set of PDFs and the A3 tune [89].

Table 1: Overview of simulation tools used to generate signal and background processes, as well as to model the UEPS. The PDF sets are also summarized. Alternative event generators or quantities varied to estimate systematic uncertainties are shown in parentheses.

Process	Matrix element (alternative)	PDF set	UEPS model (alternative model)	Prediction order for total cross section
$ggFH$	PowHEG Box v2 [23–27] NNLOPS [26, 30, 43] (MG5_AMC@NLO) [49, 86]	PDF4LHC15NNLO [57]	PYTHIA 8 [28] (HERWIG 7) [48]	N^3 LO QCD + NLO EW [11, 33–42]
$VBFH$	PowHEG Box v2 [23–25, 43] (MG5_AMC@NLO)	PDF4LHC15NLO	PYTHIA 8 (HERWIG 7)	NNLO QCD + NLO EW [44–46]
VH excluding $gg \rightarrow ZH$	PowHEG Box v2	PDF4LHC15NLO	PYTHIA 8	NNLO QCD + NLO EW [52–56]
$t\bar{t}H$	PowHEG Box v2	NNPDF3.0NLO	PYTHIA 8	NLO [11]
$gg \rightarrow ZH$	PowHEG Box v2	PDF4LHC15NLO	PYTHIA 8	NNLO QCD + NLO EW [90, 91]
$qq \rightarrow WW$	SHERPA 2.2.2 [69]	NNPDF3.0NNLO [50]	SHERPA 2.2.2 [70, 71, 73–76] (SHERPA 2.2.2 [71, 72]; μ_q)	NLO [77, 78, 92]
$qq \rightarrow WWqq$	MG5_AMC@NLO [49]	NNPDF3.0NLO	PYTHIA 8 (HERWIG 7)	LO
$gg \rightarrow WW/ZZ$	SHERPA 2.2.2	NNPDF3.0NNLO	SHERPA 2.2.2	NLO [93]
$WZ/V\gamma^*/ZZ$	SHERPA 2.2.2	NNPDF3.0NNLO	SHERPA 2.2.2	NLO [94]
$V\gamma$	SHERPA 2.2.8 [69]	NNPDF3.0NNLO	SHERPA 2.2.8	NLO [94]
VVV	SHERPA 2.2.2	NNPDF3.0NNLO	SHERPA 2.2.2	NLO
$t\bar{t}$	PowHEG Box v2 (MG5_AMC@NLO)	NNPDF3.0NLO	PYTHIA 8 (HERWIG 7)	NNLO+NNLL [95–101]
Wt	PowHEG Box v2 (MG5_AMC@NLO)	NNPDF3.0NLO	PYTHIA 8 (HERWIG 7)	NNLO [102, 103]
Z/γ^*	SHERPA 2.2.1 (MG5_AMC@NLO)	NNPDF3.0NNLO	SHERPA 2.2.1	NNLO [79]

4 Event reconstruction

Primary vertices in the event are reconstructed from tracks in the ID with $p_T > 500$ MeV. Events are required to have at least one primary vertex with at least two associated tracks. The hard-scatter vertex is selected as the vertex with the highest $\sum p_T^2$, where the sum is over all the tracks associated with that particular vertex.

Electron candidates are reconstructed by matching energy clusters in the electromagnetic calorimeter to well-reconstructed tracks that are extrapolated to the calorimeter [104]. All candidate electron tracks are fitted using a Gaussian sum filter [105] to account for bremsstrahlung energy losses. Electron candidates are required to satisfy $|\eta| < 2.47$, excluding the transition region $1.37 < |\eta| < 1.52$ between the barrel and end caps of the LAr calorimeter. Muon candidates are reconstructed from a global fit of matching tracks from the inner detector and muon spectrometer [106]. They are required to satisfy $|\eta| < 2.5$. In order to reject particles misidentified as prompt leptons, several identification requirements as well as isolation and impact parameter criteria [104, 106] are applied. For electrons, a likelihood-based identification method [104] is employed, which takes into account a number of discriminating variables such as electromagnetic shower shapes, track properties, transition radiation response, and the quality of the cluster-to-track matching. Electron candidates with $15 \text{ GeV} < E_T < 25 \text{ GeV}$ must satisfy the “tight” likelihood working point, which has an efficiency of approximately 70% for these electrons. For $E_T > 25 \text{ GeV}$, where misidentification backgrounds (discussed further in Sec. 6.4) are less important, electron candidates must satisfy the “medium” likelihood working point, which has an efficiency of approximately 85% for an electron with $p_T \sim 40 \text{ GeV}$. For muons, a cut-based identification method [106] is employed, using the “tight” working point with an efficiency of $\sim 95\%$ so as to maximize the sample purity. The impact parameter requirements are $|z_0 \sin \theta| < 0.5 \text{ mm}$ and $|d_0|/\sigma_{d_0} < 5$ (3) for electrons (muons).⁵ Leptons are required to be isolated from other activity in the event by placing upper bounds on both other transverse energy (using topological clusters in the calorimeter) within a cone of size $\Delta R = 0.2$ around the lepton and other p_T (using tracks) within a cone of variable size no larger than $\Delta R = 0.2$ (0.3) for electrons (muons). At least one of the offline reconstructed leptons must be matched to an online object that triggered the recording of the event. In the case where the $e\text{-}\mu$ trigger is solely responsible for the event being recorded, each lepton must correspond to one of the trigger objects. This trigger matching scheme also requires the p_T of the lepton to be at least 1 GeV above the trigger-level threshold.

Jets are reconstructed using the anti- k_t algorithm with a radius parameter of $R = 0.4$ and particle-flow objects as input [107–109]. The four-momentum of the jets is corrected for the response of the noncompensating calorimeter, signal losses due to noise threshold effects, energy loss in inactive material, and contamination from pileup (defined as additional pp interactions in the same and neighboring bunch crossings) [110]. For jets entering the analysis, a kinematic selection of $p_T > 20 \text{ GeV}$ and $|\eta| < 4.5$ is applied. In the context of event categorization, only jets with $p_T > 30 \text{ GeV}$ are considered for jet counting. Furthermore, a jet-vertex-tagger multivariate discriminant selection that reduces contamination from pileup [111] is applied to jets with $20 < p_T < 60 \text{ GeV}$ and $|\eta| < 2.4$, utilizing calorimeter and tracking information to separate hard-scatter jets from pileup jets. Jets with $p_T > 20 \text{ GeV}$ and $|\eta| < 2.5$ containing b -hadrons (b -jets) are identified using a neural-network discriminant based on a number of lower-level taggers which utilize relevant quantities such as the associated track impact parameters and information from secondary vertices. The working point that is adopted has an average 85% b -jet tagging efficiency, as estimated from simulated $t\bar{t}$ events [112, 113].

The following procedure is adopted in the case of overlapping objects. If two electrons share an ID track, the lower- E_T electron is removed. If a muon shares an ID track with an electron, the electron is removed. For electrons and jets, the jet is removed if $\Delta R(\text{jet}, e) < 0.2$ and the jet is not tagged as a b -jet. For any surviving jets, the electron is removed if $\Delta R(\text{jet}, e) < 0.4$. For muons and jets, the jet is removed if $\Delta R(\text{jet}, \mu) < 0.2$, the jet has less than three associated tracks with $p_T > 500 \text{ MeV}$, and the jet is not tagged as a b -jet. For any surviving jets, the muon is removed if $\Delta R(\text{jet}, \mu) < 0.4$.

⁵ z_0 and d_0 are the longitudinal and transverse impact parameters, respectively. d_0 is defined by the point of closest approach of the track to the beamline in the $r\text{-}\phi$ plane, while z_0 is the longitudinal distance to the hard-scatter primary vertex from this point.

The quantity $E_{\text{T}}^{\text{miss}}$ is calculated as the negative vector sum of the p_{T} of all the selected leptons and jets, together with reconstructed tracks that are not associated with these objects but are consistent with originating from the primary pp collision [114]. A second definition of missing transverse momentum (in this case denoted by $p_{\text{T}}^{\text{miss}}$) uses tracks for the hadronic hard term as well, replacing the calorimeter-measured jets with their associated tracks instead. The $p_{\text{T}}^{\text{miss}}$ observable is used directly in the selection of events because of its ability to discriminate better against the $Z/\gamma^* \rightarrow \tau\tau$ background, while the $E_{\text{T}}^{\text{miss}}$ observable is used to build signal-sensitive variables such as m_{T} due to its superior resolution.

5 Event selection and categorization

The initial sample of events is required to satisfy the data quality and trigger criteria, as well as to contain exactly two leptons identified as discussed in the previous section, with different flavor and opposite charge. In addition, the higher- p_{T} (leading) lepton is required to have $p_{\text{T}} > 22$ GeV and the subleading lepton is required to have $p_{\text{T}} > 15$ GeV. Di- τ -lepton backgrounds from low-mass Drell-Yan (DY) production and meson resonances are removed by requiring a dilepton invariant mass $m_{\ell\ell} > 10$ GeV. In the analysis categories targeting the ggF production mode, a $p_{\text{T}}^{\text{miss}} > 20$ GeV selection is applied, which significantly reduces both the $Z/\gamma^* \rightarrow \tau\tau$ background and the multijet backgrounds with misidentified leptons. The above criteria define the event preselection. Figure 1 shows the jet multiplicity distribution at the preselection level. All histograms in this paper include underflow and overflow events unless otherwise stated. The different background compositions as a function of jet multiplicity motivate the division of the data sample into separate N_{jet} categories. Four main analysis categories are defined: the $N_{\text{jet}} = 0$ category targeting the ggF production mode as described in Sec. 5.1, the $N_{\text{jet}} = 1$ category targeting the ggF production mode as described in Sec. 5.2, the $N_{\text{jet}} \geq 2$ category targeting the VBF production mode as described in Sec. 5.3, and the $N_{\text{jet}} \geq 2$ category targeting the ggF production mode as described in Sec. 5.4. To reject background from top-quark production, events containing b -jets with $p_{\text{T}} > 20$ GeV are vetoed in all analysis categories. The remaining selections used to define the analysis SRs are described separately for each category of events below, while Table 2 provides a summary of the full set of SR selections.

5.1 $N_{\text{jet}} = 0$ category

Events with a significant mismeasurement of the missing transverse momentum are suppressed by requiring $E_{\text{T}}^{\text{miss}}$ to point away from the dilepton transverse momentum ($\Delta\phi_{\ell\ell, E_{\text{T}}^{\text{miss}}} > \pi/2$). In the absence of a jet to balance the dilepton system, the magnitude of the dilepton momentum $p_{\text{T}}^{\ell\ell}$ is expected to be small in DY events. A requirement of $p_{\text{T}}^{\ell\ell} > 30$ GeV further reduces the DY contribution while retaining the majority of the signal events.

Continuum WW production and resonant Higgs boson production can be separated by exploiting the spin-0 property of the Higgs boson, which, when combined with the $V - A$ nature of the W boson decay, leads to a small opening angle between the charged leptons. A requirement of $m_{\ell\ell} < 55$ GeV, which combines the small lepton opening angle with the kinematics of a low-mass Higgs boson ($m_H = 125$ GeV), significantly reduces both the WW and DY backgrounds. A requirement of $\Delta\phi_{\ell\ell} < 1.8$ significantly reduces the remaining DY background while retaining most of the signal. The $m_{\ell\ell}$ and $\Delta\phi_{\ell\ell}$ selections in the $N_{\text{jet}} = 0$ category are indicated by dashed lines in Figs. 2(a) and 2(b), with an arrow at the top pointing to the region retained. The $N_{\text{jet}} = 0$ SR is further split into four subregions with boundaries in $m_{\ell\ell}$ at

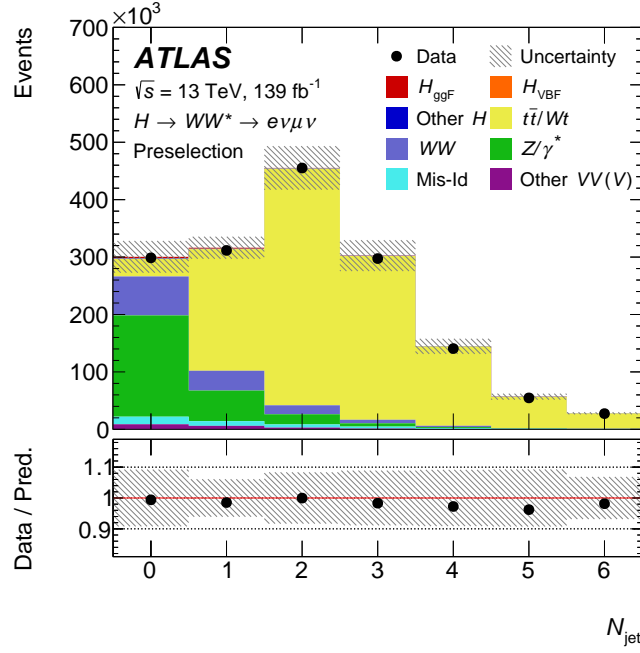


Figure 1: Jet multiplicity distribution, for jets with $p_T > 30$ GeV and $|\eta| < 4.5$, after applying the preselection criteria (prefit normalizations). The hatched band shows the normalization component of the total prefit uncertainty, assuming SM Higgs boson production. The various background components are discussed in more detail in Sec. 6.

Table 2: Event selection criteria used to define the SRs in the $H \rightarrow WW^* \rightarrow e\nu\mu\nu$ analysis. The definitions of the variables can be found in the text of this paper.

Category	$N_{\text{jet}, (p_T > 30 \text{ GeV})} = 0$ ggF	$N_{\text{jet}, (p_T > 30 \text{ GeV})} = 1$ ggF	$N_{\text{jet}, (p_T > 30 \text{ GeV})} \geq 2$ ggF	$N_{\text{jet}, (p_T > 30 \text{ GeV})} \geq 2$ VBF
Preselection	Two isolated, different-flavor leptons ($\ell = e, \mu$) with opposite charge $p_T^{\text{lead}} > 22 \text{ GeV}, p_T^{\text{sublead}} > 15 \text{ GeV}$ $m_{\ell\ell} > 10 \text{ GeV}$			
	$p_T^{\text{miss}} > 20 \text{ GeV}$			
Background rejection	$N_{b\text{-jet}, (p_T > 20 \text{ GeV})} = 0$			
	$\Delta\phi_{\ell\ell, E_T^{\text{miss}}} > \pi/2$ $p_T^{\ell\ell} > 30 \text{ GeV}$	$m_{\tau\tau} < m_Z - 25 \text{ GeV}$ $\max(m_T^\ell) > 50 \text{ GeV}$		
$H \rightarrow WW^* \rightarrow e\nu\mu\nu$ topology	$m_{\ell\ell} < 55 \text{ GeV}$ $\Delta\phi_{\ell\ell} < 1.8$			central jet veto outside lepton veto $m_{jj} > 120 \text{ GeV}$
	fail central jet veto or fail outside lepton veto $ m_{jj} - 85 > 15 \text{ GeV}$ or $\Delta y_{jj} > 1.2$			
Discriminating fit variable	m_T			DNN

$m_{\ell\ell} \leq 30$ GeV and $m_{\ell\ell} > 30$ GeV as well as in the p_T of the subleading lepton at $p_T^{\text{sublead}} \leq 20$ GeV and $p_T^{\text{sublead}} > 20$ GeV.

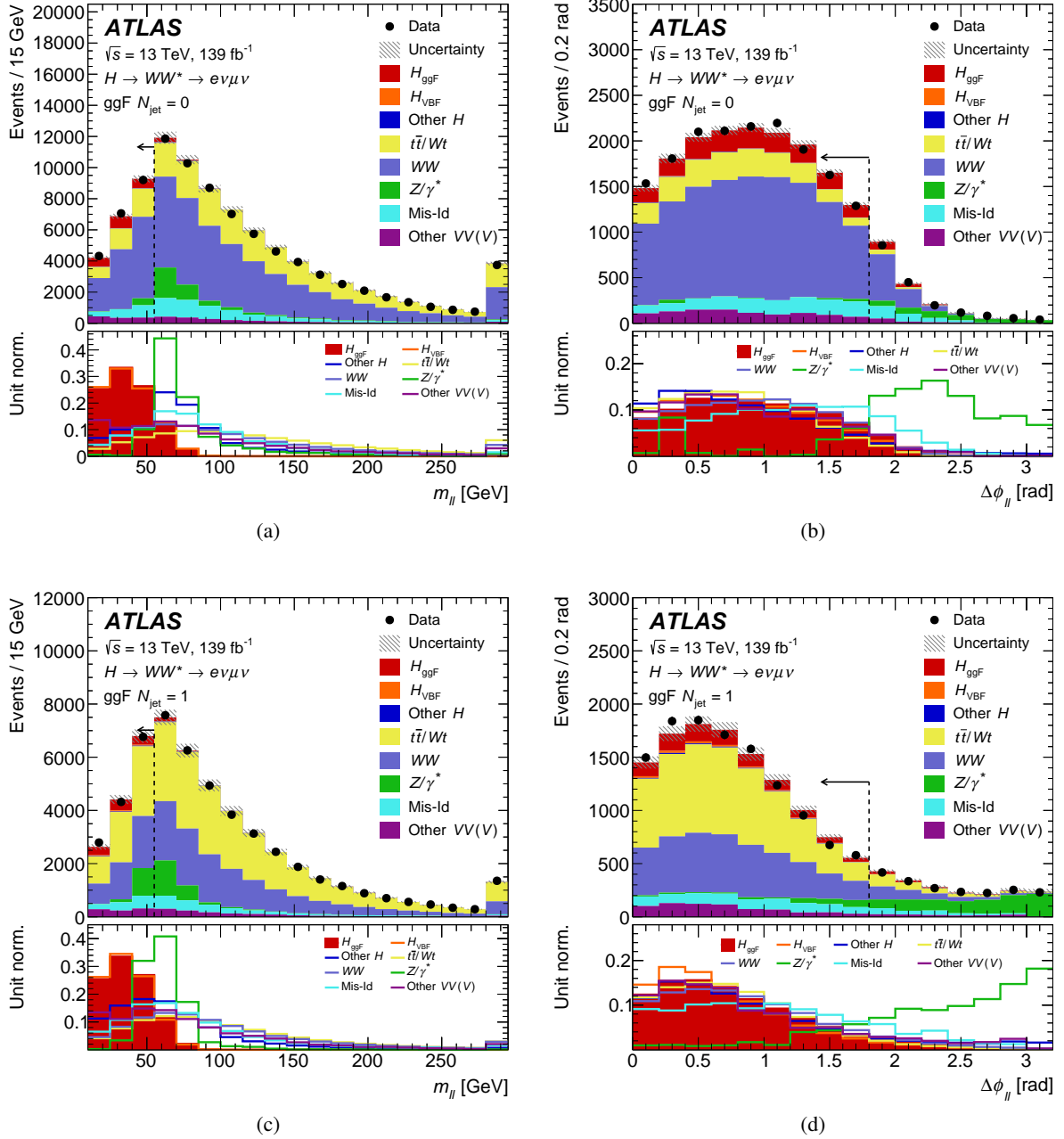


Figure 2: Distributions of (a) $m_{\ell\ell}$ and (b) $\Delta\phi_{\ell\ell}$ in the $N_{\text{jet}} = 0$ category as well as (c) $m_{\ell\ell}$ and (d) $\Delta\phi_{\ell\ell}$ in the $N_{\text{jet}} = 1$ category, after the preselection and background rejection steps, and also after the selection on $m_{\ell\ell}$ for the $\Delta\phi_{\ell\ell}$ plots. The dashed lines indicate where the selection on the observable is made. The distributions are normalized to their nominal yields, before the final fit to all SRs and CRs (prefit normalizations). The hatched band shows the normalization component of the total prefit uncertainty, assuming SM Higgs boson production. The bottom panels show the normalized distributions for the signal and backgrounds, from which it can be inferred which background processes are primarily removed by the indicated selections.

5.2 $N_{\text{jet}} = 1$ category

A requirement is applied to the maximum transverse mass defined as the maximum value of $m_{\text{T}}^{\ell_i}$, $\max(m_{\text{T}}^{\ell})$, where

$$m_{\text{T}}^{\ell_i} = \sqrt{2 p_{\text{T}}^{\ell_i} \cdot E_{\text{T}}^{\text{miss}} \cdot (1 - \cos \Delta\phi(\ell_i, E_{\text{T}}^{\text{miss}}))},$$

and ℓ_i can be either the leading or the subleading lepton. This quantity tends to have small values for the DY background and large values for the signal process. It also has small values for multijet production, where misidentified leptons are frequently measured with energy lower than the jets from which they originate. Therefore, these backgrounds are substantially reduced with a requirement of $\max(m_{\text{T}}^{\ell}) > 50$ GeV. The one-jet requirement improves the rejection of $Z/\gamma^* \rightarrow \tau\tau$ background. Using the direction and magnitude of the measured missing transverse momentum and projecting it along the directions defined by the two reconstructed charged leptons, the mass of the leptonically decaying τ -lepton pair, $m_{\tau\tau}$, can be reconstructed using the so-called collinear approximation [115]. A requirement of $m_{\tau\tau} < m_Z - 25$ GeV⁶ significantly reduces the remaining DY contribution and is applied in all categories with $N_{\text{jet}} \geq 1$. The same $\Delta\phi_{\ell\ell}$ and $m_{\ell\ell}$ selections as described in Sec. 5.1 are also applied in the $N_{\text{jet}} = 1$ category and are illustrated in Figs. 2(c) and 2(d), respectively. The $N_{\text{jet}} = 1$ SR is further split into four subregions with the same boundaries as defined for the $N_{\text{jet}} = 0$ category.

5.3 VBF-enriched $N_{\text{jet}} \geq 2$ category

The VBF process is characterized by the kinematics of the two leading jets in the event, which are predominantly emitted in the forward region, and by the relatively low levels of hadronic activity between them due to the mediating weak bosons that do not exchange color. In order to construct a SR enriched in this VBF topology, events are rejected if they contain additional jets with $p_{\text{T}} > 30$ GeV that lie in the pseudorapidity gap between the two leading jets (central jet veto) or if either lepton lies outside the pseudorapidity gap between the two leading jets (outside lepton veto). Furthermore, the invariant mass of the two leading jets, m_{jj} , is required to be above 120 GeV to ensure orthogonality to analyses targeting the $V(\rightarrow qq)H$ production mode.

The events in this category are analyzed using a DNN that is implemented through Keras [116] and TensorFlow [117], considering VBF Higgs boson production as signal and the other processes as background (including ggF Higgs boson production). The hyperparameters are optimized to find the best-performing set. The architecture of the DNN exhibits seven dense hidden layers, with the first hidden layer consisting of 256 nodes and each successive layer decreasing in size. Nodes in the hidden layers use rectified linear units as activation functions, while the output node utilizes a sigmoid activation function. Cross-entropy is used to calculate the loss, and dropout is used as a regularization method to prevent overtraining. A total of 15 kinematic variables built from the leptons (ℓ), jets (j), and $E_{\text{T}}^{\text{miss}}$ in the event are used as inputs to the DNN. The following variables are chosen to provide discrimination based on the VBF topology: m_{jj} ; the difference between the two jet rapidities (Δy_{jj}); the lepton η -centrality ($\sum_{\ell} C_{\ell}$, where $C_{\ell} = |2\eta_{\ell} - \sum \eta_j|/\Delta\eta_{jj}$), which quantifies the positions of the leptons relative to the leading jets in pseudorapidity [118]; the p_{T} of the three leading jets ($p_{\text{T}}^{j_1}, p_{\text{T}}^{j_2}, p_{\text{T}}^{j_3}$, where $p_{\text{T}}^{j_3}$ is set to 0 GeV if there is no third jet in the event); and the invariant masses of all four possible lepton-jet pairs between the leptons and the two leading jets ($m_{\ell_1 j_1}, m_{\ell_1 j_2}, m_{\ell_2 j_1}, m_{\ell_2 j_2}$). The variables $m_{\ell\ell}$, $\Delta\phi_{\ell\ell}$, and m_{T} are also utilized, targeting the features of the $H \rightarrow WW^*$ decay. Two additional variables are also included: the

⁶ For this selection, m_Z is set to 91.1876 GeV.

total transverse momentum (p_T^{tot}), defined as the magnitude of the vectorial sum of the p_T of all selected objects, and the E_T^{miss} significance, which provides separation between events with real undetected high- p_T particles and events where the E_T^{miss} is the result of resolution effects [119]. The observables providing the best discrimination between signal and background are m_{jj} and Δy_{jj} , and their distributions in the $N_{\text{jet}} \geq 2$ VBF SR are shown in Fig. 3. The DNN output reflects how ‘‘VBF-like’’ the event’s kinematics are, and

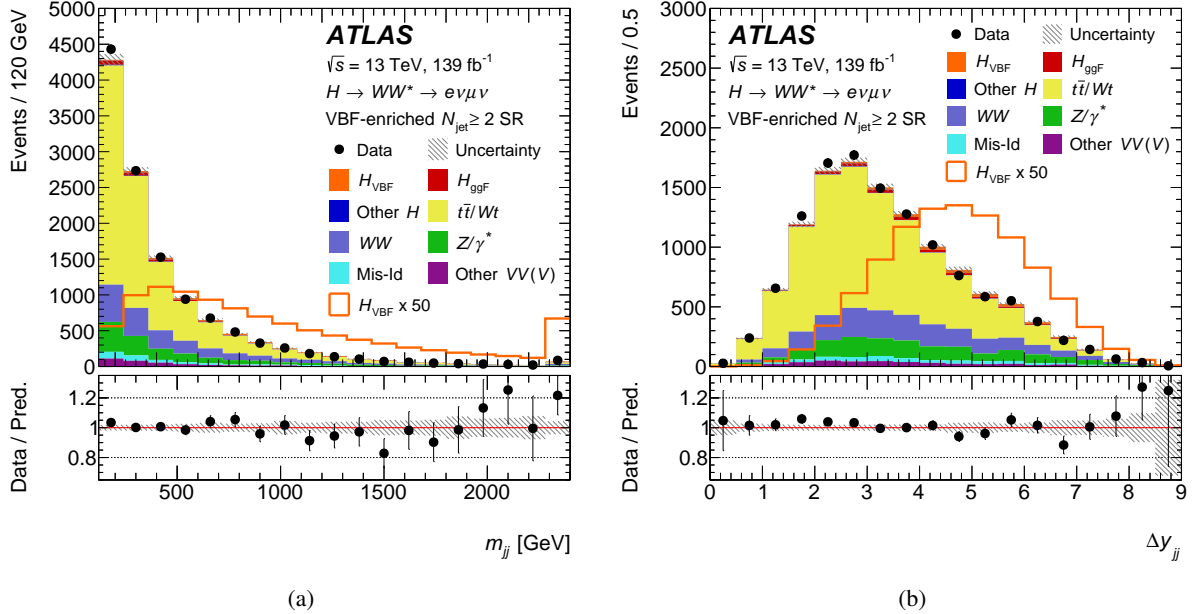


Figure 3: Distributions of (a) m_{jj} and (b) Δy_{jj} in the $N_{\text{jet}} \geq 2$ VBF SR. The solid line shows the expected VBF signal scaled by a factor of 50. The signal and background yields are normalized to the output from the final fit to all SRs and CRs. The hatched band shows the normalization component of the total postfit uncertainty, assuming SM Higgs boson production. The last bin of each distribution is inclusive (includes the overflow).

thus is used as a classifier, with the signal purity improving as the output value increases. The DNN bin boundaries in the VBF-sensitive range are chosen with an algorithm that aims to make the bins as narrow as possible, while also requiring at least ten expected signal and background events each per bin as well as at most 20% statistical uncertainty in the background. This method helps to mitigate the risk of strong statistical fluctuations in the fit, and yields narrower bins on average for larger values of the DNN output, giving a total of seven bins: $[0-0.25, 0.25-0.52, 0.52-0.68, 0.68-0.77, 0.77-0.83, 0.83-0.87, 0.87-1.00]$. In the bin with the highest DNN output, the expected VBF signal-to-background ratio is approximately 2 to 1.

5.4 ggF-enriched $N_{\text{jet}} \geq 2$ category

The ggF-enriched $N_{\text{jet}} \geq 2$ category is forced to be mutually exclusive to the VBF-enriched $N_{\text{jet}} \geq 2$ category by requiring events to fail either the central jet veto or outside lepton veto. Furthermore, $V(\rightarrow qq)H$ production is suppressed by rejecting events in a region defined by $|m_{jj} - 85| \leq 15$ GeV and $\Delta y_{jj} \leq 1.2$. The same $\Delta\phi_{\ell\ell}$ and $m_{\ell\ell}$ selections as described in Sec. 5.1 are also applied in the ggF-enriched $N_{\text{jet}} \geq 2$ category and are shown in Figs. 4(a) and 4(b), respectively, together with the $m_{\tau\tau}$ selection in Fig. 4(c). The ggF-enriched $N_{\text{jet}} \geq 2$ SR is further split into two subregions with a boundary at $m_{\ell\ell} = 30$ GeV.

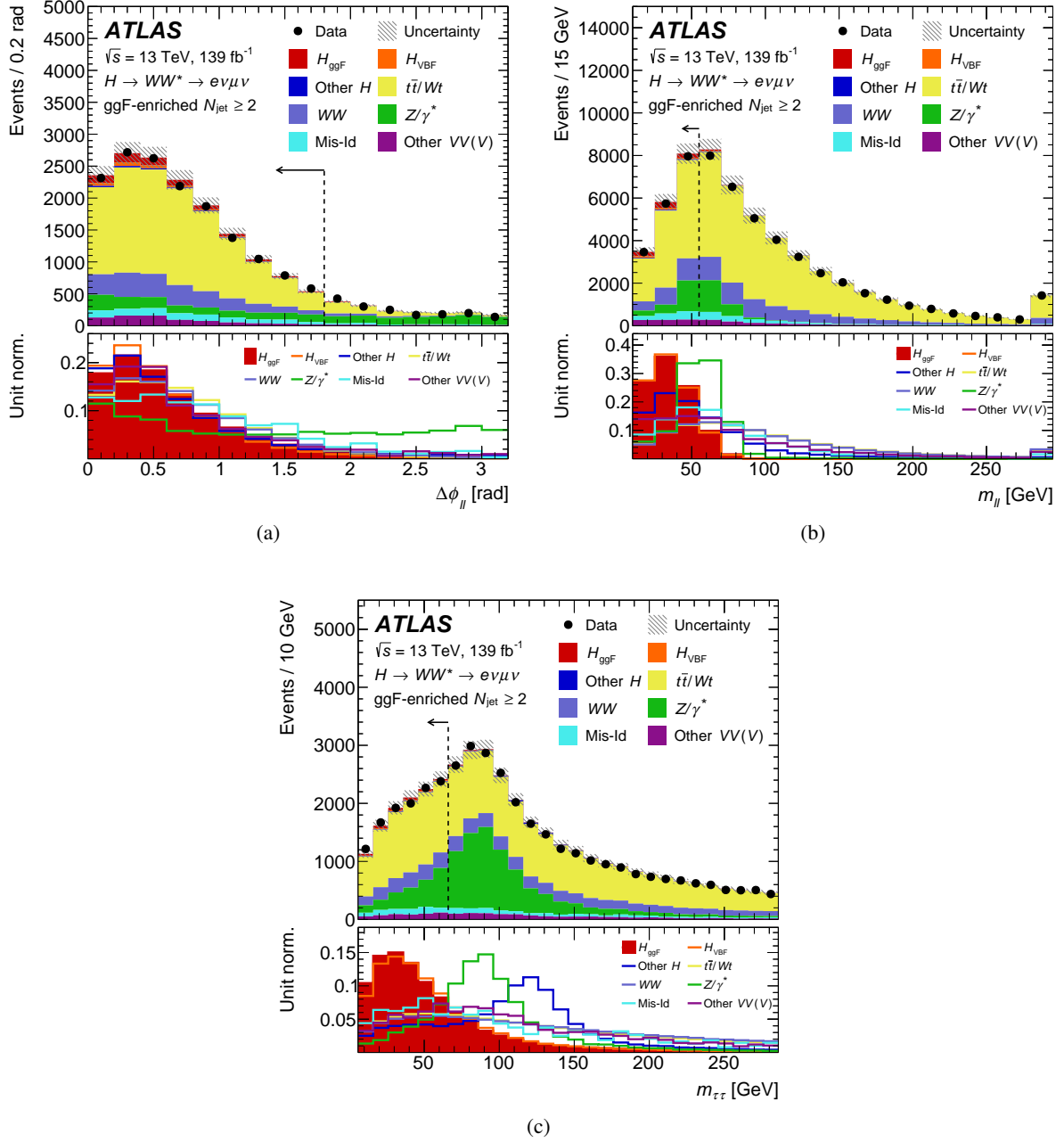


Figure 4: Distributions of (a) $\Delta\phi_{\ell\ell}$, (b) $m_{\ell\ell}$, and (c) $m_{\tau\tau}$ in the ggF-enriched $N_{\text{jet}} \geq 2$ category, after requiring all selections up to the corresponding observable. Underflow and overflow events are not included in (c). The dashed lines indicate where the selection on the observable is made. The distributions are normalized to their nominal yields, before the final fit to all SRs and CRs (prefit normalizations). The hatched band shows the normalization component of the total prefit uncertainty, assuming SM Higgs boson production. The bottom panels show the normalized distributions for the signal and backgrounds, from which it can be inferred which background processes are primarily removed by the indicated selections.

5.5 STXS categorization

In order to optimize the measurements in bins aligned with those of the Stage-1.2 STXS framework, several STXS kinematic fiducial regions are merged and the separation of the selected events into SRs differs slightly from the description above. The STXS bin merging strategy, referred to as Reduced Stage-1.2, and the reconstructed SRs are illustrated in Fig. 5. For the exclusive $N_{\text{jet}} = 0$ ggH category, only a single STXS

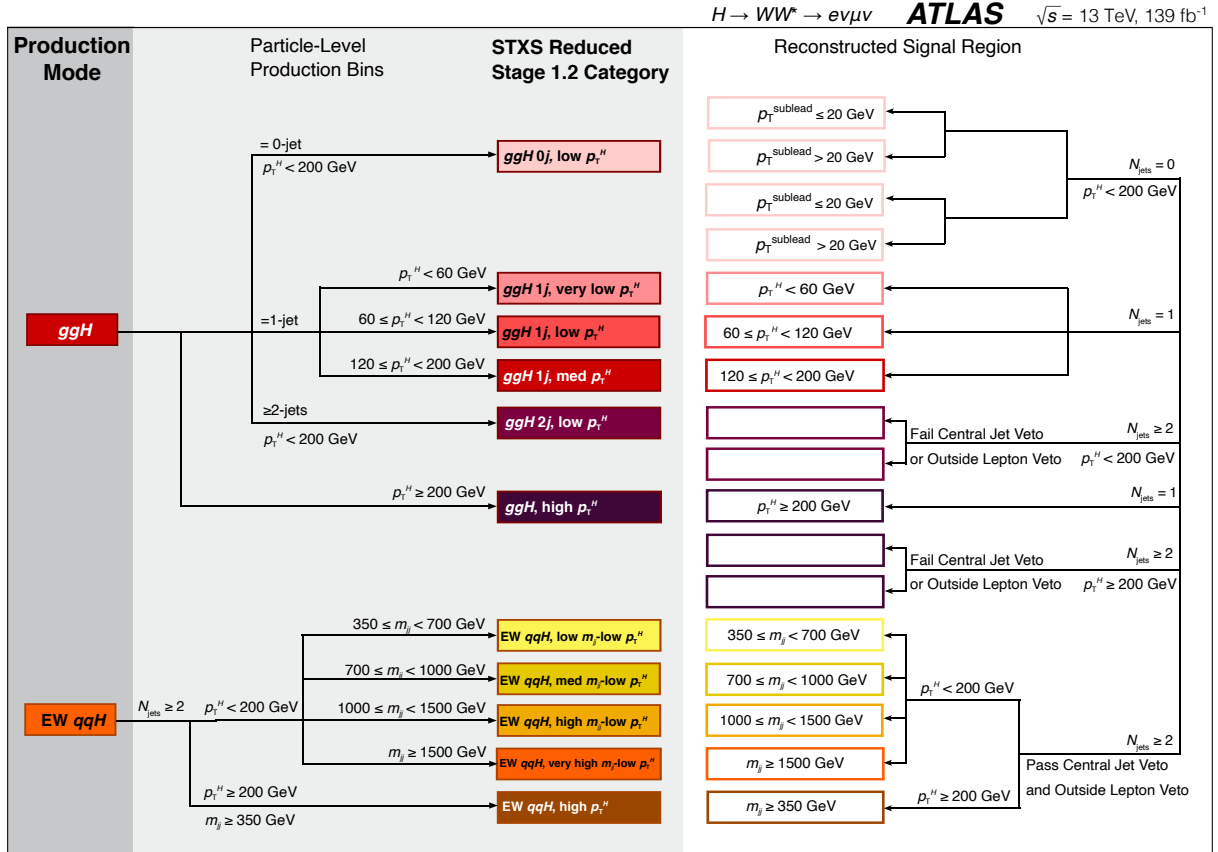


Figure 5: Two sets (Production Mode Stage and Reduced Stage 1.2) of exclusive phase-space regions (production bins) defined at parton level for the measurement of the Higgs boson production cross sections (left and middle-left shaded panels), and the corresponding reconstructed signal regions (right panel). The description of the production bins as well as the corresponding reconstructed signal regions is given in Sec. 5.5. The colors of each reconstructed signal region box indicate the STXS bin which provides the largest relative contribution.

cross section is measured, with the same SR splitting as defined in Sec. 5.1 and applying a $p_T^H < 200$ GeV selection. For the exclusive $N_{\text{jet}} = 1$ ggH category, all three Stage-1.2 measurements are retained, with the SR split along the same p_T^H bin boundaries. For the exclusive $N_{\text{jet}} \geq 2$ ggH category with $p_T^H < 200$ GeV, only a single STXS cross section is measured, with the same SR splitting as defined in Sec. 5.4 but also including a $p_T^H < 200$ GeV selection. For the N_{jet} inclusive ggH category with $p_T^H \geq 200$ GeV, only a single STXS cross section is measured, using both the $N_{\text{jet}} = 1$ SR with an added $p_T^H \geq 200$ GeV selection and the same ggF-enriched $N_{\text{jet}} \geq 2$ SR with splitting as defined in Sec. 5.4 but also including a $p_T^H \geq 200$ GeV selection. No events with $N_{\text{jet}} = 0$ at the event-generation level are reconstructed in the region with $p_T^H \geq 200$ GeV. For the exclusive $N_{\text{jet}} \geq 2$ EW qqH categories targeting VBF production,

the bins separated by p_T^{Hjj} value⁷ are merged, and so are the bins separated by m_{jj} for $p_T^H \geq 200$ GeV, resulting in a total of five measured cross sections. The same SR described in Sec. 5.3 is used, but split into five subregions with the same boundaries that define the measured EW qqH STXS cross sections. In addition, the same DNN and training is used for the final fit's discriminating variable. The exclusive $N_{\text{jet}} \geq 2$ EW qqH category with $m_{jj} < 350$ GeV that targets $V(\rightarrow q\bar{q})H$ production and also the $V(\rightarrow \text{leptons})H$ and $t\bar{t}H$ categories to which this analysis is not sensitive are fixed to their expected yields in the fit. Figure 6 shows the relative contributions of the different merged STXS bins in all reconstructed SRs. In each case, the target categories provide the largest contribution in the corresponding SRs which aim to select them.

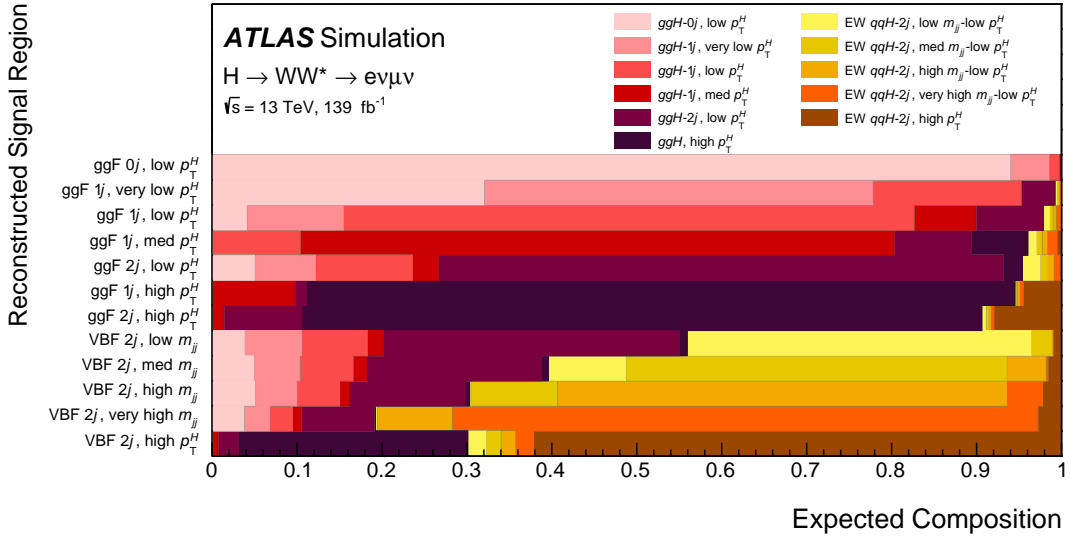


Figure 6: Relative SM signal composition in terms of the measured STXS bin for each reconstructed signal region.

6 Background estimation

The background contamination in the SRs originates from various processes: nonresonant WW , top-quark pair ($t\bar{t}$) and single-top-quark (Wt), diboson (WZ , ZZ , $W\gamma$, $W\gamma^*$, and $Z\gamma$) and Drell-Yan (mainly $Z/\gamma^* \rightarrow \tau\tau$, hereafter denoted by Z/γ^*) production. Other background contributions arise from W +jets and multijet production with misidentified leptons, which are either nonprompt leptons from decays of heavy-flavor hadrons or jets misidentified as prompt leptons. The backgrounds with misidentified leptons are estimated using a data-driven technique. Dedicated data regions with low expected signal, hereafter called control regions (CRs), are used to normalize the predictions of the WW , top-quark, and $Z/\gamma^* \rightarrow \tau\tau$ backgrounds. Table 3 summarizes the selections used to define the CRs, which start from the preselection defined in Table 2. The background estimates for the remaining background processes, most notably the diboson processes other than WW , are obtained from simulated samples normalized to the theoretical cross sections for these processes.

⁷ p_T^{Hjj} is defined at the reconstruction level as the transverse momentum of the system composed of the two leptons + E_T^{miss} + two leading jets in the event.

Table 3: Event selection criteria used to define the control regions in the $H \rightarrow WW^* \rightarrow e\nu\mu\nu$ analysis. Every control region selection starts from the selection labeled ‘‘Preselection’’ in Table 2, and $N_{b\text{-jet},(20 < p_T < 30 \text{ GeV})}$ represents the number of b -jets with $20 < p_T < 30 \text{ GeV}$.

CR	$N_{\text{jet},(p_T > 30 \text{ GeV})} = 0$ ggF	$N_{\text{jet},(p_T > 30 \text{ GeV})} = 1$ ggF	$N_{\text{jet},(p_T > 30 \text{ GeV})} \geq 2$ ggF	$N_{\text{jet},(p_T > 30 \text{ GeV})} \geq 2$ VBF	
$qq \rightarrow WW$	$N_{b\text{-jet},(p_T > 20 \text{ GeV})} = 0$				
	$\Delta\phi_{\ell\ell, E_T^{\text{miss}}} > \pi/2$ $p_T^{\ell\ell} > 30 \text{ GeV}$ $55 < m_{\ell\ell} < 110 \text{ GeV}$ $\Delta\phi_{\ell\ell} < 2.6$	$m_{\ell\ell} > 80 \text{ GeV}$			
		$ m_{\tau\tau} - m_Z > 25 \text{ GeV}$	$m_{\tau\tau} < m_Z - 25 \text{ GeV}$		
		$\max(m_T^{\ell}) > 50 \text{ GeV}$	$m_{T2} > 165 \text{ GeV}$	fail central jet veto or fail outside lepton veto	
			$ m_{jj} - 85 > 15 \text{ GeV}$ or $\Delta y_{jj} > 1.2$		
$t\bar{t}/Wt$	$N_{b\text{-jet},(20 < p_T < 30 \text{ GeV})} > 0$ $\Delta\phi_{\ell\ell, E_T^{\text{miss}}} > \pi/2$ $p_T^{\ell\ell} > 30 \text{ GeV}$ $\Delta\phi_{\ell\ell} < 2.8$	$N_{b\text{-jet},(p_T > 30 \text{ GeV})} = 1$	$N_{b\text{-jet},(p_T > 20 \text{ GeV})} = 0$	$N_{b\text{-jet},(p_T > 20 \text{ GeV})} = 1$	
		$N_{b\text{-jet},(20 < p_T < 30 \text{ GeV})} = 0$	$m_{\tau\tau} < m_Z - 25 \text{ GeV}$		
		$\max(m_T^{\ell}) > 50 \text{ GeV}$	$m_{\ell\ell} > 80 \text{ GeV}$	$\Delta\phi_{\ell\ell} < 1.8$	central jet veto outside lepton veto
			$m_{T2} < 165 \text{ GeV}$	fail central jet veto or fail outside lepton veto	
		$ m_{jj} - 85 > 15 \text{ GeV}$ or $\Delta y_{jj} > 1.2$			
Z/γ^*	$N_{b\text{-jet},(p_T > 20 \text{ GeV})} = 0$				
	$\Delta\phi_{\ell\ell} > 2.8$	$m_{\ell\ell} < 80 \text{ GeV}$ no p_T^{miss} requirement	$m_{\ell\ell} < 55 \text{ GeV}$	$m_{\ell\ell} < 70 \text{ GeV}$	
		$m_{\tau\tau} > m_Z - 25 \text{ GeV}$		$ m_{\tau\tau} - m_Z \leq 25 \text{ GeV}$ central jet veto outside lepton veto	
	$\max(m_T^{\ell}) > 50 \text{ GeV}$	fail central jet veto or fail outside lepton veto			
		$ m_{jj} - 85 > 15 \text{ GeV}$ or $\Delta y_{jj} > 1.2$			

6.1 WW background

The nonresonant WW background mainly originates from the quark-initiated process (labeled $qqWW$) with a small additional contribution from the gluon-initiated process proceeding via a box-diagram ($ggWW$). The $ggWW$ process produces approximately 10% of the total WW background contribution and is estimated from simulated samples normalized to the theoretical cross sections. The $qqWW$ process is normalized to the observed yields in dedicated CRs, defined separately for each analysis category. The CRs are orthogonal to the SRs and enriched in the WW process. For the $N_{\text{jet}} = 0$ category, the selected $m_{\ell\ell}$ region is modified to $55 < m_{\ell\ell} < 110 \text{ GeV}$ and the $\Delta\phi_{\ell\ell}$ selection is relaxed to $\Delta\phi_{\ell\ell} < 2.6$ (from $\Delta\phi_{\ell\ell} < 1.8$ in the SRs). The upper bound on the $m_{\ell\ell}$ selection reduces the contamination from top-quark processes in the WW CR, whereas the $\Delta\phi_{\ell\ell}$ selection removes most of the $Z/\gamma^* \rightarrow \tau\tau$ contamination. The WW

CR in the $N_{\text{jet}} = 1$ category differs from the SR by requiring $m_{\ell\ell} > 80$ GeV and $|m_{\tau\tau} - m_Z| > 25$ GeV. For the $N_{\text{jet}} \geq 2$ categories, it is difficult to find a region with high WW process purity because of the overwhelming background from top-quark processes. For the ggF-enriched $N_{\text{jet}} \geq 2$ category, the $qqWW$ process is normalized to the yield in the CR, whereas the $qqWW$ background in the VBF-enriched $N_{\text{jet}} \geq 2$ category is estimated from simulated samples normalized to the theoretical cross section. The WW CR for the ggF-enriched $N_{\text{jet}} \geq 2$ category is defined by requiring $m_{\ell\ell} > 80$ GeV and $m_{T2} > 165$ GeV. The m_{T2} variable [120] is defined as

$$m_{T2}^2 = \min_{\not{p}_1 + \not{p}_2 = \not{p}_T} \left[\max\{m_T^2(p_T^a, \not{p}_1), m_T^2(p_T^b, \not{p}_2)\} \right],$$

where the minimization is over all possible two-momenta, $\not{p}_{1,2}$, such that their sum gives the observed missing transverse momentum \not{p}_T , and where each of p_T^a and p_T^b is the combined transverse momentum of a charged lepton and a jet. The m_{T2} selection is indicated by a dashed line in Fig. 7, with an arrow at the top pointing to the region retained. For all WW CRs, a b -jet veto is maintained.

The WW CRs have prefit WW process purities of 67% ($N_{\text{jet}} = 0$), 34% ($N_{\text{jet}} = 1$), and 39% (ggF-enriched $N_{\text{jet}} \geq 2$). The postfit background normalization factors, from the fit described in Sec. 8 are summarized in Table 4. Figure 8 presents the postfit m_T distributions in the $N_{\text{jet}} = 0$, $N_{\text{jet}} = 1$, and ggF-enriched $N_{\text{jet}} \geq 2$ CRs.

6.2 Top-quark backgrounds

The top-quark backgrounds affecting this analysis are associated with the $t\bar{t}$ and Wt processes. They are normalized to the observed combined top yields in CRs, defined separately for each analysis category. The uncertainties in the relative contributions of $t\bar{t}$ and Wt are accounted for by considering their relevant uncertainties separately, while their ratios are similar between respective CRs and SRs. The CRs are orthogonal to the SRs, normally by inverting the b -jet veto. The exception is in the ggF-enriched $N_{\text{jet}} \geq 2$ category, where the top-quark CR is defined with a b -jet veto and orthogonality to the SR and WW CR is achieved by requiring $m_{\ell\ell} > 80$ GeV and $m_{T2} < 165$ GeV, respectively. This is possible due to the $N_{\text{jet}} \geq 2$ categories having high top-quark event purity even with a b -jet veto, and this definition reduces the uncertainties from the b -jet selection in this category. For the $N_{\text{jet}} = 0$ category, the top-quark CR requires the presence of a reconstructed jet with $20 < p_T < 30$ GeV which is identified as coming from a b -quark.

The top-quark CRs have prefit top-quark process purities of 89% ($N_{\text{jet}} = 0$), 98% ($N_{\text{jet}} = 1$), 71% (ggF-enriched $N_{\text{jet}} \geq 2$), and 97% (VBF-enriched $N_{\text{jet}} \geq 2$). The postfit background normalization factors are summarized in Table 4. Figure 9 presents the postfit m_T distributions in the $N_{\text{jet}} = 0$, $N_{\text{jet}} = 1$, and ggF-enriched $N_{\text{jet}} \geq 2$ CRs, as well as the postfit DNN output distribution in the VBF-enriched $N_{\text{jet}} \geq 2$ CR.

6.3 $Z/\gamma^* \rightarrow \tau\tau$ background

The $Z/\gamma^* \rightarrow \tau\tau$ background is normalized in dedicated CRs, defined separately for each analysis category. For the $N_{\text{jet}} = 0$ category, the reconstructed leptons are required to have a large opening angle, $\Delta\phi_{\ell\ell} > 2.8$. For the $N_{\text{jet}} = 1$ and $N_{\text{jet}} \geq 2$ categories, the main selection that separates the $Z/\gamma^* \rightarrow \tau\tau$ CR from the SR is that the $Z/\gamma^* \rightarrow \tau\tau$ CR includes the region in $m_{\tau\tau}$ around the nominal Z boson mass. For all $Z/\gamma^* \rightarrow \tau\tau$

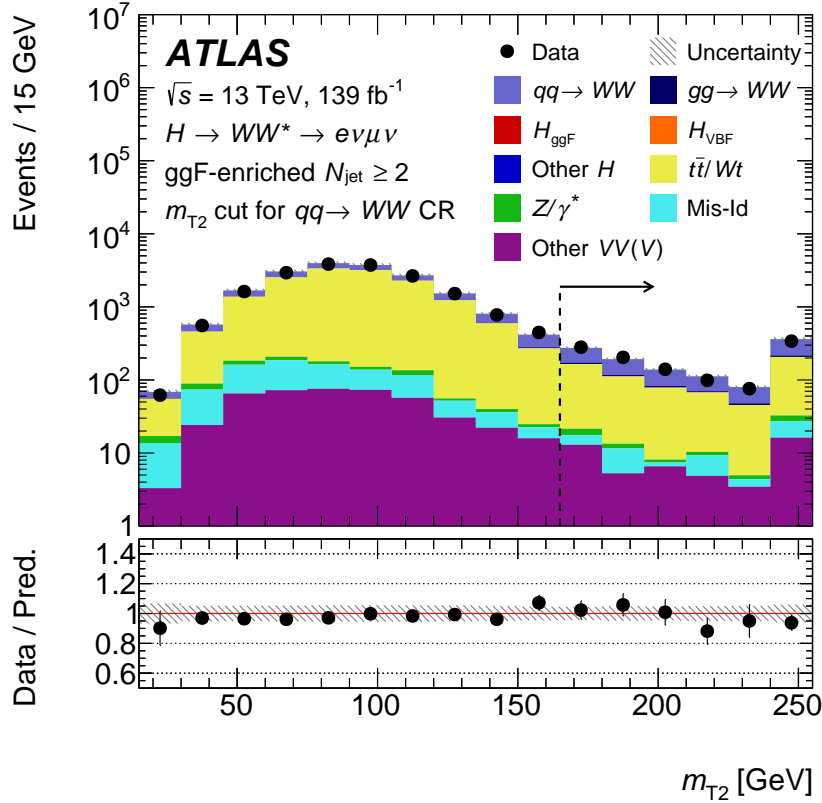


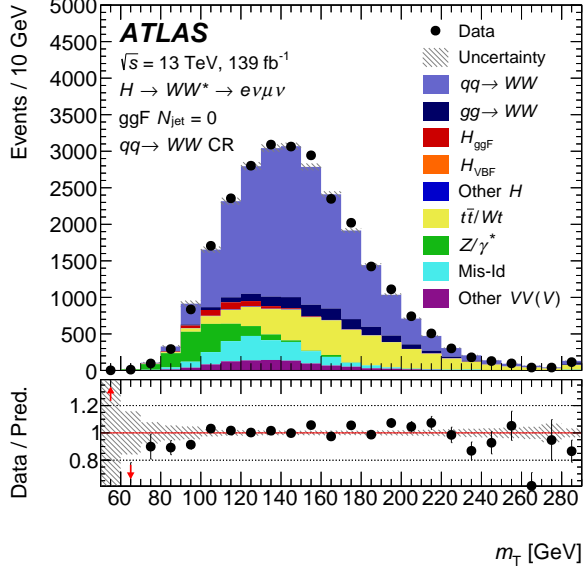
Figure 7: Distribution of the m_{T2} variable used in the definition of the WW CR for the ggF-enriched $N_{\text{jet}} \geq 2$ category and after the prior selections summarized in Table 3 have been applied. The dashed line indicates where the selection on the observable is made. The distributions are normalized to their nominal yields, before the final fit to all SRs and CRs (prefit normalizations). The hatched band shows the normalization component of the total prefit uncertainty.

CRs, a b -jet veto is maintained. These CRs have prefit $Z/\gamma^* \rightarrow \tau\tau$ process purities of 94% ($N_{\text{jet}}=0$), 76% ($N_{\text{jet}}=1$), 76% (ggF-enriched $N_{\text{jet}} \geq 2$), and 77% (VBF-enriched $N_{\text{jet}} \geq 2$). The postfit background normalization factors are summarized in Table 4. Figure 10 presents the postfit m_T distributions in the $N_{\text{jet}}=0$, $N_{\text{jet}}=1$, and ggF-enriched $N_{\text{jet}} \geq 2$ CRs as well as the postfit DNN output distribution in the VBF-enriched $N_{\text{jet}} \geq 2$ CR.

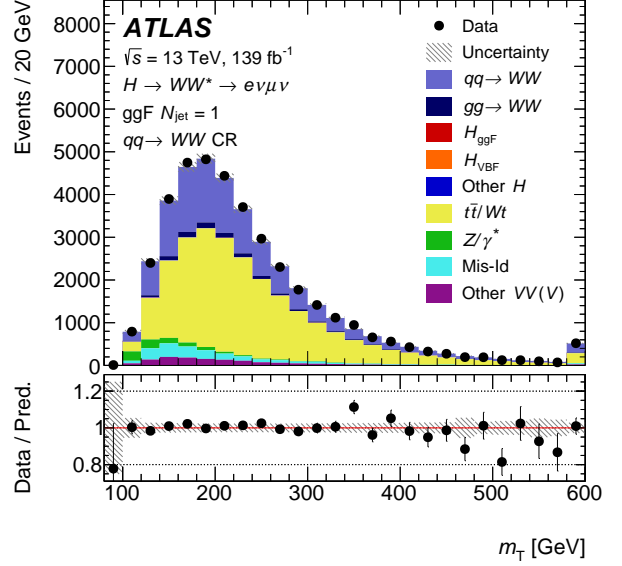
6.4 Backgrounds with misidentified leptons

The backgrounds originating from either one or two misidentified (Mis-Id) leptons are primarily due to W +jets and multijet processes, respectively. They are estimated using a data-driven technique⁸ where control samples are established in which all nominal selections are applied with the exception that one of the two lepton candidates fails to meet all of the identification criteria defined in Sec. 4, but satisfies a looser set of identification criteria (referred to as an anti-identified lepton). The expected Mis-Id background yields in the signal and control regions are extrapolated from the observed number of events in the corresponding samples with anti-identified leptons, after subtracting the expected contribution from processes with two

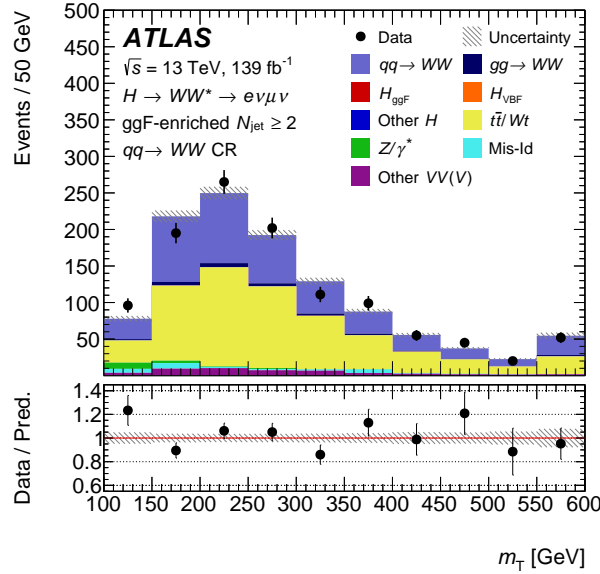
⁸ The method to estimate the Mis-ID backgrounds is based on previous ggF+VBF $H \rightarrow WW^*$ analyses by ATLAS [121, 122].



(a)



(b)



(c)

Figure 8: Postfit m_T distributions in the (a) $N_{\text{jet}} = 0$, (b) $N_{\text{jet}} = 1$, and (c) ggF -enriched $N_{\text{jet}} \geq 2$ WW CRs with signal (normalized to postfit measurement) and background modeled contributions. The red arrow in the lower panel of (a) indicates that the central value of the data lies above the window. The last bin of each distribution is inclusive (includes the overflow). The hatched band shows the total uncertainty, assuming SM Higgs boson production. Some contributions are too small to be visible.

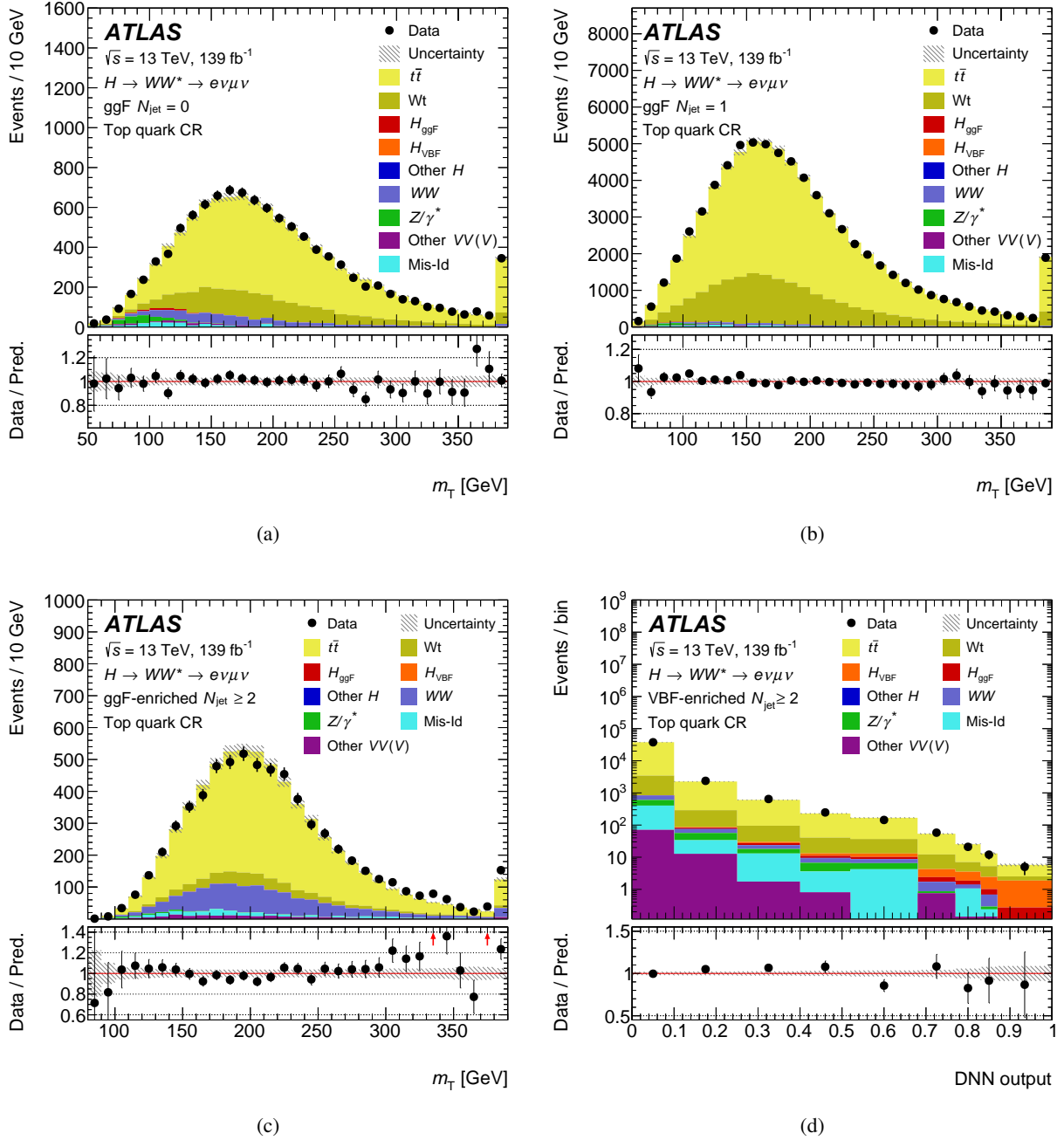


Figure 9: Postfit m_T distributions in the (a) $N_{\text{jet}} = 0$, (b) $N_{\text{jet}} = 1$, and (c) ggF-enriched $N_{\text{jet}} \geq 2$ top-quark CRs, as well as (d) the postfit DNN output distribution in the VBF-enriched $N_{\text{jet}} \geq 2$ top-quark CR, with signal (normalized to postfit measurement) and background modeled contributions. The first two bins of the DNN output distribution used in the final fit, $[0-0.25, 0.25-0.52]$, are split here into four bins, $[0-0.1, 0.1-0.25, 0.25-0.4, 0.4-0.52]$, to illustrate the shape of the steeply falling background. The red arrows in the lower panel of (c) indicate that the central value of the data lies above the window. The last bin of each m_T distribution is inclusive (includes the overflow). The hatched band shows the total uncertainty, assuming SM Higgs boson production. Some contributions are too small to be visible.

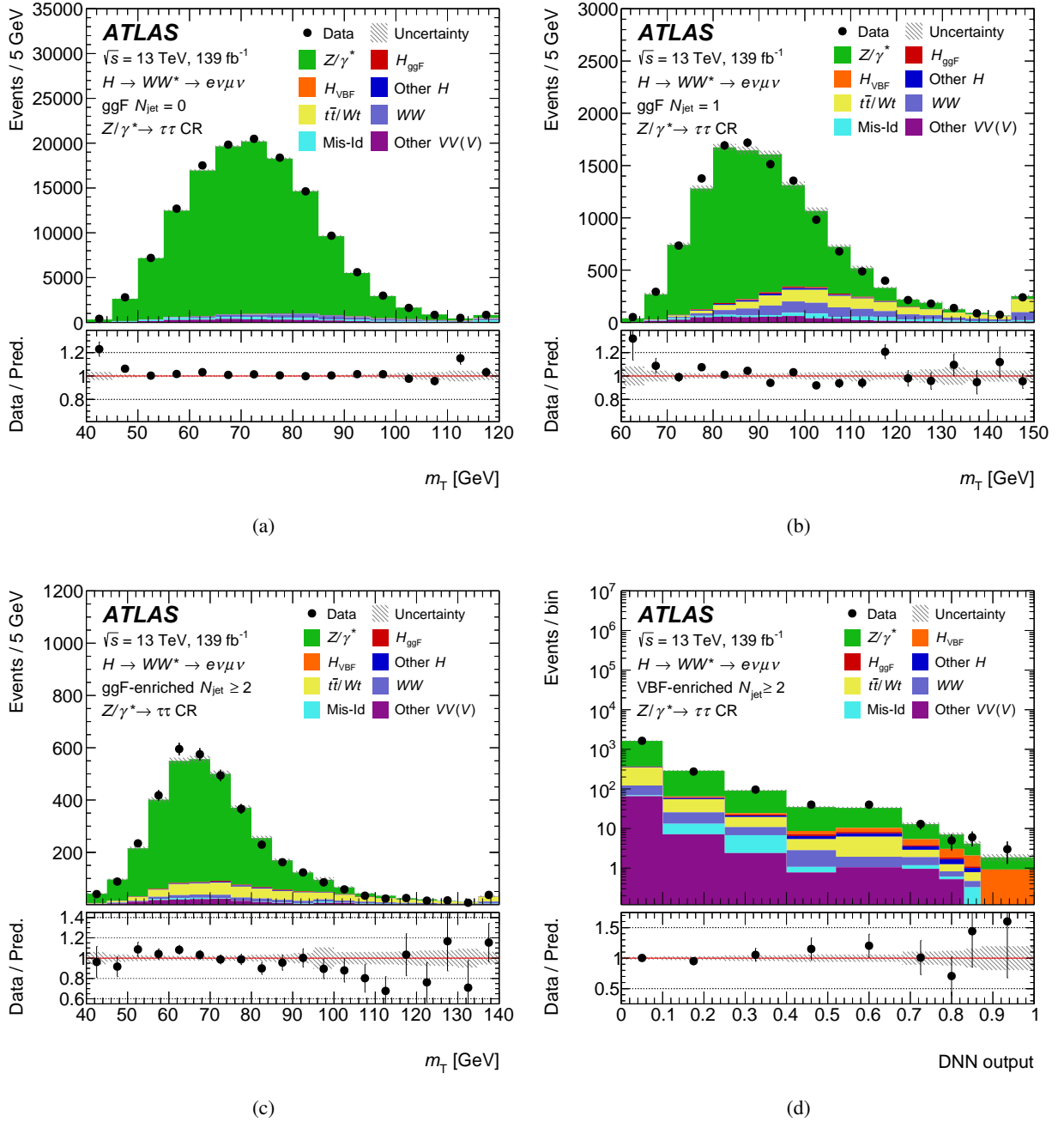


Figure 10: Postfit m_T distributions in the (a) $N_{\text{jet}} = 0$, (b) $N_{\text{jet}} = 1$, and (c) ggF-enriched $N_{\text{jet}} \geq 2$ $Z/\gamma^* \rightarrow \tau\tau$ CRs, as well as (d) the postfit DNN output distribution in the VBF-enriched $N_{\text{jet}} \geq 2$ $Z/\gamma^* \rightarrow \tau\tau$ CR, with signal (normalized to postfit measurement) and background modeled contributions. The first two bins of the DNN output distribution used in the final fit, $[0-0.25, 0.25-0.52]$, are split here into four bins, $[0-0.1, 0.1-0.25, 0.25-0.4, 0.4-0.52]$, to illustrate the shape of the steeply falling background. The last bin of each m_T distribution is inclusive (includes the overflow). The hatched band shows the total uncertainty, assuming SM Higgs boson production. Some contributions are too small to be visible.

Table 4: Postfit normalization factors which scale the corresponding estimated yields in the relevant signal region; the dash indicates where a MC-based normalization is used. The quoted uncertainties include both the statistical and systematic contributions.

Category	WW	$t\bar{t}/Wt$	Z/γ^*
$N_{\text{jet}} = 0$ ggF	$1.02^{+0.07}_{-0.07}$	$0.93^{+0.22}_{-0.17}$	$0.96^{+0.07}_{-0.06}$
$N_{\text{jet}} = 1$ ggF	$0.85^{+0.16}_{-0.15}$	$1.05^{+0.19}_{-0.16}$	$0.98^{+0.10}_{-0.09}$
$N_{\text{jet}} \geq 2$ ggF	$0.81^{+0.34}_{-0.33}$	$0.96^{+0.23}_{-0.18}$	$0.98^{+0.18}_{-0.17}$
$N_{\text{jet}} \geq 2$ VBF		$0.92^{+0.33}_{-0.21}$	$0.93^{+0.23}_{-0.19}$

prompt leptons. The method appropriately accounts for all processes with misidentified leptons, as long as they are represented in the sample with one anti-identified lepton and the extrapolation factor is similar to the nominal value. The small contribution from multijet processes with two misidentified leptons is accounted for in the extrapolation by applying a correction term evaluated in a sample where both lepton candidates are anti-identified. The correction is largest in the VBF-enriched $N_{\text{jet}} \geq 2$ category, for which a direct $p_{\text{T}}^{\text{miss}}$ selection is not applied. In this case, the multijet processes constitute approximately 25% of the total misidentified lepton yield in the SR.

The extrapolation factor that is used to extrapolate the expected Mis-Id background yields in the control samples to the SRs is determined in a sample of Z +jets-enriched events, where a three-lepton selection is applied to target events with a leptonically decaying Z boson plus a misidentified lepton candidate recoiling against the Z boson. It is defined as the ratio of the number of events in which the misidentified lepton candidate is identified to the number of events in which it is anti-identified and is measured in bins of lepton p_{T} (and $|\eta|$) in the case of electrons (muons). A correction factor is used to account for the fact that the sources of misidentified leptons, such as hadrons, nonprompt leptons from heavy-flavor decays, and photons, contribute in different ratios to the Z +jets-enriched sample in which the extrapolation factor is derived and the largest source of Mis-Id background in the SR (W +jets events). This sample composition correction factor is determined from the ratio of extrapolation factors measured in W +jets and Z +jets MC simulation.

6.5 Control regions for the STXS measurements

For the cross-section measurements in the STXS framework, the CRs defined above for the WW , top-quark, and $Z/\gamma^* \rightarrow \tau\tau$ processes are further split into smaller CRs corresponding to the various STXS SRs. For the $N_{\text{jet}} = 0$ CRs, no further splitting is needed and identical CRs are used. For the $N_{\text{jet}} = 1$ category, the CRs for the WW , top-quark, and $Z/\gamma^* \rightarrow \tau\tau$ processes are each divided into four regions defined by $p_{\text{T}}^H < 60$ GeV, $60 \leq p_{\text{T}}^H < 120$ GeV, $120 \leq p_{\text{T}}^H < 200$ GeV, and $p_{\text{T}}^H \geq 200$ GeV. The CRs for the WW , top-quark, and $Z/\gamma^* \rightarrow \tau\tau$ processes in the ggF-enriched $N_{\text{jet}} \geq 2$ category are further divided into regions with $p_{\text{T}}^H < 200$ GeV and $p_{\text{T}}^H \geq 200$ GeV. The $p_{\text{T}}^H \geq 200$ GeV STXS category targeting the ggF production mode is common to all jet multiplicities. For the VBF-enriched $N_{\text{jet}} \geq 2$ category, the top-quark and $Z/\gamma^* \rightarrow \tau\tau$ CRs are split into three regions each. Two regions are defined for $p_{\text{T}}^H < 200$ GeV by $350 \leq m_{jj} < 700$ GeV and $m_{jj} \geq 700$ GeV, while one region is defined for $p_{\text{T}}^H \geq 200$ GeV.

7 Systematic uncertainties

Uncertainties from both experimental and theoretical sources affect the results of the analysis. This section describes the estimation of their effects on the signal and background normalizations as well as, where applicable, their effects on the shape of the final discriminant. The relative impacts that various sources of systematic uncertainties have on the measured ggF and VBF cross sections are obtained from the likelihood fit described in Sec. 8 and are listed in Table 6.

7.1 Experimental uncertainties

The uncertainties related to the reconstruction of the objects used in the analysis are determined using data-driven methods on high-statistics samples of processes such as $Z \rightarrow \ell\ell$. Uncertainties associated with the selected leptons originate from the reconstruction and identification efficiency, the energy (or momentum) scale and resolution, and the isolation efficiency [104, 106]. For jets, uncertainties arise from the jet energy scale and resolution [110], the jet-vertex tagger’s performance, and the b -jet identification [113]. Furthermore, uncertainties due to the trigger selection [18, 19] and the soft term in the reconstruction of E_T^{miss} [114] are estimated. The uncertainty in the modeling of pileup for simulated samples is estimated by varying the reweighting to the profile in data within its uncertainties. The uncertainty in the combined 2015–2018 integrated luminosity is 1.7% [21], obtained using the LUCID-2 detector [123] for the primary luminosity measurements. The integrated luminosity uncertainty is only applied to the Higgs boson signal and to background processes that are normalized to theoretical predictions.

Three sources of uncertainty related to the extrapolation factor used in the data-driven Mis-Id background estimate are considered: the statistical uncertainty of the extrapolation factor itself, an uncertainty related to the subtraction of processes with two prompt leptons from the Z +jets-enriched sample used to derive the extrapolation factor, and an uncertainty in the sample composition correction factor. Together, they amount to a total uncertainty on the electron (muon) extrapolation factor ranging from 10% (12%) at low p_T to 35% (75%) at high p_T where there is a small number of Mis-Id leptons.

The largest experimental uncertainties affecting the ggF measurement come from the b -jet identification, the pileup modeling, the jet energy resolution, and the Mis-Id background estimate. For the VBF measurement, the largest experimental uncertainty comes from the E_T^{miss} reconstruction.

7.2 Theoretical uncertainties

Uncertainties from the renormalization and factorization scale choices, underlying-event modeling, and choice of PDF are estimated for all processes. For signal, top, and Z/γ^* processes, the uncertainties from the parton shower and the matrix-element matching are estimated by comparing predictions from the nominal and alternative generators that are described in Sec. 3.2. For the prediction of $qqWW$ and of WZ , ZZ , and $V\gamma^*$ production (VV), variations of the matching scale and nonperturbative effects are considered instead of an alternative program for estimating the matrix-element matching uncertainties. The uncertainty from the resummation scale is estimated for the SHERPA samples.

For signal processes, the approach described in Refs. [11, 124] is used to estimate the variations due to the impact of higher-order contributions not included in the calculations and of migration effects on the N_{jet} ggF cross sections. In particular, the uncertainties from the choice of factorization and renormalization

scales, the choice of resummation scales, and the ggF migrations between the 0-jet and 1-jet phase-space bins or between the 1-jet and ≥ 2 -jet bins are considered [11, 125–128].

The $ggWW$ process is simulated at LO precision for up to one additional parton emission. Therefore, a conservative $-50\%/+100\%$ normalization uncertainty is assigned to this process for the $N_{\text{jet}} \geq 2$ categories and to the STXS measurement in the region with $p_{\text{T}}^H \geq 200$ GeV targeting the ggF production mode. A similar $-50\%/+100\%$ normalization uncertainty is also assigned to the $V\gamma$ sample, due to a mismodeling of the $\gamma \rightarrow e$ misidentification rate which primarily affects events with $m_{\text{T}} \lesssim 80$ GeV and can be seen in Fig. 11(a). The EW WW process, which contributes most significantly in the highest VBF DNN bin, is assigned an additional normalization uncertainty of 15% due to NLO EW corrections, as calculated using the leading-log approximation [129, 130]. For Wt , an additional uncertainty estimated by comparing samples with different diagram removal schemes [84] is applied. A normalization uncertainty of 12%, as estimated in the sample with a three-lepton selection described in Sec. 6.4, is also applied to the non- WW and VVV backgrounds. For backgrounds which are normalized to CR yields, uncertainties are estimated for the CR-to-SR extrapolation factors. Only uncertainties that change the ratios of SR yields to CR yields affect the extrapolation. The uncertainties in the extrapolation factors are treated as uncorrelated between different jet multiplicities and between the CRs for the STXS measurement.

The uncertainties in the STXS measurements are estimated for each SR separately, where the 11 STXS bins are treated as different processes, and cover the migration of events between STXS SRs. Merged SRs are used to determine the uncertainties when only a small number of events are available in the simulated samples in a particular SR.

The largest theoretical uncertainties affecting the ggF signal come from the measurement of exclusive jet multiplicities and from the parton shower. For the VBF signal, the comparisons of different event generators for the matrix-element matching and for the parton shower result in the largest uncertainties in the measurement. For background processes, the theoretical uncertainties in the WW and top-quark backgrounds result in the largest contributions to the overall uncertainty.

8 Fit procedure

Results are obtained from a profile likelihood fit [131] to data in the signal and control regions. Uncertainties enter the fit as nuisance parameters in the likelihood function. Theoretical uncertainties affecting the signal and the experimental uncertainties affecting both signal and background are in general correlated between signal and control regions in all analysis categories. Theoretical uncertainties in the backgrounds and the background normalization factors are uncorrelated between different analysis categories.

The m_{T} distribution is used as the final fit discriminant in each of four regions defined by $m_{\ell\ell}$ and subleading lepton p_{T} in both the $N_{\text{jet}} = 0$ and $N_{\text{jet}} = 1$ categories, as described in Secs. 5.1 and 5.2. The same binning of the m_{T} distribution is used in all regions: $[0-90, 90-100, 100-110, 110-120, 120-130, 130-\infty]$. The SR in the ggF-enriched $N_{\text{jet}} \geq 2$ category is split into two bins of $m_{\ell\ell}$, but there is no split in subleading lepton p_{T} . In both regions, the m_{T} distribution is divided into six bins with the same boundaries as for the $N_{\text{jet}} = 0$ and $N_{\text{jet}} = 1$ categories. For the VBF-enriched $N_{\text{jet}} \geq 2$ category, the DNN output is used as the discriminating fit variable. The distribution is divided into seven bins with the boundaries defined in Sec. 5.3.

For the STXS measurements, two modifications are made: the four STXS regions in the $N_{\text{jet}} = 1$ category are no longer split into bins defined by $m_{\ell\ell}$ and subleading lepton p_{T} , while the STXS measurements

targeting the VBF production mode define four bins for the DNN output with boundaries [0–0.5, 0.5–0.7, 0.7–0.84, 0.84–1.00].

The cross sections for the ggF and VBF production modes are determined in a simultaneous fit to all nominal SRs and CRs in the $N_{\text{jet}}=0$, $N_{\text{jet}}=1$, and $N_{\text{jet}}\geq 2$ categories. The ggF and VBF cross sections are the two unconstrained POIs in this fit. A second fit is performed using these same regions, but measuring a single POI for the combined ggF and VBF yield. In both fits, the other Higgs boson production modes are fixed to their expected yields. A third fit is made to all the STXS regions, where the 11 cross sections measured are POIs. No nuisance parameters are significantly pulled or constrained in any of the fits.

9 Signal region yields and results

Table 5 shows the postfit SR yields for all of the four analysis categories defined in Sec. 5. The uncertainty in the total expected yield reflects incomplete knowledge of the observed yield in each analysis category and is not indicative of the precision of the analysis. Furthermore, the relative error in the yields of the background processes for which dedicated CRs are defined is in many cases less than the relative error in the corresponding normalization factor displayed in Table 4 due to effects of anticorrelation with some nuisance parameters modeling theory uncertainties.

Table 5: Postfit MC and data yields in the ggF and VBF SRs. Yields in the bin with the highest VBF DNN output are also presented. The quoted uncertainties correspond to the statistical uncertainties, together with the experimental and theory modeling systematic uncertainties. The sum of all the contributions may differ from the total value due to rounding. Moreover, the uncertainty in the total yield differs from the sum in quadrature of the single-process uncertainties due to the effect of anticorrelations between the sources of their systematic uncertainties, which are larger than their MC statistical uncertainties.

Process	$N_{\text{jet}}=0$ ggF	$N_{\text{jet}}=1$ ggF	$N_{\text{jet}}\geq 2$ ggF	$N_{\text{jet}}\geq 2$ VBF	
				Inclusive	DNN: [0.87, 1.0]
H_{ggF}	2100 ± 220	1100 ± 130	440 ± 90	209 ± 40	2.6 ± 0.9
H_{VBF}	23 ± 9	103 ± 30	46 ± 12	180 ± 40	28.8 ± 5.5
Other Higgs	40 ± 20	55 ± 28	55 ± 27	29 ± 15	0.04 ± 0.02
WW	9700 ± 350	3500 ± 410	1500 ± 470	2100 ± 340	4.6 ± 1.2
$t\bar{t}/Wt$	2200 ± 210	5300 ± 340	6100 ± 500	7600 ± 370	2.6 ± 0.8
Z/γ^*	140 ± 50	280 ± 40	930 ± 70	1300 ± 300	0.6 ± 0.1
Other VV	1400 ± 130	840 ± 100	470 ± 90	380 ± 80	0.6 ± 0.1
Mis-Id	1200 ± 130	720 ± 90	470 ± 50	330 ± 40	1.7 ± 0.2
Total	$16\,770 \pm 130$	$11\,940 \pm 110$	$10\,030 \pm 100$	$12\,200 \pm 180$	42.0 ± 5.1
Observed	16 726	11 917	9 982	12 189	38

The m_T distributions for the separate $N_{\text{jet}}=0$, $N_{\text{jet}}=1$, and ggF-enriched $N_{\text{jet}}\geq 2$ SRs, as well as the combination of ggF SRs, are shown in Fig. 11. The bottom panels of Fig. 11 display the difference between the data and the total estimated background compared to the m_T distribution of a SM Higgs boson with $m_H = 125.09$ GeV. The total signal observed in all categories (see Table 5) is about 4000 events and agrees, in both shape and rate, with the expected SM signal. The observed (expected) signal yield in the ggF-enriched $N_{\text{jet}}\geq 2$ category, with the VBF contribution fixed to the Standard Model prediction, reaches a significance of 2.2σ (1.6σ) above the background expectation.

The VBF DNN output distribution in the final signal region is presented in Fig. 12. The observed (expected) VBF signal reaches a significance of 5.8σ (6.2σ) above the background expectation.

Figure 13 shows the best-fit values and uncertainties of the $H \rightarrow WW^*$ cross section for the ggF and VBF processes and their combination, normalized to the corresponding SM prediction. The cross sections times branching ratio for the ggF and VBF production modes for a Higgs boson with mass $m_H = 125.09$ GeV in the $H \rightarrow WW^*$ decay channel, $\sigma_{\text{ggF}} \cdot \mathcal{B}_{H \rightarrow WW^*}$ and $\sigma_{\text{VBF}} \cdot \mathcal{B}_{H \rightarrow WW^*}$, are simultaneously measured to be

$$\begin{aligned} \sigma_{\text{ggF}} \cdot \mathcal{B}_{H \rightarrow WW^*} &= 12.0 \pm 1.4 \text{ pb} \\ &= 12.0 \pm 0.6 \text{ (stat.)}_{-0.8}^{+0.9} \text{ (exp. syst.)}_{-0.5}^{+0.6} \text{ (sig. theo.)} \pm 0.8 \text{ (bkg. theo.) pb} \\ \sigma_{\text{VBF}} \cdot \mathcal{B}_{H \rightarrow WW^*} &= 0.75_{-0.16}^{+0.19} \text{ pb} \\ &= 0.75 \pm 0.11 \text{ (stat.)}_{-0.06}^{+0.07} \text{ (exp. syst.)}_{-0.08}^{+0.12} \text{ (sig. theo.)}_{-0.06}^{+0.07} \text{ (bkg. theo.) pb,} \end{aligned}$$

compared to the SM predicted values of 10.4 ± 0.5 and 0.81 ± 0.02 pb for ggF and VBF [11],⁹ respectively. The combined cross section times branching ratio, $\sigma_{\text{ggF+VBF}} \cdot \mathcal{B}_{H \rightarrow WW^*}$, obtained from fitting a single POI, is measured to be

$$\begin{aligned} \sigma_{\text{ggF+VBF}} \cdot \mathcal{B}_{H \rightarrow WW^*} &= 12.3 \pm 1.3 \text{ pb} \\ &= 12.3 \pm 0.6 \text{ (stat.)}_{-0.7}^{+0.8} \text{ (exp. syst.)} \pm 0.6 \text{ (sig. theo.)} \pm 0.7 \text{ (bkg. theo.) pb,} \end{aligned}$$

compared to the SM predicted value of 11.3 ± 0.5 pb.

Table 6 shows the relative impact of the main uncertainties on the measured values for $\sigma_{\text{ggF+VBF}} \cdot \mathcal{B}_{H \rightarrow WW^*}$, $\sigma_{\text{ggF}} \cdot \mathcal{B}_{H \rightarrow WW^*}$, and $\sigma_{\text{VBF}} \cdot \mathcal{B}_{H \rightarrow WW^*}$. The measurements are dominated by systematic uncertainties. For the ggF measurement, uncertainties from experimental and theoretical sources are comparable. For the VBF measurement, signal theory uncertainties make up the largest contribution and the dominant ones are those related to the modeling of potential jets in addition to the tagging jets.

The 68% and 95% confidence level two-dimensional contours of $\sigma_{\text{ggF}} \cdot \mathcal{B}_{H \rightarrow WW^*}$ and $\sigma_{\text{VBF}} \cdot \mathcal{B}_{H \rightarrow WW^*}$ are shown in Fig. 14 and are consistent with the SM predictions.

Figure 15 shows a summary of the $H \rightarrow WW^*$ cross sections measured in each of the 11 STXS bins, normalized to the corresponding SM prediction. The correlation matrix for the measured cross sections is shown in Fig. 16. The largest correlations between the measured cross sections are around 30% and are primarily caused by the migration of signal events between STXS bins and reconstructed signal regions. The measured cross sections for the five STXS bins targeting EW qqH production are on average lower than the VBF cross section measured in the two-POI fit. Events with high m_{jj} or high p_{T}^H carry a larger statistical weight than events at low m_{jj} in the two-POI fit, and in these STXS bins, the measured value is close to 1. Table 7 provides the central value and uncertainties of each of the measured STXS cross sections, together with the SM predictions. The results are compatible with the Standard Model predictions, with a p -value of 53%.

⁹ The uncertainties in the predicted cross sections include the uncertainty in the Higgs boson mass.

Table 6: Breakdown of the main contributions to the total uncertainty in $\sigma_{\text{ggF+VBF}} \cdot \mathcal{B}_{H \rightarrow WW^*}$, $\sigma_{\text{ggF}} \cdot \mathcal{B}_{H \rightarrow WW^*}$, and $\sigma_{\text{VBF}} \cdot \mathcal{B}_{H \rightarrow WW^*}$, relative to the measured value. The individual sources of systematic uncertainties are grouped together. The sum in quadrature of the individual components differs from the total uncertainty due to correlations between the components.

Source	$\frac{\Delta\sigma_{\text{ggF+VBF}} \cdot \mathcal{B}_{H \rightarrow WW^*}}{\sigma_{\text{ggF+VBF}} \cdot \mathcal{B}_{H \rightarrow WW^*}}$ [%]	$\frac{\Delta\sigma_{\text{ggF}} \cdot \mathcal{B}_{H \rightarrow WW^*}}{\sigma_{\text{ggF}} \cdot \mathcal{B}_{H \rightarrow WW^*}}$ [%]	$\frac{\Delta\sigma_{\text{VBF}} \cdot \mathcal{B}_{H \rightarrow WW^*}}{\sigma_{\text{VBF}} \cdot \mathcal{B}_{H \rightarrow WW^*}}$ [%]
Data statistical uncertainties	4.6	5.1	15
Total systematic uncertainties	9.5	11	18
MC statistical uncertainties	3.0	3.8	4.9
Experimental uncertainties	5.2	6.3	6.7
Flavor tagging	2.3	2.7	1.0
Jet energy scale	0.9	1.1	3.7
Jet energy resolution	2.0	2.4	2.1
$E_{\text{T}}^{\text{miss}}$	0.7	2.2	4.9
Muons	1.8	2.1	0.8
Electrons	1.3	1.6	0.4
Mis-Id extrapolation factors	2.1	2.4	0.8
Pileup	2.4	2.5	1.3
Luminosity	2.1	2.0	2.2
Theoretical uncertainties	6.8	7.8	16
ggF	3.8	4.3	4.6
VBF	3.2	0.7	12
WW	3.5	4.2	5.5
Top	2.9	3.8	6.4
Z $\tau\tau$	1.8	2.3	1.0
Other VV	2.3	2.9	1.5
Other Higgs	0.9	0.4	0.4
Background normalizations	3.6	4.5	4.9
WW	2.2	2.8	0.6
Top	1.9	2.3	3.4
Z $\tau\tau$	2.7	3.1	3.4
Total	10	12	23

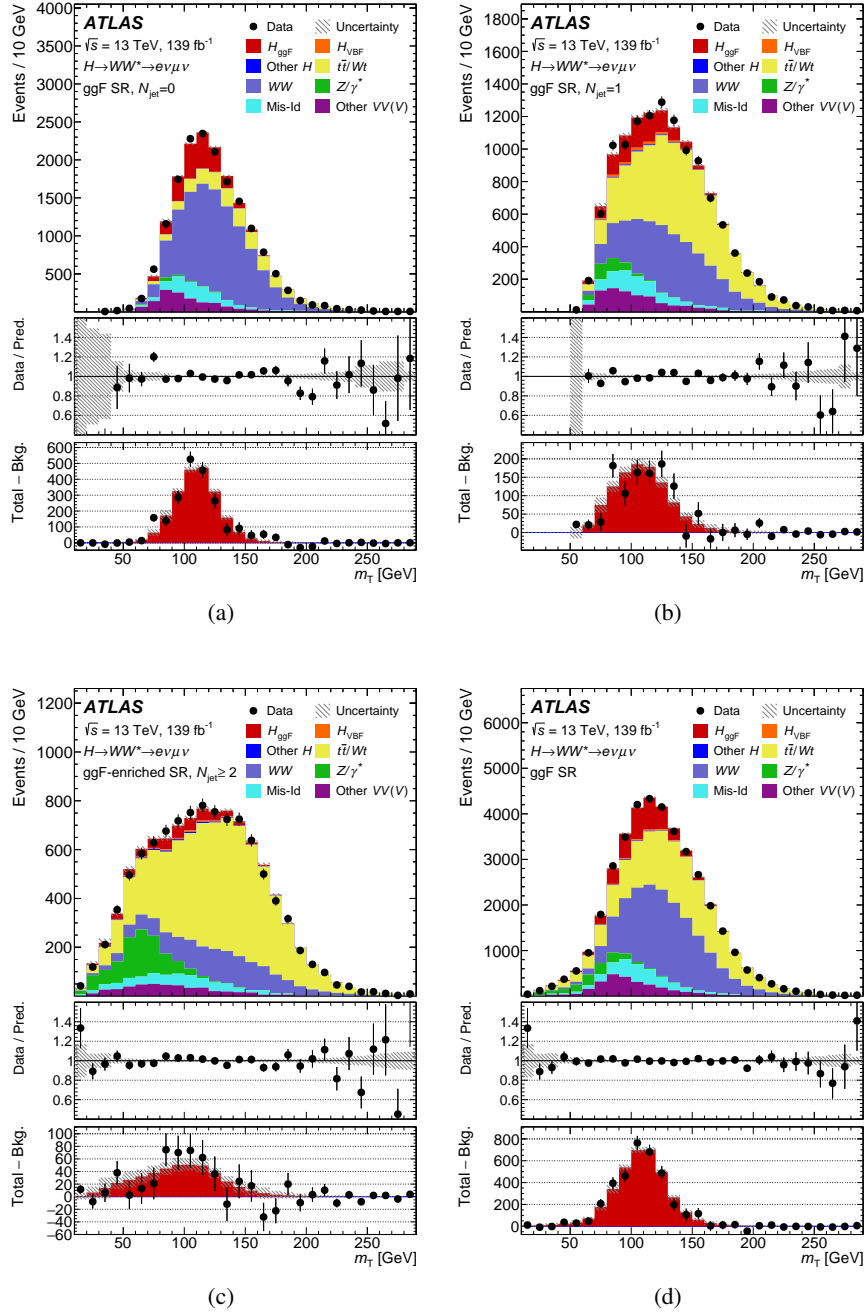


Figure 11: Postfit m_T distributions with the signal and the background modeled contributions in the (a) $N_{\text{jet}} = 0$, (b) $N_{\text{jet}} = 1$, (c) ggF-enriched $N_{\text{jet}} \geq 2$, and (d) combined ggF signal regions. Underflow and overflow events are not included. The hatched band shows the total uncertainty, assuming SM Higgs boson production. The middle panel shows the ratio of the data to the sum of the fitted signal and background. The bottom panel displays the difference between the data and the estimated background compared to the simulated signal distribution, where the hatched band indicates the combined statistical and systematic uncertainty for the fitted signal and background.

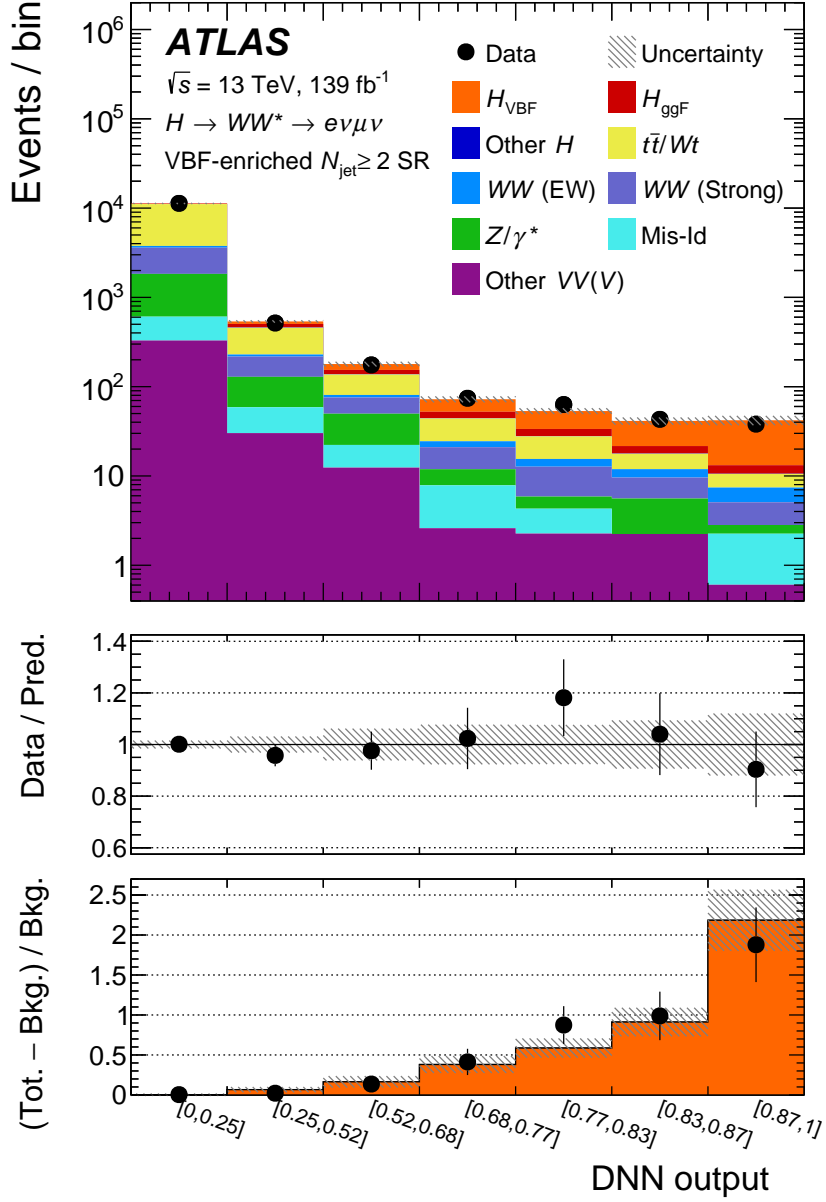


Figure 12: Postfit distribution of the DNN output in the VBF signal region. The hatched band shows the total uncertainty, assuming SM Higgs boson production. The middle panel shows the ratio of the data to the sum of the fitted signal and background. The bottom panel displays the signal-to-background ratio, where the hatched band indicates the combined statistical and systematic uncertainty for the fitted signal and background.

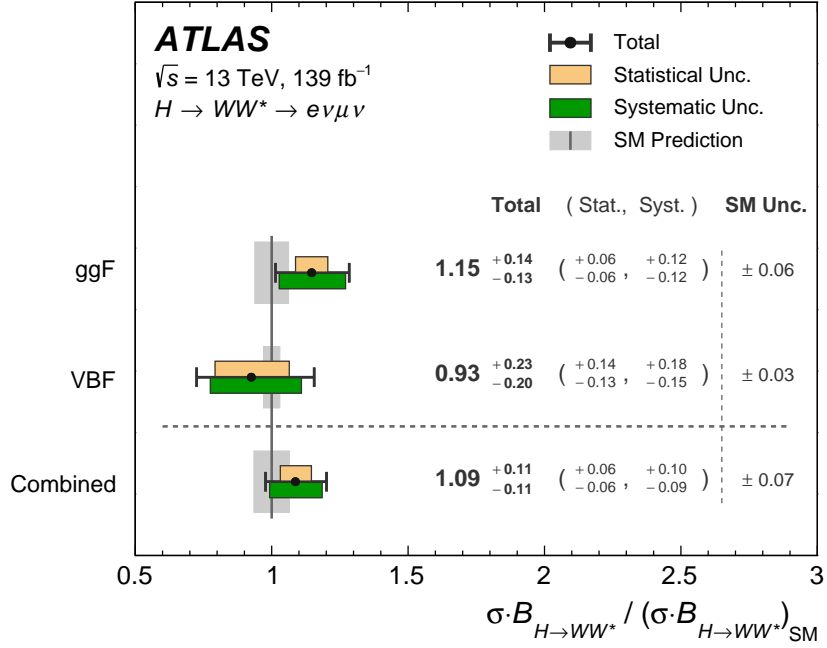


Figure 13: Best-fit values and uncertainties of the $H \rightarrow WW^*$ cross section for the ggF and VBF processes and their combination, normalized to the corresponding SM prediction. The black error bars, green boxes, and tan boxes show the total, systematic, and statistical uncertainties in the measurements, respectively. The gray bands represent the theory uncertainty of the corresponding Higgs production mode.

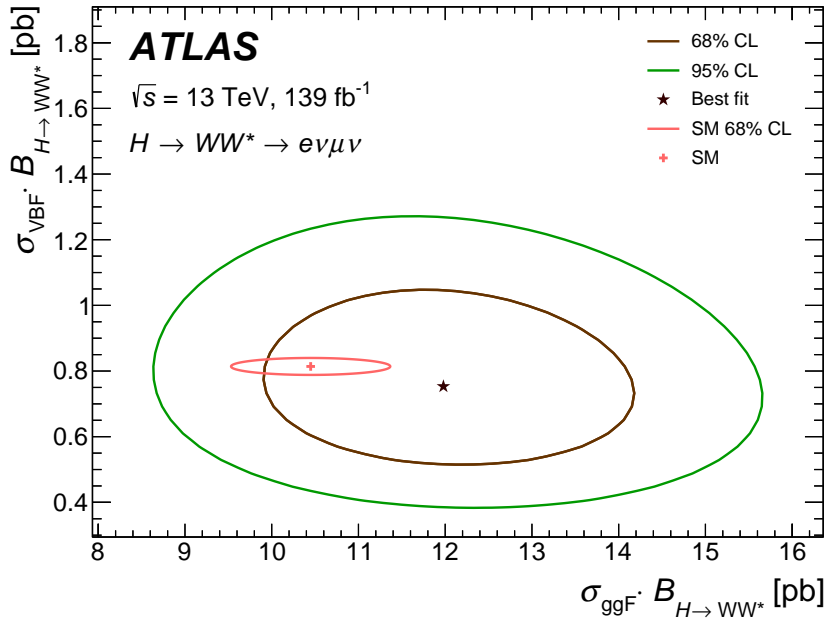


Figure 14: 68% and 95% confidence level (C.L.) two-dimensional contours of $\sigma_{\text{ggF}} \cdot \mathcal{B}_{H \rightarrow WW^*}$ vs $\sigma_{\text{VBF}} \cdot \mathcal{B}_{H \rightarrow WW^*}$, compared to the SM prediction shown by the red marker. The 68% C.L. contour for the SM predictions of the ggF and VBF cross sections times branching ratio [11] is indicated by the red ellipse.

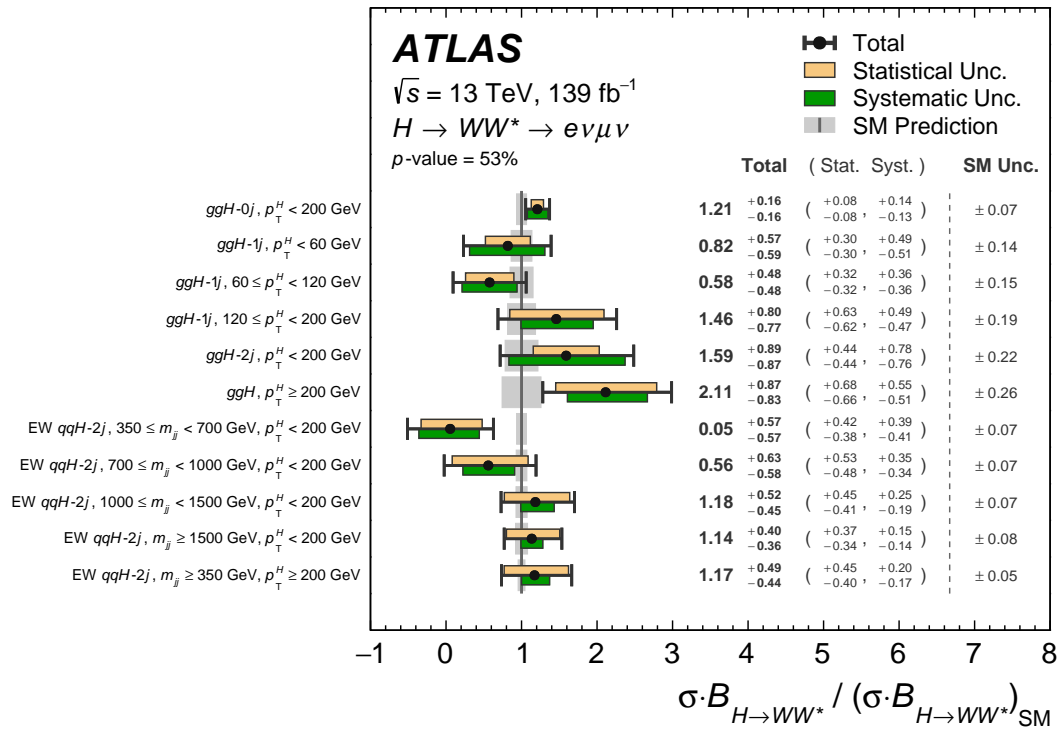


Figure 15: Best-fit value and uncertainties for the $H \rightarrow WW^*$ cross section measured in each of the STXS bins, normalized to the corresponding SM prediction. The black error bars, green boxes, and tan boxes show the total, systematic, and statistical uncertainties in the measurements, respectively. The gray bands represent the theory uncertainty of the signal yield in the corresponding STXS bin.

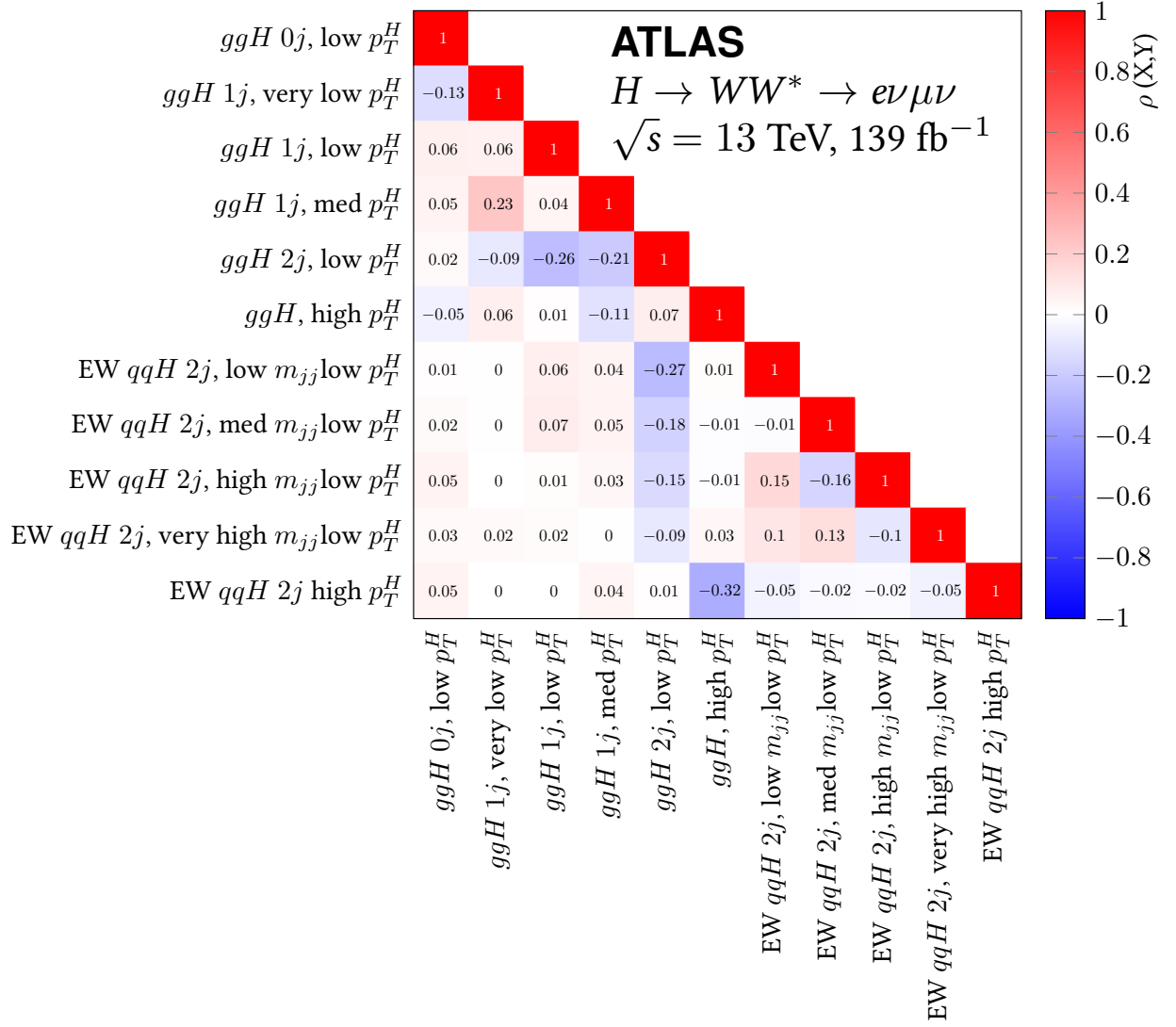


Figure 16: Correlations between the cross-section measurements in the 11 STXS bins for the $H \rightarrow WW^* \rightarrow e\nu\mu\nu$ analysis.

Table 7: Best-fit values and uncertainties for the production cross section times $H \rightarrow WW^*$ branching ratio ($\sigma_i \cdot \mathcal{B}_{H \rightarrow WW^*}$) in each STXS bin.

STXS bin ($\sigma_i \cdot \mathcal{B}_{H \rightarrow WW^*}$)	Value		Uncertainty [fb]				SM prediction [fb]
	[fb]	Total	Stat.	Exp. Syst.	Sig. Theo.	Bkg. Theo.	
$ggH-0j$, low p_T^H $p_T^H < 200$ GeV	7100	+950 -910	+480 -470	+570 -530	+320 -260	+490 -480	5870 ± 390
$ggH-1j$, very low p_T^H $p_T^H < 60$ GeV	1140	+800 -820	+420 -410	+380 -380	+80 -70	+570 -600	1400 ± 190
$ggH-1j$, low p_T^H $60 \leq p_T^H < 120$ GeV	540	+470 -470	+310 -310	+230 -230	+42 -47	+270 -280	970 ± 150
$ggH-1j$, med p_T^H $120 \leq p_T^H < 200$ GeV	230	+130 -120	+100 -100	+60 -60	+10 -10	+50 -50	160 ± 30
$ggH-2j$, low p_T^H $p_T^H < 200$ GeV	1610	+900 -890	+440 -440	+430 -420	+300 -150	+640 -650	1010 ± 220
ggH , high p_T^H $p_T^H \geq 200$ GeV	260	+100 -100	+80 -80	+40 -40	+40 -20	+40 -40	122 ± 31
EW $qqH-2j$, low m_{jj} -low p_T^H $350 \leq m_{jj} < 700$ GeV, $p_T^H < 200$ GeV	6	+63 -62	+46 -42	+31 -34	+11 -14	+24 -26	109 ± 7
EW $qqH-2j$, med m_{jj} -low p_T^H $700 \leq m_{jj} < 1000$ GeV, $p_T^H < 200$ GeV	31	+35 -33	+30 -27	+15 -14	+8 -7	+11 -10	56 ± 4
EW $qqH-2j$, high m_{jj} -low p_T^H $1000 \leq m_{jj} < 1500$ GeV, $p_T^H < 200$ GeV	60	+26 -23	+23 -21	+7 -7	+9 -5	+5 -5	51 ± 4
EW $qqH-2j$, very high m_{jj} -low p_T^H $m_{jj} \geq 1500$ GeV, $p_T^H < 200$ GeV	57	+20 -18	+18 -17	+5 -5	+3 -3	+4 -4	50 ± 4
EW $qqH-2j$, high p_T^H $m_{jj} \geq 350$ GeV, $p_T^H \geq 200$ GeV	37	+16 -14	+14 -13	+4 -3	+4 -3	+3 -3	32 ± 1

10 Conclusions

The $H \rightarrow WW^* \rightarrow e\nu\mu\nu$ decay channel was used to measure Higgs boson production by gluon-gluon fusion and vector-boson fusion. The measurements are based on a dataset of proton-proton collisions with an integrated luminosity of 139 fb^{-1} recorded with the ATLAS detector at the LHC in 2015–2018 at a center-of-mass energy of 13 TeV. The ggF and VBF cross sections times the $H \rightarrow WW^*$ branching ratio are simultaneously measured to be 12.0 ± 0.6 (stat.) $_{-0.8}^{+0.9}$ (exp. syst.) $_{-0.5}^{+0.6}$ (sig. theo.) ± 0.8 (bkg. theo.) and 0.75 ± 0.11 (stat.) $_{-0.06}^{+0.07}$ (exp. syst.) $_{-0.08}^{+0.12}$ (sig. theo.) $_{-0.06}^{+0.07}$ (bkg. theo.) pb, in agreement with the Standard Model predictions of 10.4 ± 0.6 and 0.81 ± 0.02 pb, respectively. These measurements are significantly more precise than the previous Higgs boson cross sections times $H \rightarrow WW^*$ branching ratio results from ATLAS because of several improvements to the analysis in addition to the larger dataset, most notably the inclusion of a dedicated signal region for the ggF production mode in conjunction with two or more reconstructed jets. Higgs boson production in the $H \rightarrow WW^*$ decay channel is further characterized through STXS measurements in a total of 11 categories. The STXS results are compatible with the Standard Model predictions, with a p -value of 53%.

Acknowledgments

We thank CERN for the very successful operation of the LHC, as well as the support staff from our institutions without whom ATLAS could not be operated efficiently.

We acknowledge the support of ANPCyT, Argentina; YerPhI, Armenia; ARC, Australia; BMWFW and FWF, Austria; ANAS, Azerbaijan; CNPq and FAPESP, Brazil; NSERC, NRC and CFI, Canada; CERN; ANID, Chile; CAS, MOST and NSFC, China; Minciencias, Colombia; MEYS CR, Czech Republic; DNRF and DNSRC, Denmark; IN2P3-CNRS and CEA-DRF/IRFU, France; SRNSFG, Georgia; BMBF, HGF and MPG, Germany; GSRI, Greece; RGC and Hong Kong SAR, China; ISF and Benoziyo Center, Israel; INFN, Italy; MEXT and JSPS, Japan; CNRST, Morocco; NWO, Netherlands; RCN, Norway; MEiN, Poland; FCT, Portugal; MNE/IFA, Romania; MESTD, Serbia; MSSR, Slovakia; ARRS and MIZŠ, Slovenia; DSI/NRF, South Africa; MICINN, Spain; SRC and Wallenberg Foundation, Sweden; SERI, SNSF and Cantons of Bern and Geneva, Switzerland; MOST, Taiwan; TENMAK, Türkiye; STFC, United Kingdom; DOE and NSF, United States of America. In addition, individual groups and members have received support from BCKDF, CANARIE, Compute Canada and CRC, Canada; PRIMUS 21/SCI/017 and UNCE SCI/013, Czech Republic; COST, ERC, ERDF, Horizon 2020 and Marie Skłodowska-Curie Actions, European Union; Investissements d’Avenir Labex, Investissements d’Avenir Idex and ANR, France; DFG and AvH Foundation, Germany; Herakleitos, Thales and Aristeia programmes co-financed by EU-ESF and the Greek NSRF, Greece; BSF-NSF and MINERVA, Israel; Norwegian Financial Mechanism 2014–2021, Norway; NCN and NAWA, Poland; La Caixa Banking Foundation, CERCA Programme Generalitat de Catalunya and PROMETEO and GenT Programmes Generalitat Valenciana, Spain; Göran Gustafssons Stiftelse, Sweden; The Royal Society and Leverhulme Trust, United Kingdom.

The crucial computing support from all WLCG partners is acknowledged gratefully, in particular from CERN, the ATLAS Tier-1 facilities at TRIUMF (Canada), NDGF (Denmark, Norway, Sweden), CC-IN2P3 (France), KIT/GridKA (Germany), INFN-CNAF (Italy), NL-T1 (Netherlands), PIC (Spain), ASGC (Taiwan), RAL (UK) and BNL (USA), the Tier-2 facilities worldwide and large non-WLCG resource providers. Major contributors of computing resources are listed in Ref. [132].

References

- [1] F. Englert and R. Brout, *Broken Symmetry and the Mass of Gauge Vector Mesons*, [Phys. Rev. Lett. **13** \(1964\) 321](#).
- [2] P. W. Higgs, *Broken symmetries, massless particles and gauge fields*, [Phys. Lett. **12** \(1964\) 132](#).
- [3] P. W. Higgs, *Broken Symmetries and the Masses of Gauge Bosons*, [Phys. Rev. Lett. **13** \(1964\) 508](#).
- [4] G. S. Guralnik, C. R. Hagen, and T. W. B. Kibble, *Global Conservation Laws and Massless Particles*, [Phys. Rev. Lett. **13** \(1964\) 585](#).
- [5] ATLAS Collaboration, *Observation of a new particle in the search for the Standard Model Higgs boson with the ATLAS detector at the LHC*, [Phys. Lett. B **716** \(2012\) 1](#), arXiv: [1207.7214 \[hep-ex\]](#).
- [6] CMS Collaboration, *Observation of a new boson at a mass of 125 GeV with the CMS experiment at the LHC*, [Phys. Lett. B **716** \(2012\) 30](#), arXiv: [1207.7235 \[hep-ex\]](#).
- [7] L. Evans and P. Bryant, *LHC Machine*, [JINST **3** \(2008\) S08001](#).
- [8] ATLAS Collaboration, *The ATLAS Experiment at the CERN Large Hadron Collider*, [JINST **3** \(2008\) S08003](#).
- [9] CMS Collaboration, *Measurement of the inclusive and differential Higgs boson production cross sections in the leptonic WW decay mode at $\sqrt{s} = 13$ TeV*, [JHEP **03** \(2021\) 003](#), arXiv: [2007.01984 \[hep-ex\]](#).
- [10] ATLAS Collaboration, *Measurements of gluon-gluon fusion and vector-boson fusion Higgs boson production cross-sections in the $H \rightarrow WW^* \rightarrow e\nu\mu\nu$ decay channel in pp collisions at $\sqrt{s} = 13$ TeV with the ATLAS detector*, [Phys. Lett. B **789** \(2019\) 508](#), arXiv: [1808.09054 \[hep-ex\]](#).
- [11] D. de Florian et al., *Handbook of LHC Higgs Cross Sections: 4. Deciphering the Nature of the Higgs Sector*, [2/2017 \(2016\)](#), arXiv: [1610.07922 \[hep-ph\]](#).
- [12] J. R. Andersen et al., “Les Houches 2015: Physics at TeV Colliders Standard Model Working Group Report,” *9th Les Houches Workshop on Physics at TeV Colliders*, 2016, arXiv: [1605.04692 \[hep-ph\]](#).
- [13] M. Dittmar and H. Dreiner, *How to find a Higgs boson with a mass between 155 and 180 GeV at the LHC*, [Phys. Rev. D **55** \(1997\) 167](#), arXiv: [hep-ph/9608317](#).
- [14] N. Berger et al., *Simplified Template Cross Sections - Stage 1.1*, (2019), arXiv: [1906.02754 \[hep-ph\]](#).
- [15] ATLAS Collaboration, *ATLAS Insertable B-Layer Technical Design Report*, ATLAS-TDR-19; CERN-LHCC-2010-013, 2010, URL: <https://cds.cern.ch/record/1291633>, Addendum: ATLAS-TDR-19-ADD-1; CERN-LHCC-2012-009, 2012, URL: <https://cds.cern.ch/record/1451888>.
- [16] B. Abbott et al., *Production and integration of the ATLAS Insertable B-Layer*, [JINST **13** \(2018\) T05008](#), arXiv: [1803.00844 \[physics.ins-det\]](#).

- [17] ATLAS Collaboration, *Performance of the ATLAS trigger system in 2015*, *Eur. Phys. J. C* **77** (2017) 317, arXiv: 1611.09661 [hep-ex].
- [18] ATLAS Collaboration, *Performance of electron and photon triggers in ATLAS during LHC Run 2*, *Eur. Phys. J. C* **80** (2020) 47, arXiv: 1909.00761 [hep-ex].
- [19] ATLAS Collaboration, *Performance of the ATLAS muon triggers in Run 2*, *JINST* **15** (2020) P09015, arXiv: 2004.13447 [physics.ins-det].
- [20] ATLAS Collaboration, *ATLAS data quality operations and performance for 2015–2018 data-taking*, *JINST* **15** (2020) P04003, arXiv: 1911.04632 [physics.ins-det].
- [21] ATLAS Collaboration, *Luminosity determination in pp collisions at $\sqrt{s} = 13$ TeV using the ATLAS detector at the LHC*, ATLAS-CONF-2019-021, 2019, URL: <https://cds.cern.ch/record/2677054>.
- [22] ATLAS Collaboration, *The ATLAS Collaboration Software and Firmware*, tech. rep., CERN, 2021, URL: <https://cds.cern.ch/record/2767187>.
- [23] P. Nason, *A new method for combining NLO QCD with shower Monte Carlo algorithms*, *JHEP* **11** (2004) 040, arXiv: hep-ph/0409146.
- [24] S. Frixione, P. Nason, and C. Oleari, *Matching NLO QCD computations with parton shower simulations: the POWHEG method*, *JHEP* **11** (2007) 070, arXiv: 0709.2092 [hep-ph].
- [25] S. Alioli, P. Nason, C. Oleari, and E. Re, *A general framework for implementing NLO calculations in shower Monte Carlo programs: the POWHEG BOX*, *JHEP* **06** (2010) 043, arXiv: 1002.2581 [hep-ph].
- [26] K. Hamilton, P. Nason, E. Re, and G. Zanderighi, *NNLOPS simulation of Higgs boson production*, *JHEP* **10** (2013) 222, arXiv: 1309.0017 [hep-ph].
- [27] K. Hamilton, P. Nason, and G. Zanderighi, *Finite quark-mass effects in the NNLOPS POWHEG+MiNLO Higgs generator*, *JHEP* **05** (2015) 140, arXiv: 1501.04637 [hep-ph].
- [28] T. Sjöstrand et al., *An introduction to PYTHIA 8.2*, *Comput. Phys. Commun.* **191** (2015) 159, arXiv: 1410.3012 [hep-ph].
- [29] K. Hamilton, P. Nason, and G. Zanderighi, *MINLO: multi-scale improved NLO*, *JHEP* **10** (2012) 155, arXiv: 1206.3572 [hep-ph].
- [30] J. M. Campbell et al., *NLO Higgs boson production plus one and two jets using the POWHEG BOX, MadGraph4 and MCFM*, *JHEP* **07** (2012) 092, arXiv: 1202.5475 [hep-ph].
- [31] K. Hamilton, P. Nason, C. Oleari, and G. Zanderighi, *Merging H/W/Z + 0 and 1 jet at NLO with no merging scale: a path to parton shower + NNLO matching*, *JHEP* **05** (2013) 082, arXiv: 1212.4504 [hep-ph].
- [32] S. Catani and M. Grazzini, *Next-to-Next-to-Leading-Order Subtraction Formalism in Hadron Collisions and its Application to Higgs-Boson Production at the Large Hadron Collider*, *Phys. Rev. Lett.* **98** (2007) 222002, arXiv: hep-ph/0703012.
- [33] C. Anastasiou et al., *High precision determination of the gluon fusion Higgs boson cross-section at the LHC*, *JHEP* **05** (2016) 058, arXiv: 1602.00695 [hep-ph].

- [34] C. Anastasiou, C. Duhr, F. Dulat, F. Herzog, and B. Mistlberger, *Higgs Boson Gluon-Fusion Production in QCD at Three Loops*, [Phys. Rev. Lett. **114** \(2015\) 212001](#), arXiv: [1503.06056 \[hep-ph\]](#).
- [35] F. Dulat, A. Lazopoulos, and B. Mistlberger, *iHixs 2 — Inclusive Higgs cross sections*, [Comput. Phys. Commun. **233** \(2018\) 243](#), arXiv: [1802.00827 \[hep-ph\]](#).
- [36] R. V. Harlander and K. J. Ozeren, *Finite top mass effects for hadronic Higgs production at next-to-next-to-leading order*, [JHEP **11** \(2009\) 088](#), arXiv: [0909.3420 \[hep-ph\]](#).
- [37] R. V. Harlander and K. J. Ozeren, *Top mass effects in Higgs production at next-to-next-to-leading order QCD: Virtual corrections*, [Phys. Lett. B **679** \(2009\) 467](#), arXiv: [0907.2997 \[hep-ph\]](#).
- [38] R. V. Harlander, H. Mantler, S. Marzani, and K. J. Ozeren, *Higgs production in gluon fusion at next-to-next-to-leading order QCD for finite top mass*, [Eur. Phys. J. C **66** \(2010\) 359](#), arXiv: [0912.2104 \[hep-ph\]](#).
- [39] A. Pak, M. Rogal, and M. Steinhauser, *Finite top quark mass effects in NNLO Higgs boson production at LHC*, [JHEP **02** \(2010\) 025](#), arXiv: [0911.4662 \[hep-ph\]](#).
- [40] S. Actis, G. Passarino, C. Sturm, and S. Uccirati, *NLO electroweak corrections to Higgs boson production at hadron colliders*, [Phys. Lett. B **670** \(2008\) 12](#), arXiv: [0809.1301 \[hep-ph\]](#).
- [41] S. Actis, G. Passarino, C. Sturm, and S. Uccirati, *NNLO computational techniques: The cases $H \rightarrow \gamma\gamma$ and $H \rightarrow gg$* , [Nucl. Phys. B **811** \(2009\) 182](#), arXiv: [0809.3667 \[hep-ph\]](#).
- [42] M. Bonetti, K. Melnikov, and L. Tancredi, *Higher order corrections to mixed QCD-EW contributions to Higgs boson production in gluon fusion*, [Phys. Rev. D **97** \(2018\) 056017](#), [Erratum: [Phys. Rev. D **97**, \(2018\) 099906](#)], arXiv: [1801.10403 \[hep-ph\]](#).
- [43] P. Nason and C. Oleari, *NLO Higgs boson production via vector-boson fusion matched with shower in POWHEG*, [JHEP **02** \(2010\) 037](#), arXiv: [0911.5299 \[hep-ph\]](#).
- [44] M. Ciccolini, A. Denner, and S. Dittmaier, *Strong and Electroweak Corrections to the Production of a Higgs Boson + 2 Jets via Weak Interactions at the Large Hadron Collider*, [Phys. Rev. Lett. **99** \(2007\) 161803](#), arXiv: [0707.0381 \[hep-ph\]](#).
- [45] M. Ciccolini, A. Denner, and S. Dittmaier, *Electroweak and QCD corrections to Higgs production via vector-boson fusion at the LHC*, [Phys. Rev. D **77** \(2008\) 013002](#), arXiv: [0710.4749 \[hep-ph\]](#).
- [46] P. Bolzoni, F. Maltoni, S.-O. Moch, and M. Zaro, *Higgs Boson Production via Vector-Boson Fusion at Next-to-Next-to-Leading Order in QCD*, [Phys. Rev. Lett. **105** \(2010\) 011801](#), arXiv: [1003.4451 \[hep-ph\]](#).
- [47] M. Bähr et al., *Herwig++ physics and manual*, [Eur. Phys. J. C **58** \(2008\) 639](#), arXiv: [0803.0883 \[hep-ph\]](#).
- [48] J. Bellm et al., *Herwig 7.0/Herwig++ 3.0 release note*, [Eur. Phys. J. C **76** \(2016\) 196](#), arXiv: [1512.01178 \[hep-ph\]](#).

- [49] J. Alwall et al., *The automated computation of tree-level and next-to-leading order differential cross sections, and their matching to parton shower simulations*, *JHEP* **07** (2014) 079, arXiv: [1405.0301 \[hep-ph\]](#).
- [50] R. D. Ball et al., *Parton distributions for the LHC run II*, *JHEP* **04** (2015) 040, arXiv: [1410.8849 \[hep-ph\]](#).
- [51] L. A. Harland-Lang, A. D. Martin, P. Motylinski, and R. S. Thorne, *Parton distributions in the LHC era: MMHT 2014 PDFs*, *Eur. Phys. J. C* **75** (2015) 204, arXiv: [1412.3989 \[hep-ph\]](#).
- [52] M. L. Ciccolini, S. Dittmaier, and M. Krämer, *Electroweak radiative corrections to associated WH and ZH production at hadron colliders*, *Phys. Rev. D* **68** (2003) 073003, arXiv: [hep-ph/0306234](#).
- [53] O. Brein, A. Djouadi, and R. Harlander, *NNLO QCD corrections to the Higgs-strahlung processes at hadron colliders*, *Phys. Lett. B* **579** (2004) 149, arXiv: [hep-ph/0307206](#).
- [54] O. Brein, R. V. Harlander, M. Wiesemann, and T. Zirke, *Top-quark mediated effects in hadronic Higgs-Strahlung*, *Eur. Phys. J. C* **72** (2012) 1868, arXiv: [1111.0761 \[hep-ph\]](#).
- [55] A. Denner, S. Dittmaier, S. Kallweit, and A. Mück, *HAWK 2.0: A Monte Carlo program for Higgs production in vector-boson fusion and Higgs strahlung at hadron colliders*, *Comput. Phys. Commun.* **195** (2015) 161, arXiv: [1412.5390 \[hep-ph\]](#).
- [56] O. Brein, R. V. Harlander, and T. J. Zirke, *vh@nnlo - Higgs Strahlung at hadron colliders*, *Comput. Phys. Commun.* **184** (2013) 998, arXiv: [1210.5347 \[hep-ph\]](#).
- [57] J. Butterworth et al., *PDF4LHC recommendations for LHC Run II*, *J. Phys. G* **43** (2016) 023001, arXiv: [1510.03865 \[hep-ph\]](#).
- [58] ATLAS Collaboration, *Measurement of the Z/ γ^* boson transverse momentum distribution in pp collisions at $\sqrt{s} = 7$ TeV with the ATLAS detector*, *JHEP* **09** (2014) 145, arXiv: [1406.3660 \[hep-ex\]](#).
- [59] A. Djouadi, J. Kalinowski, and M. Spira, *HDECAY: a program for Higgs boson decays in the Standard Model and its supersymmetric extension*, *Comput. Phys. Commun.* **108** (1998) 56, arXiv: [hep-ph/9704448](#).
- [60] M. Spira, *QCD Effects in Higgs Physics*, *Fortsch. Phys.* **46** (1998) 203, arXiv: [hep-ph/9705337](#).
- [61] A. Djouadi, M. M. Muhlleitner, and M. Spira, *Decays of Supersymmetric Particles: the program SUSY-HIT (SUSpect-SdecaY-Hdecay-InTerface)*, *Acta Phys. Polon. B* **38** (2007) 635, arXiv: [hep-ph/0609292](#).
- [62] A. Bredenstein, A. Denner, S. Dittmaier, and M. M. Weber, *Radiative corrections to the semileptonic and hadronic Higgs-boson decays $H \rightarrow WW/ZZ \rightarrow 4$ fermions*, *JHEP* **02** (2007) 080, arXiv: [hep-ph/0611234](#).
- [63] A. Bredenstein, A. Denner, S. Dittmaier, and M. M. Weber, *Precise predictions for the Higgs-boson decay $H \rightarrow WW/ZZ \rightarrow 4$ leptons*, *Phys. Rev. D* **74** (2006) 013004, arXiv: [hep-ph/0604011](#).
- [64] A. Bredenstein, A. Denner, S. Dittmaier, and M. M. Weber, *Precision calculations for the Higgs decays $H \rightarrow ZZ/WW \rightarrow 4$ leptons*, *Nucl. Phys. B Proc. Suppl.* **160** (2006) 131, arXiv: [hep-ph/0607060](#).

- [65] ATLAS and CMS Collaborations, *Combined Measurement of the Higgs Boson Mass in pp Collisions at $\sqrt{s} = 7$ and 8 TeV with the ATLAS and CMS Experiments*, [Phys. Rev. Lett. **114** \(2015\) 191803](#), arXiv: [1503.07589 \[hep-ex\]](#).
- [66] S. Frixione, G. Ridolfi, and P. Nason, *A positive-weight next-to-leading-order Monte Carlo for heavy flavour hadroproduction*, [JHEP **09** \(2007\) 126](#), arXiv: [0707.3088 \[hep-ph\]](#).
- [67] H. B. Hartanto, B. Jäger, L. Reina, and D. Wackerroth, *Higgs boson production in association with top quarks in the POWHEG BOX*, [Phys. Rev. D **91** \(2015\) 094003](#), arXiv: [1501.04498 \[hep-ph\]](#).
- [68] ATLAS Collaboration, *ATLAS Pythia 8 tunes to 7 TeV data*, ATL-PHYS-PUB-2014-021, 2014, URL: <https://cds.cern.ch/record/1966419>.
- [69] E. Bothmann et al., *Event Generation with Sherpa 2.2*, [SciPost Phys. **7** \(2019\) 034](#), arXiv: [1905.09127 \[hep-ph\]](#).
- [70] S. Höche, F. Krauss, S. Schumann, and F. Siegert, *QCD matrix elements and truncated showers*, [JHEP **05** \(2009\) 053](#), arXiv: [0903.1219 \[hep-ph\]](#).
- [71] S. Schumann and F. Krauss, *A parton shower algorithm based on Catani–Seymour dipole factorisation*, [JHEP **03** \(2008\) 038](#), arXiv: [0709.1027 \[hep-ph\]](#).
- [72] S. Höche, S. Schumann, and F. Siegert, *Hard photon production and matrix-element parton-shower merging*, [Phys. Rev. D **81** \(2010\) 034026](#), arXiv: [0912.3501 \[hep-ph\]](#).
- [73] T. Gleisberg and S. Höche, *Comix, a new matrix element generator*, [JHEP **12** \(2008\) 039](#), arXiv: [0808.3674 \[hep-ph\]](#).
- [74] S. Höche, F. Krauss, M. Schönherr, and F. Siegert, *A critical appraisal of NLO+PS matching methods*, [JHEP **09** \(2012\) 049](#), arXiv: [1111.1220 \[hep-ph\]](#).
- [75] S. Höche, F. Krauss, M. Schönherr, and F. Siegert, *QCD matrix elements + parton showers. The NLO case*, [JHEP **04** \(2013\) 027](#), arXiv: [1207.5030 \[hep-ph\]](#).
- [76] S. Catani, F. Krauss, B. R. Webber, and R. Kuhn, *QCD Matrix Elements + Parton Showers*, [JHEP **11** \(2001\) 063](#), arXiv: [hep-ph/0109231](#).
- [77] F. Cascioli, P. Maierhöfer, and S. Pozzorini, *Scattering Amplitudes with Open Loops*, [Phys. Rev. Lett. **108** \(2012\) 111601](#), arXiv: [1111.5206 \[hep-ph\]](#).
- [78] A. Denner, S. Dittmaier, and L. Hofer, *COLLIER: A fortran-based complex one-loop library in extended regularizations*, [Comput. Phys. Commun. **212** \(2017\) 220](#), arXiv: [1604.06792 \[hep-ph\]](#).
- [79] C. Anastasiou, L. Dixon, K. Melnikov, and F. Petriello, *High-precision QCD at hadron colliders: Electroweak gauge boson rapidity distributions at next-to-next-to leading order*, [Phys. Rev. D **69** \(2004\) 094008](#), arXiv: [hep-ph/0312266](#).
- [80] R. D. Ball et al., *Parton distributions with LHC data*, [Nucl. Phys. B **867** \(2013\) 244](#), arXiv: [1207.1303 \[hep-ph\]](#).

- [81] T. Sjöstrand, S. Mrenna, and P. Skands, *A brief introduction to PYTHIA 8.1*, *Comput. Phys. Commun.* **178** (2008) 852, arXiv: [0710.3820 \[hep-ph\]](#).
- [82] ATLAS Collaboration, *Studies on top-quark Monte Carlo modelling for Top2016*, ATL-PHYS-PUB-2016-020, 2016, URL: <https://cds.cern.ch/record/2216168>.
- [83] M. Czakon et al., *Top-pair production at the LHC through NNLO QCD and NLO EW*, *JHEP* **10** (2017) 186.
- [84] S. Frixione, E. Laenen, P. Motylinski, C. White, and B. R. Webber, *Single-top hadroproduction in association with a W boson*, *JHEP* **07** (2008) 029, arXiv: [0805.3067 \[hep-ph\]](#).
- [85] D. J. Lange, *The EvtGen particle decay simulation package*, *Nucl. Instrum. Meth. A* **462** (2001) 152.
- [86] R. Frederix and S. Frixione, *Merging meets matching in MC@NLO*, *JHEP* **12** (2012) 061, arXiv: [1209.6215 \[hep-ph\]](#).
- [87] ATLAS Collaboration, *The ATLAS Simulation Infrastructure*, *Eur. Phys. J. C* **70** (2010) 823, arXiv: [1005.4568 \[physics.ins-det\]](#).
- [88] GEANT4 Collaboration, S. Agostinelli, et al., *GEANT4 – a simulation toolkit*, *Nucl. Instrum. Meth. A* **506** (2003) 250.
- [89] ATLAS Collaboration, *The Pythia 8 A3 tune description of ATLAS minimum bias and inelastic measurements incorporating the Donnachie–Landshoff diffractive model*, ATL-PHYS-PUB-2016-017, 2016, URL: <https://cds.cern.ch/record/2206965>.
- [90] L. Altenkamp, S. Dittmaier, R. V. Harlander, H. Rzehak, and T. J. E. Zirke, *Gluon-induced Higgs-strahlung at next-to-leading order QCD*, *JHEP* **02** (2013) 078, arXiv: [1211.5015 \[hep-ph\]](#).
- [91] R. V. Harlander, A. Kulesza, V. Theeuwes, and T. Zirke, *Soft gluon resummation for gluon-induced Higgs Strahlung*, *JHEP* **11** (2014) 082, arXiv: [1410.0217 \[hep-ph\]](#).
- [92] F. Buccioni et al., *OpenLoops 2*, *Eur. Phys. J. C* **79** (2019) 866, arXiv: [1907.13071 \[hep-ph\]](#).
- [93] F. Caola, K. Melnikov, R. Rötsch, and L. Tancredi, *QCD corrections to W^+W^- production through gluon fusion*, *Phys. Lett. B* **754** (2016) 275, arXiv: [1511.08617 \[hep-ph\]](#).
- [94] F. Cascioli et al., *Precise Higgs-background predictions: merging NLO QCD and squared quark-loop corrections to four-lepton + 0,1 jet production*, *JHEP* **01** (2014) 046, arXiv: [1309.0500 \[hep-ph\]](#).
- [95] M. Beneke, P. Falgari, S. Klein, and C. Schwinn, *Hadronic top-quark pair production with NNLL threshold resummation*, *Nucl. Phys. B* **855** (2012) 695, arXiv: [1109.1536 \[hep-ph\]](#).
- [96] M. Cacciari, M. Czakon, M. Mangano, A. Mitov, and P. Nason, *Top-pair production at hadron colliders with next-to-next-to-leading logarithmic soft-gluon resummation*, *Phys. Lett. B* **710** (2012) 612, arXiv: [1111.5869 \[hep-ph\]](#).
- [97] P. Bärnreuther, M. Czakon, and A. Mitov, *Percent-Level-Precision Physics at the Tevatron: Next-to-Next-to-Leading Order QCD Corrections to $q\bar{q} \rightarrow t\bar{t} + X$* , *Phys. Rev. Lett.* **109** (2012) 132001, arXiv: [1204.5201 \[hep-ph\]](#).

- [98] M. Czakon and A. Mitov, *NNLO corrections to top-pair production at hadron colliders: the all-fermionic scattering channels*, *JHEP* **12** (2012) 054, arXiv: [1207.0236 \[hep-ph\]](#).
- [99] M. Czakon and A. Mitov, *NNLO corrections to top pair production at hadron colliders: the quark-gluon reaction*, *JHEP* **01** (2013) 080, arXiv: [1210.6832 \[hep-ph\]](#).
- [100] M. Czakon, P. Fiedler, and A. Mitov, *Total Top-Quark Pair-Production Cross Section at Hadron Colliders Through $O(\alpha_S^4)$* , *Phys. Rev. Lett.* **110** (2013) 252004, arXiv: [1303.6254 \[hep-ph\]](#).
- [101] M. Czakon and A. Mitov, *Top++: A program for the calculation of the top-pair cross-section at hadron colliders*, *Comput. Phys. Commun.* **185** (2014) 2930, arXiv: [1112.5675 \[hep-ph\]](#).
- [102] N. Kidonakis, *Two-loop soft anomalous dimensions for single top quark associated production with a W^- or H^-* , *Phys. Rev. D* **82** (2010) 054018, arXiv: [1005.4451 \[hep-ph\]](#).
- [103] N. Kidonakis, *Top Quark Production*, Helmholtz International Summer School on Physics of Heavy Quarks and Hadrons, 2014, arXiv: [1311.0283 \[hep-ph\]](#).
- [104] ATLAS Collaboration, *Electron and photon performance measurements with the ATLAS detector using the 2015–2017 LHC proton–proton collision data*, *JINST* **14** (2019) P12006, arXiv: [1908.00005 \[hep-ex\]](#).
- [105] ATLAS Collaboration, *Improved electron reconstruction in ATLAS using the Gaussian Sum Filter-based model for bremsstrahlung*, ATLAS-CONF-2012-047, 2012, URL: <https://cds.cern.ch/record/1449796>.
- [106] ATLAS Collaboration, *Muon reconstruction and identification efficiency in ATLAS using the full Run 2 pp collision data set at $\sqrt{s} = 13$ TeV*, *Eur. Phys. J. C* **81** (2021) 578, arXiv: [2012.00578 \[hep-ex\]](#).
- [107] M. Cacciari, G. P. Salam, and G. Soyez, *The anti- k_t jet clustering algorithm*, *JHEP* **04** (2008) 063, arXiv: [0802.1189 \[hep-ph\]](#).
- [108] M. Cacciari, G. P. Salam, and G. Soyez, *FastJet user manual*, *Eur. Phys. J. C* **72** (2012) 1896, arXiv: [1111.6097 \[hep-ph\]](#).
- [109] ATLAS Collaboration, *Jet reconstruction and performance using particle flow with the ATLAS Detector*, *Eur. Phys. J. C* **77** (2017) 466, arXiv: [1703.10485 \[hep-ex\]](#).
- [110] ATLAS Collaboration, *Jet energy scale measurements and their systematic uncertainties in proton–proton collisions at $\sqrt{s} = 13$ TeV with the ATLAS detector*, *Phys. Rev. D* **96** (2017) 072002, arXiv: [1703.09665 \[hep-ex\]](#).
- [111] ATLAS Collaboration, *Tagging and suppression of pileup jets with the ATLAS detector*, ATLAS-CONF-2014-018, 2014, URL: <https://cds.cern.ch/record/1700870>.
- [112] ATLAS Collaboration, *Optimisation and performance studies of the ATLAS b-tagging algorithms for the 2017-18 LHC run*, ATL-PHYS-PUB-2017-013, 2017, URL: <https://cds.cern.ch/record/2273281>.

- [113] ATLAS Collaboration, *ATLAS b -jet identification performance and efficiency measurement with $t\bar{t}$ events in pp collisions at $\sqrt{s} = 13$ TeV*, *Eur. Phys. J. C* **79** (2019) 970, arXiv: [1907.05120](https://arxiv.org/abs/1907.05120) [[hep-ex](#)].
- [114] ATLAS Collaboration, *Performance of missing transverse momentum reconstruction with the ATLAS detector using proton–proton collisions at $\sqrt{s} = 13$ TeV*, *Eur. Phys. J. C* **78** (2018) 903, arXiv: [1802.08168](https://arxiv.org/abs/1802.08168) [[hep-ex](#)].
- [115] T. Plehn, D. L. Rainwater, and D. Zeppenfeld, *A Method for identifying $H \rightarrow \tau^+\tau^- \rightarrow e^\pm\mu^\mp + \text{missing } p_T$ at the CERN LHC*, *Phys. Rev. D* **61** (2000) 093005, arXiv: [hep-ph/9911385](https://arxiv.org/abs/hep-ph/9911385).
- [116] F. Chollet et al., *Keras*, 2015, URL: <https://keras.io>.
- [117] M. Abadi et al., *TensorFlow: Large-Scale Machine Learning on Heterogeneous Distributed Systems*, 2016, URL: <https://arxiv.org/abs/1603.04467>.
- [118] V. Barger, R. J. N. Phillips, and D. Zeppenfeld, *Minijet veto: a tool for the heavy Higgs search at the LHC*, *Phys. Lett. B* **346** (1995) 106, arXiv: [hep-ph/9412276](https://arxiv.org/abs/hep-ph/9412276).
- [119] ATLAS Collaboration, *Object-based missing transverse momentum significance in the ATLAS Detector*, ATLAS-CONF-2018-038, 2018, URL: <https://cds.cern.ch/record/2630948>.
- [120] C. G. Lester and D. J. Summers, *Measuring masses of semiinvisibly decaying particles pair produced at hadron colliders*, *Phys. Lett. B* **463** (1999) 99, arXiv: [hep-ph/9906349](https://arxiv.org/abs/hep-ph/9906349).
- [121] ATLAS Collaboration, *Observation and measurement of Higgs boson decays to WW^* with the ATLAS detector*, *Phys. Rev. D* **92** (2015) 012006, arXiv: [1412.2641](https://arxiv.org/abs/1412.2641) [[hep-ex](#)].
- [122] ATLAS Collaboration, *Measurements of gluon-gluon fusion and vector-boson fusion Higgs boson production cross-sections in the $H \rightarrow WW^* \rightarrow e\nu\mu\nu$ decay channel in pp collisions at $\sqrt{s} = 13$ TeV with the ATLAS detector*, *Phys. Lett. B* **789** (2019) 508, arXiv: [1808.09054](https://arxiv.org/abs/1808.09054) [[hep-ex](#)].
- [123] G. Avoni et al., *The new LUCID-2 detector for luminosity measurement and monitoring in ATLAS*, *JINST* **13** (2018) P07017.
- [124] I. W. Stewart and F. J. Tackmann, *Theory uncertainties for Higgs mass and other searches using jet bins*, *Phys. Rev. D* **85** (2012) 034011, arXiv: [1107.2117](https://arxiv.org/abs/1107.2117) [[hep-ph](#)].
- [125] I. W. Stewart, F. J. Tackmann, J. R. Walsh, and S. Zuberi, *Jet p_T resummation in Higgs production at NNLL' + NNLO*, *Phys. Rev. D* **89** (2014) 054001, arXiv: [1307.1808](https://arxiv.org/abs/1307.1808) [[hep-ph](#)].
- [126] X. Liu and F. Petriello, *Reducing theoretical uncertainties for exclusive Higgs-boson plus one-jet production at the LHC*, *Phys. Rev. D* **87** (2013) 094027, arXiv: [1303.4405](https://arxiv.org/abs/1303.4405) [[hep-ph](#)].
- [127] R. Boughezal, X. Liu, F. Petriello, F. J. Tackmann, and J. R. Walsh, *Combining resummed Higgs predictions across jet bins*, *Phys. Rev. D* **89** (2014) 074044, arXiv: [1312.4535](https://arxiv.org/abs/1312.4535) [[hep-ph](#)].

- [128] S. Gangal and F. J. Tackmann,
Next-to-leading-order uncertainties in Higgs+2 jets from gluon fusion,
[Phys. Rev. D **87** \(2013\) 093008](#), arXiv: [1302.5437 \[hep-ph\]](#).
- [129] B. Biedermann, A. Denner, and M. Pellen,
Large Electroweak Corrections to Vector-Boson Scattering at the Large Hadron Collider,
[Phys. Rev. Lett. **118** \(2017\)](#), arXiv: [1611.02951 \[hep-ph\]](#).
- [130] A. Denner and S. Pozzorini, *One-loop leading logarithms in electroweak radiative corrections*,
[Eur. Phys. J. C **18** \(2001\) 461](#), arXiv: [hep-ph/0010201](#).
- [131] G. Cowan, K. Cranmer, E. Gross, and O. Vitells,
Asymptotic formulae for likelihood-based tests of new physics, [Eur. Phys. J. C **71** \(2011\) 1554](#),
arXiv: [1007.1727 \[physics.data-an\]](#), Erratum: [Eur. Phys. J. C **73** \(2013\) 2501](#).
- [132] ATLAS Collaboration, *ATLAS Computing Acknowledgements*, ATL-SOFT-PUB-2021-003,
URL: <https://cds.cern.ch/record/2776662>.

The ATLAS Collaboration

G. Aad ¹⁰¹, B. Abbott ¹¹⁹, D.C. Abbott ¹⁰², A. Abed Abud ³⁶, K. Abeling ⁵⁵, S.H. Abidi ²⁹, A. Aboulhorma ^{35e}, H. Abramowicz ¹⁵⁰, H. Abreu ¹⁴⁹, Y. Abulaiti ¹¹⁶, A.C. Abusleme Hoffman ^{136a}, B.S. Acharya ^{68a,68b,o}, B. Achkar ⁵⁵, L. Adam ⁹⁹, C. Adam Bourdarios ⁴, L. Adamczyk ^{84a}, L. Adamek ¹⁵⁴, S.V. Addepalli ²⁶, J. Adelman ¹¹⁴, A. Adiguzel ^{21c}, S. Adorni ⁵⁶, T. Adye ¹³³, A.A. Affolder ¹³⁵, Y. Afik ³⁶, M.N. Agaras ¹³, J. Agarwala ^{72a,72b}, A. Aggarwal ⁹⁹, C. Agheorghiesei ^{27c}, J.A. Aguilar-Saavedra ^{129f}, A. Ahmad ³⁶, F. Ahmadov ^{38,y}, W.S. Ahmed ¹⁰³, X. Ai ⁴⁸, G. Aielli ^{75a,75b}, I. Aizenberg ¹⁶⁸, M. Akbiyik ⁹⁹, T.P.A. Åkesson ⁹⁷, A.V. Akimov ³⁷, K. Al Khoury ⁴¹, G.L. Alberghi ^{23b}, J. Albert ¹⁶⁴, P. Albicocco ⁵³, M.J. Alconada Verzini ⁸⁹, S. Alderweireldt ⁵², M. Aleksa ³⁶, I.N. Aleksandrov ³⁸, C. Alexa ^{27b}, T. Alexopoulos ¹⁰, A. Alfonsi ¹¹³, F. Alfonsi ^{23b}, M. Alhroob ¹¹⁹, B. Ali ¹³¹, S. Ali ¹⁴⁷, M. Aliev ³⁷, G. Alimonti ^{70a}, C. Allaire ³⁶, B.M.M. Allbrooke ¹⁴⁵, P.P. Allport ²⁰, A. Aloisio ^{71a,71b}, F. Alonso ⁸⁹, C. Alpigiani ¹³⁷, E. Alunno Camelia ^{75a,75b}, M. Alvarez Estevez ⁹⁸, M.G. Alviggi ^{71a,71b}, Y. Amaral Coutinho ^{81b}, A. Ambler ¹⁰³, C. Amelung ³⁶, C.G. Ames ¹⁰⁸, D. Amidei ¹⁰⁵, S.P. Amor Dos Santos ^{129a}, S. Amoroso ⁴⁸, K.R. Amos ¹⁶², C.S. Amrouche ⁵⁶, V. Ananiev ¹²⁴, C. Anastopoulos ¹³⁸, N. Andari ¹³⁴, T. Andeen ¹¹, J.K. Anders ¹⁹, S.Y. Andrean ^{47a,47b}, A. Andreazza ^{70a,70b}, S. Angelidakis ⁹, A. Angerami ^{41.ab}, A.V. Anisenkov ³⁷, A. Annovi ^{73a}, C. Antel ⁵⁶, M.T. Anthony ¹³⁸, E. Antipov ¹²⁰, M. Antonelli ⁵³, D.J.A. Antrim ^{17a}, F. Anulli ^{74a}, M. Aoki ⁸², J.A. Aparisi Pozo ¹⁶², M.A. Aparo ¹⁴⁵, L. Aperio Bella ⁴⁸, C. Appelt ¹⁸, N. Aranzabal ³⁶, V. Araujo Ferraz ^{81a}, C. Arcangeletti ⁵³, A.T.H. Arce ⁵¹, E. Arena ⁹¹, J-F. Arguin ¹⁰⁷, S. Argyropoulos ⁵⁴, J.-H. Arling ⁴⁸, A.J. Armbruster ³⁶, O. Arnaez ¹⁵⁴, H. Arnold ¹¹³, Z.P. Arrubarrena Tame ¹⁰⁸, G. Artoni ^{74a,74b}, H. Asada ¹¹⁰, K. Asai ¹¹⁷, S. Asai ¹⁵², N.A. Asbah ⁶¹, E.M. Asimakopoulou ¹⁶⁰, J. Assahsah ^{35d}, K. Assamagan ²⁹, R. Astalos ^{28a}, R.J. Atkin ^{33a}, M. Atkinson ¹⁶¹, N.B. Atlay ¹⁸, H. Atmani ^{62b}, P.A. Atmasiddha ¹⁰⁵, K. Augsten ¹³¹, S. Auricchio ^{71a,71b}, A.D. Auriol ²⁰, V.A. Austrup ¹⁷⁰, G. Avner ¹⁴⁹, G. Avolio ³⁶, K. Axiotis ⁵⁶, M.K. Ayoub ^{14c}, G. Azuelos ^{107,ah}, D. Babal ^{28a}, H. Bachacou ¹³⁴, K. Bachas ^{151,r}, A. Bachi ³⁴, F. Backman ^{47a,47b}, A. Badea ⁶¹, P. Bagnaia ^{74a,74b}, M. Bahmani ¹⁸, A.J. Bailey ¹⁶², V.R. Bailey ¹⁶¹, J.T. Baines ¹³³, C. Bakalis ¹⁰, O.K. Baker ¹⁷¹, P.J. Bakker ¹¹³, E. Bakos ¹⁵, D. Bakshi Gupta ⁸, S. Balaji ¹⁴⁶, R. Balasubramanian ¹¹³, E.M. Baldin ³⁷, P. Balek ¹³², E. Ballabene ^{70a,70b}, F. Balli ¹³⁴, L.M. Baltes ^{63a}, W.K. Balunas ³², J. Balz ⁹⁹, E. Banas ⁸⁵, M. Bandieramonte ¹²⁸, A. Bandyopadhyay ²⁴, S. Bansal ²⁴, L. Barak ¹⁵⁰, E.L. Barberio ¹⁰⁴, D. Barberis ^{57b,57a}, M. Barbero ¹⁰¹, G. Barbour ⁹⁵, K.N. Barends ^{33a}, T. Barillari ¹⁰⁹, M-S. Barisits ³⁶, J. Barkeloo ¹²², T. Barklow ¹⁴², R.M. Barnett ^{17a}, P. Baron ¹²¹, D.A. Baron Moreno ¹⁰⁰, A. Baroncelli ^{62a}, G. Barone ²⁹, A.J. Barr ¹²⁵, L. Barranco Navarro ^{47a,47b}, F. Barreiro ⁹⁸, J. Barreiro Guimarães da Costa ^{14a}, U. Barron ¹⁵⁰, S. Barsov ³⁷, F. Bartels ^{63a}, R. Bartoldus ¹⁴², A.E. Barton ⁹⁰, P. Bartos ^{28a}, A. Basalae ⁴⁸, A. Basan ⁹⁹, M. Baselga ⁴⁹, I. Bashta ^{76a,76b}, A. Bassalat ^{66.ad}, M.J. Basso ¹⁵⁴, C.R. Basson ¹⁰⁰, R.L. Bates ⁵⁹, S. Batlamous ^{35e}, J.R. Batley ³², B. Batool ¹⁴⁰, M. Battaglia ¹³⁵, M. Bauge ^{74a,74b}, P. Bauer ²⁴, A. Bayirli ^{21a}, J.B. Beacham ⁵¹, T. Beau ¹²⁶, P.H. Beauchemin ¹⁵⁷, F. Becherer ⁵⁴, P. Bechtel ²⁴, H.P. Beck ^{19,q}, K. Becker ¹⁶⁶, C. Becot ⁴⁸, A.J. Beddall ^{21d}, V.A. Bednyakov ³⁸, C.P. Bee ¹⁴⁴, L.J. Beamster ¹⁵, T.A. Beermann ³⁶, M. Begalli ^{81b}, M. Begel ²⁹, A. Behera ¹⁴⁴, J.K. Behr ⁴⁸, C. Beirao Da Cruz E Silva ³⁶, J.F. Beirer ^{55,36}, F. Beisiegel ²⁴, M. Belfkir ¹⁵⁸, G. Bella ¹⁵⁰, L. Bellagamba ^{23b}, A. Bellerive ³⁴, P. Bellos ²⁰, K. Beloborodov ³⁷, K. Belotskiy ³⁷, N.L. Belyaev ³⁷, D. Benchekroun ^{35a}, Y. Benhammou ¹⁵⁰, D.P. Benjamin ²⁹,

M. Benoit ²⁹, J.R. Bensinger ²⁶, S. Bentvelsen ¹¹³, L. Beresford ³⁶, M. Beretta ⁵³, D. Berge ¹⁸,
E. Bergeaas Kuutmann ¹⁶⁰, N. Berger ⁴, B. Bergmann ¹³¹, J. Beringer ^{17a}, S. Berlendis ⁷,
G. Bernardi ⁵, C. Bernius ¹⁴², F.U. Bernlochner ²⁴, T. Berry ⁹⁴, P. Berta ¹³², A. Berthold ⁵⁰,
I.A. Bertram ⁹⁰, O. Bessidskaia Bylund ¹⁷⁰, S. Bethke ¹⁰⁹, A. Betti ⁴⁴, A.J. Bevan ⁹³,
S. Bhatta ¹⁴⁴, D.S. Bhattacharya ¹⁶⁵, P. Bhattarai ²⁶, V.S. Bhopatkar ⁶, R. Bi ¹²⁸, R. Bi ^{29,ak},
R.M. Bianchi ¹²⁸, O. Biebel ¹⁰⁸, R. Bielski ¹²², N.V. Biesuz ^{73a,73b}, M. Biglietti ^{76a},
T.R.V. Billoud ¹³¹, M. Bindi ⁵⁵, A. Bingul ^{21b}, C. Bini ^{74a,74b}, S. Biondi ^{23b,23a}, A. Biondini ⁹¹,
C.J. Birch-sykes ¹⁰⁰, G.A. Bird ^{20,133}, M. Birman ¹⁶⁸, T. Bisanz ³⁶, D. Biswas ^{169,k},
A. Bitadze ¹⁰⁰, K. Bjørke ¹²⁴, I. Bloch ⁴⁸, C. Blocker ²⁶, A. Blue ⁵⁹, U. Blumenschein ⁹³,
J. Blumenthal ⁹⁹, G.J. Bobbink ¹¹³, V.S. Bobrovnikov ³⁷, M. Boehler ⁵⁴, D. Bogavac ¹³,
A.G. Bogdanchikov ³⁷, C. Bohm ^{47a}, V. Boisvert ⁹⁴, P. Bokan ⁴⁸, T. Bold ^{84a}, M. Bomben ⁵,
M. Bona ⁹³, M. Boonekamp ¹³⁴, C.D. Booth ⁹⁴, A.G. Borbély ⁵⁹, H.M. Borecka-Bielska ¹⁰⁷,
L.S. Borgna ⁹⁵, G. Borissov ⁹⁰, D. Bortoletto ¹²⁵, D. Boscherini ^{23b}, M. Bosman ¹³,
J.D. Bossio Sola ³⁶, K. Bouaouda ^{35a}, J. Boudreau ¹²⁸, E.V. Bouhova-Thacker ⁹⁰,
D. Boumediene ⁴⁰, R. Bouquet ⁵, A. Boveia ¹¹⁸, J. Boyd ³⁶, D. Boye ²⁹, I.R. Boyko ³⁸,
J. Bracinik ²⁰, N. Brahimy ^{62d,62c}, G. Brandt ¹⁷⁰, O. Brandt ³², F. Braren ⁴⁸, B. Brau ¹⁰²,
J.E. Brau ¹²², W.D. Breaden Madden ⁵⁹, K. Brendlinger ⁴⁸, R. Brenner ¹⁶⁸, L. Brenner ³⁶,
R. Brenner ¹⁶⁰, S. Bressler ¹⁶⁸, B. Brickwedde ⁹⁹, D. Britton ⁵⁹, D. Britzger ¹⁰⁹, I. Brock ²⁴,
G. Brooijmans ⁴¹, W.K. Brooks ^{136f}, E. Brost ²⁹, P.A. Bruckman de Renstrom ⁸⁵, B. Brüers ⁴⁸,
D. Bruncko ^{28b,*}, A. Bruni ^{23b}, G. Bruni ^{23b}, M. Bruschi ^{23b}, N. Brusino ^{74a,74b},
L. Bryngemark ¹⁴², T. Buanes ¹⁶, Q. Buat ¹³⁷, P. Buchholz ¹⁴⁰, A.G. Buckley ⁵⁹,
I.A. Budagov ^{38,*}, M.K. Bugge ¹²⁴, O. Bulekov ³⁷, B.A. Bullard ⁶¹, S. Burdin ⁹¹,
C.D. Burgard ⁴⁸, A.M. Burger ⁴⁰, B. Burghgrave ⁸, J.T.P. Burr ³², C.D. Burton ¹¹,
J.C. Burzynski ¹⁴¹, E.L. Busch ⁴¹, V. Büscher ⁹⁹, P.J. Bussey ⁵⁹, J.M. Butler ²⁵, C.M. Buttar ⁵⁹,
J.M. Butterworth ⁹⁵, W. Buttinger ¹³³, C.J. Buxo Vazquez ¹⁰⁶, A.R. Buzykaev ³⁷, G. Cabras ^{23b},
S. Cabrera Urbán ¹⁶², D. Caforio ⁵⁸, H. Cai ¹²⁸, Y. Cai ^{14a,14d}, V.M.M. Cairo ³⁶, O. Cakir ^{3a},
N. Calace ³⁶, P. Calafiura ^{17a}, G. Calderini ¹²⁶, P. Calfayan ⁶⁷, G. Callea ⁵⁹, L.P. Caloba ^{81b},
D. Calvet ⁴⁰, S. Calvet ⁴⁰, T.P. Calvet ¹⁰¹, M. Calvetti ^{73a,73b}, R. Camacho Toro ¹²⁶,
S. Camarda ³⁶, D. Camarero Munoz ⁹⁸, P. Camarri ^{75a,75b}, M.T. Camerlingo ^{76a,76b},
D. Cameron ¹²⁴, C. Camincher ¹⁶⁴, M. Campanelli ⁹⁵, A. Camplani ⁴², V. Canale ^{71a,71b},
A. Canesse ¹⁰³, M. Cano Bret ⁷⁹, J. Cantero ¹⁶², Y. Cao ¹⁶¹, F. Capocasa ²⁶, M. Capua ^{43b,43a},
A. Carbone ^{70a,70b}, R. Cardarelli ^{75a}, J.C.J. Cardenas ⁸, F. Cardillo ¹⁶², T. Carli ³⁶,
G. Carlino ^{71a}, B.T. Carlson ^{128,s}, E.M. Carlson ^{164,155a}, L. Carminati ^{70a,70b}, M. Carnesale ^{74a,74b},
S. Caron ¹¹², E. Carquin ^{136f}, S. Carrá ⁴⁸, G. Carratta ^{23b,23a}, J.W.S. Carter ¹⁵⁴, T.M. Carter ⁵²,
M.P. Casado ^{13,h}, A.F. Casha ¹⁵⁴, E.G. Castiglia ¹⁷¹, F.L. Castillo ^{63a}, L. Castillo Garcia ¹³,
V. Castillo Gimenez ¹⁶², N.F. Castro ^{129a,129e}, A. Catinaccio ³⁶, J.R. Catmore ¹²⁴, V. Cavaliere ²⁹,
N. Cavalli ^{23b,23a}, V. Cavalanni ^{73a,73b}, E. Celebi ^{21a}, F. Celli ¹²⁵, M.S. Centonze ^{69a,69b},
K. Cerny ¹²¹, A.S. Cerqueira ^{81a}, A. Cerri ¹⁴⁵, L. Cerrito ^{75a,75b}, F. Cerutti ^{17a}, A. Cervelli ^{23b},
S.A. Cetin ^{21d}, Z. Chadi ^{35a}, D. Chakraborty ¹¹⁴, M. Chala ^{129f}, J. Chan ¹⁶⁹, W.S. Chan ¹¹³,
W.Y. Chan ¹⁵², J.D. Chapman ³², B. Chargeishvili ^{148b}, D.G. Charlton ²⁰, T.P. Charman ⁹³,
M. Chatterjee ¹⁹, S. Chekanov ⁶, S.V. Chekulaev ^{155a}, G.A. Chelkov ^{38,a}, A. Chen ¹⁰⁵,
B. Chen ¹⁵⁰, B. Chen ¹⁶⁴, C. Chen ^{62a}, H. Chen ^{14c}, H. Chen ²⁹, J. Chen ^{62c}, J. Chen ²⁶,
S. Chen ¹⁵², S.J. Chen ^{14c}, X. Chen ^{62c}, X. Chen ^{14b,ag}, Y. Chen ^{62a}, C.L. Cheng ¹⁶⁹,
H.C. Cheng ^{64a}, A. Cheplakov ³⁸, E. Cheremushkina ⁴⁸, E. Cherepanova ³⁸,
R. Cherkaoui El Moursli ^{35e}, E. Cheu ⁷, K. Cheung ⁶⁵, L. Chevalier ¹³⁴, V. Chiarella ⁵³,
G. Chiarelli ^{73a}, G. Chiodini ^{69a}, A.S. Chisholm ²⁰, A. Chitan ^{27b}, Y.H. Chiu ¹⁶⁴,
M.V. Chizhov ³⁸, K. Choi ¹¹, A.R. Chomont ^{74a,74b}, Y. Chou ¹⁰², E.Y.S. Chow ¹¹³,

T. Chowdhury [ID^{33g}](#), L.D. Christopher [ID^{33g}](#), K.L. Chu [ID^{64a}](#), M.C. Chu [ID^{64a}](#), X. Chu [ID^{14a,14d}](#),
 J. Chudoba [ID¹³⁰](#), J.J. Chwastowski [ID⁸⁵](#), D. Cieri [ID¹⁰⁹](#), K.M. Ciesla [ID⁸⁵](#), V. Cindro [ID⁹²](#), A. Ciocio [ID^{17a}](#),
 F. Cirotto [ID^{71a,71b}](#), Z.H. Citron [ID^{168,1}](#), M. Citterio [ID^{70a}](#), D.A. Ciubotaru [ID^{27b}](#), B.M. Ciungu [ID¹⁵⁴](#),
 A. Clark [ID⁵⁶](#), P.J. Clark [ID⁵²](#), J.M. Clavijo Columbie [ID⁴⁸](#), S.E. Clawson [ID¹⁰⁰](#), C. Clement [ID^{47a,47b}](#),
 J. Clercx [ID⁴⁸](#), L. Clissa [ID^{23b,23a}](#), Y. Coadou [ID¹⁰¹](#), M. Cobal [ID^{68a,68c}](#), A. Coccaro [ID^{57b}](#),
 R.F. Coelho Barrue [ID^{129a}](#), R. Coelho Lopes De Sa [ID¹⁰²](#), S. Coelli [ID^{70a}](#), H. Cohen [ID¹⁵⁰](#),
 A.E.C. Coimbra [ID¹⁴⁹](#), B. Cole [ID⁴¹](#), J. Collot [ID⁶⁰](#), P. Conde Muiño [ID^{129a,129g}](#), S.H. Connell [ID^{33c}](#),
 I.A. Connelly [ID⁵⁹](#), E.I. Conroy [ID¹²⁵](#), F. Conventi [ID^{71a,ai}](#), H.G. Cooke [ID²⁰](#), A.M. Cooper-Sarkar [ID¹²⁵](#),
 F. Cormier [ID¹⁶³](#), L.D. Corpe [ID³⁶](#), M. Corradi [ID^{74a,74b}](#), E.E. Corrigan [ID⁹⁷](#), F. Corriveau [ID^{103,x}](#),
 A. Cortes-Gonzalez [ID¹⁸](#), M.J. Costa [ID¹⁶²](#), F. Costanza [ID⁴](#), D. Costanzo [ID¹³⁸](#), B.M. Cote [ID¹¹⁸](#),
 G. Cowan [ID⁹⁴](#), J.W. Cowley [ID³²](#), K. Cranmer [ID¹¹⁶](#), S. Crépe-Renaudin [ID⁶⁰](#), F. Crescioli [ID¹²⁶](#),
 M. Cristinziani [ID¹⁴⁰](#), M. Cristoforetti [ID^{77a,77b,c}](#), V. Croft [ID¹⁵⁷](#), G. Crosetti [ID^{43b,43a}](#), A. Cueto [ID³⁶](#),
 T. Cuhadar Donszelmann [ID¹⁵⁹](#), H. Cui [ID^{14a,14d}](#), Z. Cui [ID⁷](#), A.R. Cukierman [ID¹⁴²](#), W.R. Cunningham [ID⁵⁹](#),
 F. Curcio [ID^{43b,43a}](#), P. Czodrowski [ID³⁶](#), M.M. Czurylo [ID^{63b}](#), M.J. Da Cunha Sargedas De Sousa [ID^{62a}](#),
 J.V. Da Fonseca Pinto [ID^{81b}](#), C. Da Via [ID¹⁰⁰](#), W. Dabrowski [ID^{84a}](#), T. Dado [ID⁴⁹](#), S. Dahbi [ID^{33g}](#),
 T. Dai [ID¹⁰⁵](#), C. Dallapiccola [ID¹⁰²](#), M. Dam [ID⁴²](#), G. D'amen [ID²⁹](#), V. D'Amico [ID^{76a,76b}](#), J. Damp [ID⁹⁹](#),
 J.R. Dandoy [ID¹²⁷](#), M.F. Daneri [ID³⁰](#), M. Danninger [ID¹⁴¹](#), V. Dao [ID³⁶](#), G. Darbo [ID^{57b}](#), S. Darmora [ID⁶](#),
 S.J. Das [ID^{29,ak}](#), A. Dattagupta [ID¹²²](#), S. D'Auria [ID^{70a,70b}](#), C. David [ID^{155b}](#), T. Davidek [ID¹³²](#),
 D.R. Davis [ID⁵¹](#), B. Davis-Purcell [ID³⁴](#), I. Dawson [ID⁹³](#), K. De [ID⁸](#), R. De Asmundis [ID^{71a}](#),
 M. De Beurs [ID¹¹³](#), S. De Castro [ID^{23b,23a}](#), N. De Groot [ID¹¹²](#), P. de Jong [ID¹¹³](#), H. De la Torre [ID¹⁰⁶](#),
 A. De Maria [ID^{14c}](#), A. De Salvo [ID^{74a}](#), U. De Sanctis [ID^{75a,75b}](#), M. De Santis [ID^{75a,75b}](#), A. De Santo [ID¹⁴⁵](#),
 J.B. De Vivie De Regie [ID⁶⁰](#), D.V. Dedovich [ID³⁸](#), J. Degens [ID¹¹³](#), A.M. Deiana [ID⁴⁴](#), F. Del Corso [ID^{23b,23a}](#),
 J. Del Peso [ID⁹⁸](#), F. Del Rio [ID^{63a}](#), F. Deliot [ID¹³⁴](#), C.M. Delitzsch [ID⁴⁹](#), M. Della Pietra [ID^{71a,71b}](#),
 D. Della Volpe [ID⁵⁶](#), A. Dell'Acqua [ID³⁶](#), L. Dell'Asta [ID^{70a,70b}](#), M. Delmastro [ID⁴](#), P.A. Delsart [ID⁶⁰](#),
 S. Demers [ID¹⁷¹](#), M. Demichev [ID³⁸](#), S.P. Denisov [ID³⁷](#), L. D'Eramo [ID¹¹⁴](#), D. Derendarz [ID⁸⁵](#),
 F. Derue [ID¹²⁶](#), P. Dervan [ID⁹¹](#), K. Desch [ID²⁴](#), K. Dette [ID¹⁵⁴](#), C. Deutsch [ID²⁴](#), P.O. Deviveiros [ID³⁶](#),
 F.A. Di Bello [ID^{74a,74b}](#), A. Di Ciaccio [ID^{75a,75b}](#), L. Di Ciaccio [ID⁴](#), A. Di Domenico [ID^{74a,74b}](#),
 C. Di Donato [ID^{71a,71b}](#), A. Di Girolamo [ID³⁶](#), G. Di Gregorio [ID^{73a,73b}](#), A. Di Luca [ID^{77a,77b}](#),
 B. Di Micco [ID^{76a,76b}](#), R. Di Nardo [ID^{76a,76b}](#), C. Diaconu [ID¹⁰¹](#), F.A. Dias [ID¹¹³](#), T. Dias Do Vale [ID¹⁴¹](#),
 M.A. Diaz [ID^{136a,136b}](#), F.G. Diaz Capriles [ID²⁴](#), M. Didenko [ID¹⁶²](#), E.B. Diehl [ID¹⁰⁵](#), L. Diehl [ID⁵⁴](#),
 S. Díez Cornell [ID⁴⁸](#), C. Diez Pardos [ID¹⁴⁰](#), C. Dimitriadi [ID^{24,160}](#), A. Dimitrievska [ID^{17a}](#), W. Ding [ID^{14b}](#),
 J. Dingfelder [ID²⁴](#), I-M. Dinu [ID^{27b}](#), S.J. Dittmeier [ID^{63b}](#), F. Dittus [ID³⁶](#), F. Djama [ID¹⁰¹](#), T. Djobava [ID^{148b}](#),
 J.I. Djuvsland [ID¹⁶](#), D. Dodsworth [ID²⁶](#), C. Doglioni [ID^{100,97}](#), J. Dolejsi [ID¹³²](#), Z. Dolezal [ID¹³²](#),
 M. Donadelli [ID^{81c}](#), B. Dong [ID^{62c}](#), J. Donini [ID⁴⁰](#), A. D'Onofrio [ID^{14c}](#), M. D'Onofrio [ID⁹¹](#), J. Dopke [ID¹³³](#),
 A. Doria [ID^{71a}](#), M.T. Dova [ID⁸⁹](#), A.T. Doyle [ID⁵⁹](#), M.A. Draguet [ID¹²⁵](#), E. Drechsler [ID¹⁴¹](#), E. Dreyer [ID¹⁶⁸](#),
 I. Drivas-koulouris [ID¹⁰](#), A.S. Drobac [ID¹⁵⁷](#), D. Du [ID^{62a}](#), T.A. du Pree [ID¹¹³](#), F. Dubinin [ID³⁷](#),
 M. Dubovsky [ID^{28a}](#), E. Duchovni [ID¹⁶⁸](#), G. Duckeck [ID¹⁰⁸](#), O.A. Ducu [ID^{36,27b}](#), D. Duda [ID¹⁰⁹](#),
 A. Dudarev [ID³⁶](#), M. D'uffizi [ID¹⁰⁰](#), L. Dufлот [ID⁶⁶](#), M. Dührssen [ID³⁶](#), C. Dülsen [ID¹⁷⁰](#), A.E. Dumitriu [ID^{27b}](#),
 M. Dunford [ID^{63a}](#), S. Dungs [ID⁴⁹](#), K. Dunne [ID^{47a,47b}](#), A. Duperrin [ID¹⁰¹](#), H. Duran Yildiz [ID^{3a}](#),
 M. Düren [ID⁵⁸](#), A. Durglishvili [ID^{148b}](#), B.L. Dwyer [ID¹¹⁴](#), G.I. Dyckes [ID^{17a}](#), M. Dyndal [ID^{84a}](#),
 S. Dysch [ID¹⁰⁰](#), B.S. Dziedzic [ID⁸⁵](#), B. Eckerova [ID^{28a}](#), M.G. Eggleston [ID⁵¹](#), E. Egidio Purcino De Souza [ID^{81b}](#),
 L.F. Ehrke [ID⁵⁶](#), G. Eigen [ID¹⁶](#), K. Einsweiler [ID^{17a}](#), T. Ekelof [ID¹⁶⁰](#), P.A. Ekman [ID⁹⁷](#), Y. El Ghazali [ID^{35b}](#),
 H. El Jarrari [ID^{35e,147}](#), A. El Moussaouy [ID^{35a}](#), V. Ellajosyula [ID¹⁶⁰](#), M. Ellert [ID¹⁶⁰](#), F. Ellinghaus [ID¹⁷⁰](#),
 A.A. Elliot [ID⁹³](#), N. Ellis [ID³⁶](#), J. Elmsheuser [ID²⁹](#), M. Elsing [ID³⁶](#), D. Emelianov [ID¹³³](#), A. Emerman [ID⁴¹](#),
 Y. Enari [ID¹⁵²](#), I. Ene [ID^{17a}](#), S. Epari [ID¹³](#), J. Erdmann [ID⁴⁹](#), A. Ereditato [ID¹⁹](#), P.A. Erland [ID⁸⁵](#),
 M. Errenst [ID¹⁷⁰](#), M. Escalier [ID⁶⁶](#), C. Escobar [ID¹⁶²](#), E. Etzion [ID¹⁵⁰](#), G. Evans [ID^{129a}](#), H. Evans [ID⁶⁷](#),
 M.O. Evans [ID¹⁴⁵](#), A. Ezhilov [ID³⁷](#), S. Ezzarqtouni [ID^{35a}](#), F. Fabbri [ID⁵⁹](#), L. Fabbri [ID^{23b,23a}](#), G. Facini [ID⁹⁵](#),

V. Fadeyev ¹³⁵, R.M. Fakhrutdinov ³⁷, S. Falciano ^{74a}, P.J. Falke ²⁴, S. Falke ³⁶, J. Faltova ¹³², Y. Fan ^{14a}, Y. Fang ^{14a,14d}, G. Fanourakis ⁴⁶, M. Fanti ^{70a,70b}, M. Faraj ^{68a,68b}, A. Farbin ⁸, A. Farilla ^{76a}, T. Farooque ¹⁰⁶, S.M. Farrington ⁵², F. Fassi ^{35e}, D. Fassouliotis ⁹, M. Faucci Giannelli ^{75a,75b}, W.J. Fawcett ³², L. Fayard ⁶⁶, O.L. Fedin ^{37,a}, G. Fedotov ³⁷, M. Feickert ¹⁶¹, L. Feligioni ¹⁰¹, A. Fell ¹³⁸, D.E. Fellers ¹²², C. Feng ^{62b}, M. Feng ^{14b}, M.J. Fenton ¹⁵⁹, A.B. Fenyuk ³⁷, L. Ferencz ⁴⁸, S.W. Ferguson ⁴⁵, J. Ferrando ⁴⁸, A. Ferrari ¹⁶⁰, P. Ferrari ¹¹³, R. Ferrari ^{72a}, D. Ferrere ⁵⁶, C. Ferretti ¹⁰⁵, F. Fiedler ⁹⁹, A. Filipčič ⁹², E.K. Filmer ¹, F. Filthaut ¹¹², M.C.N. Fiolhais ^{129a,129c,b}, L. Fiorini ¹⁶², F. Fischer ¹⁴⁰, W.C. Fisher ¹⁰⁶, T. Fitschen ^{20,66}, I. Fleck ¹⁴⁰, P. Fleischmann ¹⁰⁵, T. Flick ¹⁷⁰, L. Flores ¹²⁷, M. Flores ^{33d,ac}, L.R. Flores Castillo ^{64a}, F.M. Follega ^{77a,77b}, N. Fomin ¹⁶, J.H. Foo ¹⁵⁴, B.C. Forland ⁶⁷, A. Formica ¹³⁴, A.C. Forti ¹⁰⁰, E. Fortin ¹⁰¹, A.W. Fortman ⁶¹, M.G. Foti ^{17a}, L. Fountas ^{9,i}, D. Fournier ⁶⁶, H. Fox ⁹⁰, P. Francavilla ^{73a,73b}, S. Francescato ⁶¹, M. Franchini ^{23b,23a}, S. Franchino ^{63a}, D. Francis ³⁶, L. Franco ⁴, L. Franconi ¹⁹, M. Franklin ⁶¹, G. Frattari ²⁶, A.C. Freegard ⁹³, P.M. Freeman ²⁰, W.S. Freund ^{81b}, N. Fritzsche ⁵⁰, A. Froch ⁵⁴, D. Froidevaux ³⁶, J.A. Frost ¹²⁵, Y. Fu ^{62a}, M. Fujimoto ¹¹⁷, E. Fullana Torregrosa ^{162,*}, J. Fuster ¹⁶², A. Gabrielli ^{23b,23a}, A. Gabrielli ³⁶, P. Gadow ⁴⁸, G. Gagliardi ^{57b,57a}, L.G. Gagnon ^{17a}, G.E. Gallardo ¹²⁵, E.J. Gallas ¹²⁵, B.J. Gallop ¹³³, R. Gamboa Goni ⁹³, K.K. Gan ¹¹⁸, S. Ganguly ¹⁵², J. Gao ^{62a}, Y. Gao ⁵², F.M. Garay Walls ^{136a,136b}, B. Garcia ^{29,ak}, C. García ¹⁶², J.E. García Navarro ¹⁶², J.A. García Pascual ^{14a}, M. Garcia-Sciveres ^{17a}, R.W. Gardner ³⁹, D. Garg ⁷⁹, R.B. Garg ^{142,p}, S. Gargiulo ⁵⁴, C.A. Garner ¹⁵⁴, V. Garonne ²⁹, S.J. Gasiorowski ¹³⁷, P. Gaspar ^{81b}, G. Gaudio ^{72a}, P. Gauzzi ^{74a,74b}, I.L. Gavrilenko ³⁷, A. Gavrilyuk ³⁷, C. Gay ¹⁶³, G. Gaycken ⁴⁸, E.N. Gazis ¹⁰, A.A. Geanta ^{27b}, C.M. Gee ¹³⁵, J. Geisen ⁹⁷, M. Geisen ⁹⁹, C. Gemme ^{57b}, M.H. Genest ⁶⁰, S. Gentile ^{74a,74b}, S. George ⁹⁴, W.F. George ²⁰, T. Gerialis ⁴⁶, L.O. Gerlach ⁵⁵, P. Gessinger-Befurt ³⁶, M. Ghasemi Bostanabad ¹⁶⁴, M. Ghneimat ¹⁴⁰, A. Ghosal ¹⁴⁰, A. Ghosh ¹⁵⁹, A. Ghosh ⁷, B. Giacobbe ^{23b}, S. Giagu ^{74a,74b}, N. Giangiacomi ¹⁵⁴, P. Giannetti ^{73a}, A. Giannini ^{62a}, S.M. Gibson ⁹⁴, M. Gignac ¹³⁵, D.T. Gil ^{84b}, A.K. Gilbert ^{84a}, B.J. Gilbert ⁴¹, D. Gillberg ³⁴, G. Gilles ¹¹³, N.E.K. Gillwald ⁴⁸, L. Ginabat ¹²⁶, D.M. Gingrich ^{2,ah}, M.P. Giordani ^{68a,68c}, P.F. Giraud ¹³⁴, G. Giugliarelli ^{68a,68c}, D. Giugni ^{70a}, F. Giuli ²⁶, I. Gkialas ^{9,i}, L.K. Gladilin ³⁷, C. Glasman ⁹⁸, G.R. Gledhill ¹²², M. Glisic ¹²², I. Gnesi ^{43b,e}, Y. Go ^{29,ak}, M. Goblirsch-Kolb ²⁶, D. Godin ¹⁰⁷, S. Goldfarb ¹⁰⁴, T. Golling ⁵⁶, M.G.D. Gololo ^{33g}, D. Golubkov ³⁷, J.P. Gombas ¹⁰⁶, A. Gomes ^{129a,129b}, A.J. Gomez Delegido ¹⁶², R. Goncalves Gama ⁵⁵, R. Gonçalo ^{129a,129c}, G. Gonella ¹²², L. Gonella ²⁰, A. Gongadze ³⁸, F. Gonnella ²⁰, J.L. Gonski ⁴¹, R.Y. González Andana ⁵², S. González de la Hoz ¹⁶², S. Gonzalez Fernandez ¹³, R. Gonzalez Lopez ⁹¹, C. Gonzalez Renteria ^{17a}, R. Gonzalez Suarez ¹⁶⁰, S. Gonzalez-Sevilla ⁵⁶, G.R. Gonzalvo Rodriguez ¹⁶², L. Goossens ³⁶, N.A. Gorasia ²⁰, P.A. Gorbounov ³⁷, B. Gorini ³⁶, E. Gorini ^{69a,69b}, A. Gorišek ⁹², A.T. Goshaw ⁵¹, M.I. Gostkin ³⁸, C.A. Gottardo ¹¹², M. Goughri ^{35b}, V. Goumarre ⁴⁸, A.G. Goussiou ¹³⁷, N. Govender ^{33c}, C. Goy ⁴, I. Grabowska-Bold ^{84a}, K. Graham ³⁴, E. Gramstad ¹²⁴, S. Grancagnolo ¹⁸, M. Grandi ¹⁴⁵, V. Gratchev ^{37,*}, P.M. Gravila ^{27f}, F.G. Gravili ^{69a,69b}, H.M. Gray ^{17a}, M. Greco ^{69a,69b}, C. Grefe ²⁴, I.M. Gregor ⁴⁸, P. Grenier ¹⁴², C. Grieco ¹³, A.A. Grillo ¹³⁵, K. Grimm ^{31,m}, S. Grinstein ^{13,u}, J.-F. Grivaz ⁶⁶, E. Gross ¹⁶⁸, J. Grosse-Knetter ⁵⁵, C. Grud ¹⁰⁵, A. Grummer ¹¹¹, J.C. Grundy ¹²⁵, L. Guan ¹⁰⁵, W. Guan ¹⁶⁹, C. Gubbels ¹⁶³, J.G.R. Guerrero Rojas ¹⁶², G. Guerrieri ^{68a,68c}, F. Guescini ¹⁰⁹, R. Gugel ⁹⁹, J.A.M. Guhit ¹⁰⁵, A. Guida ⁴⁸, T. Guillemain ⁴, E. Guilloton ^{166,133}, S. Guindon ³⁶, F. Guo ^{14a,14d}, J. Guo ^{62c}, L. Guo ⁶⁶, Y. Guo ¹⁰⁵, R. Gupta ⁴⁸, S. Gurbuz ²⁴, G. Gustavino ³⁶, M. Guth ⁵⁶, P. Gutierrez ¹¹⁹, L.F. Gutierrez Zagazeta ¹²⁷, C. Gutschow ⁹⁵, C. Guyot ¹³⁴, C. Gwenlan ¹²⁵, C.B. Gwilliam ⁹¹,

E.S. Haaland ¹²⁴, A. Haas ¹¹⁶, M. Habedank ⁴⁸, C. Haber ^{17a}, H.K. Hadavand ⁸, A. Hadeif ⁹⁹,
 S. Hadzic ¹⁰⁹, M. Haleem ¹⁶⁵, J. Haley ¹²⁰, J.J. Hall ¹³⁸, G.D. Hallewell ¹⁰¹, L. Halser ¹⁹,
 K. Hamano ¹⁶⁴, H. Hamdaoui ^{35e}, M. Hamer ²⁴, G.N. Hamity ⁵², J. Han ^{62b}, K. Han ^{62a},
 L. Han ^{14c}, L. Han ^{62a}, S. Han ^{17a}, Y.F. Han ¹⁵⁴, K. Hanagaki ⁸², M. Hance ¹³⁵,
 D.A. Hangal ^{41,ab}, M.D. Hank ³⁹, R. Hankache ¹⁰⁰, J.B. Hansen ⁴², J.D. Hansen ⁴²,
 P.H. Hansen ⁴², K. Hara ¹⁵⁶, D. Harada ⁵⁶, T. Harenberg ¹⁷⁰, S. Harkusha ³⁷, Y.T. Harris ¹²⁵,
 P.F. Harrison ¹⁶⁶, N.M. Hartman ¹⁴², N.M. Hartmann ¹⁰⁸, Y. Hasegawa ¹³⁹, A. Hasib ⁵²,
 S. Haug ¹⁹, R. Hauser ¹⁰⁶, M. Havranek ¹³¹, C.M. Hawkes ²⁰, R.J. Hawkins ³⁶,
 S. Hayashida ¹¹⁰, D. Hayden ¹⁰⁶, C. Hayes ¹⁰⁵, R.L. Hayes ¹⁶³, C.P. Hays ¹²⁵, J.M. Hays ⁹³,
 H.S. Hayward ⁹¹, F. He ^{62a}, Y. He ¹⁵³, Y. He ¹²⁶, M.P. Heath ⁵², V. Hedberg ⁹⁷,
 A.L. Heggelund ¹²⁴, N.D. Hehir ⁹³, C. Heidegger ⁵⁴, K.K. Heidegger ⁵⁴, W.D. Heidorn ⁸⁰,
 J. Heilman ³⁴, S. Heim ⁴⁸, T. Heim ^{17a}, B. Heinemann ^{48,ae}, J.G. Heinlein ¹²⁷, J.J. Heinrich ¹²²,
 L. Heinrich ³⁶, J. Hejbal ¹³⁰, L. Helary ⁴⁸, A. Held ¹¹⁶, S. Hellesund ¹²⁴, C.M. Helling ¹⁶³,
 S. Hellman ^{47a,47b}, C. Helsens ³⁶, R.C.W. Henderson ⁹⁰, L. Henkelmann ³²,
 A.M. Henriques Correia ³⁶, H. Herde ¹⁴², Y. Hernández Jiménez ¹⁴⁴, H. Herr ⁹⁹, M.G. Herrmann ¹⁰⁸,
 T. Herrmann ⁵⁰, G. Herten ⁵⁴, R. Hertenberger ¹⁰⁸, L. Hervas ³⁶, N.P. Hessey ^{155a}, H. Hibi ⁸³,
 E. Higón-Rodríguez ¹⁶², S.J. Hillier ²⁰, I. Hinchliffe ^{17a}, F. Hinterkeuser ²⁴, M. Hirose ¹²³,
 S. Hirose ¹⁵⁶, D. Hirschbuehl ¹⁷⁰, B. Hiti ⁹², J. Hobbs ¹⁴⁴, R. Hobincu ^{27e}, N. Hod ¹⁶⁸,
 M.C. Hodgkinson ¹³⁸, B.H. Hodgkinson ³², A. Hoecker ³⁶, J. Hofer ⁴⁸, D. Hohn ⁵⁴, T. Holm ²⁴,
 M. Holzbock ¹⁰⁹, L.B.A.H. Hommels ³², B.P. Honan ¹⁰⁰, J. Hong ^{62c}, T.M. Hong ¹²⁸,
 Y. Hong ⁵⁵, J.C. Honig ⁵⁴, A. Hönle ¹⁰⁹, B.H. Hooberman ¹⁶¹, W.H. Hopkins ⁶, Y. Horii ¹¹⁰,
 S. Hou ¹⁴⁷, J. Howarth ⁵⁹, J. Hoya ⁸⁹, M. Hrabovsky ¹²¹, A. Hrynevich ³⁷, T. Hryn'ova ⁴,
 P.J. Hsu ⁶⁵, S.-C. Hsu ¹³⁷, Q. Hu ^{41,ab}, Y.F. Hu ^{14a,14d,aj}, D.P. Huang ⁹⁵, S. Huang ^{64b},
 X. Huang ^{14c}, Y. Huang ^{62a}, Y. Huang ^{14a}, Z. Huang ¹⁰⁰, Z. Hubacek ¹³¹, M. Huebner ²⁴,
 F. Huegging ²⁴, T.B. Huffman ¹²⁵, M. Huhtinen ³⁶, S.K. Huiberts ¹⁶, R. Hulskén ¹⁰³,
 N. Huseynov ^{12,a}, J. Huston ¹⁰⁶, J. Huth ⁶¹, R. Hyneman ¹⁴², S. Hyrych ^{28a}, G. Iacobucci ⁵⁶,
 G. Iakovidis ²⁹, I. Ibragimov ¹⁴⁰, L. Iconomidou-Fayard ⁶⁶, P. Iengo ^{71a,71b}, R. Iguchi ¹⁵²,
 T. Iizawa ⁵⁶, Y. Ikegami ⁸², A. Ilg ¹⁹, N. Ilic ¹⁵⁴, H. Imam ^{35a}, T. Ingebretsen Carlson ^{47a,47b},
 G. Introzzi ^{72a,72b}, M. Iodice ^{76a}, V. Ippolito ^{74a,74b}, M. Ishino ¹⁵², W. Islam ¹⁶⁹, C. Issever ^{18,48},
 S. Istin ^{21a,al}, H. Ito ¹⁶⁷, J.M. Iturbe Ponce ^{64a}, R. Iuppa ^{77a,77b}, A. Ivina ¹⁶⁸, J.M. Izen ⁴⁵,
 V. Izzo ^{71a}, P. Jacka ^{130,131}, P. Jackson ¹, R.M. Jacobs ⁴⁸, B.P. Jaeger ¹⁴¹, C.S. Jagfeld ¹⁰⁸,
 G. Jäkel ¹⁷⁰, K. Jakobs ⁵⁴, T. Jakoubek ¹⁶⁸, J. Jamieson ⁵⁹, K.W. Janas ^{84a}, G. Jarlskog ⁹⁷,
 A.E. Jaspan ⁹¹, T. Javůrek ³⁶, M. Javurkova ¹⁰², F. Jeanneau ¹³⁴, L. Jeanty ¹²², J. Jejelava ^{148a,z},
 P. Jenni ^{54,f}, C.E. Jessiman ³⁴, S. Jézéquel ⁴, J. Jia ¹⁴⁴, X. Jia ⁶¹, X. Jia ^{14a,14d}, Z. Jia ^{14c},
 Y. Jiang ^{62a}, S. Jiggins ⁵², J. Jimenez Pena ¹⁰⁹, S. Jin ^{14c}, A. Jinaru ^{27b}, O. Jinnouchi ¹⁵³,
 H. Jivan ^{33g}, P. Johansson ¹³⁸, K.A. Johns ⁷, C.A. Johnson ⁶⁷, D.M. Jones ³², E. Jones ¹⁶⁶,
 R.W.L. Jones ⁹⁰, T.J. Jones ⁹¹, J. Jovicevic ¹⁵, X. Ju ^{17a}, J.J. Junggeburth ³⁶, A. Juste Rozas ^{13,u},
 S. Kabana ^{136e}, A. Kaczmarek ⁸⁵, M. Kado ^{74a,74b}, H. Kagan ¹¹⁸, M. Kagan ¹⁴², A. Kahn ⁴¹,
 A. Kahn ¹²⁷, C. Kahra ⁹⁹, T. Kaji ¹⁶⁷, E. Kajomovitz ¹⁴⁹, N. Kakati ¹⁶⁸, C.W. Kalderon ²⁹,
 A. Kamenshchikov ¹⁵⁴, N.J. Kang ¹³⁵, Y. Kano ¹¹⁰, D. Kar ^{33g}, K. Karava ¹²⁵,
 M.J. Kareem ^{155b}, E. Karentzos ⁵⁴, I. Karkanas ¹⁵¹, S.N. Karpov ³⁸, Z.M. Karpova ³⁸,
 V. Kartvelishvili ⁹⁰, A.N. Karyukhin ³⁷, E. Kasimi ¹⁵¹, C. Kato ^{62d}, J. Katzy ⁴⁸, S. Kaur ³⁴,
 K. Kawade ¹³⁹, K. Kawagoe ⁸⁸, T. Kawaguchi ¹¹⁰, T. Kawamoto ¹³⁴, G. Kawamura ⁵⁵,
 E.F. Kay ¹⁶⁴, F.I. Kaya ¹⁵⁷, S. Kazakos ¹³, V.F. Kazanin ³⁷, Y. Ke ¹⁴⁴, J.M. Keaveney ^{33a},
 R. Keeler ¹⁶⁴, G.V. Kehris ⁶¹, J.S. Keller ³⁴, A.S. Kelly ⁹⁵, D. Kelsey ¹⁴⁵, J.J. Kempster ²⁰,
 J. Kendrick ²⁰, K.E. Kennedy ⁴¹, O. Kepka ¹³⁰, B.P. Kerridge ¹⁶⁶, S. Kersten ¹⁷⁰,
 B.P. Kerševan ⁹², L. Keszeghova ^{28a}, S. Ketabchi Haghighat ¹⁵⁴, M. Khandoga ¹²⁶,

A. Khanov ¹²⁰, A.G. Kharlamov ³⁷, T. Kharlamova ³⁷, E.E. Khoda ¹³⁷, T.J. Khoo ¹⁸,
 G. Khorauli ¹⁶⁵, J. Khubua ^{148b}, Y.A.R. Khwaira ⁶⁶, M. Kiehn ³⁶, A. Kilgallon ¹²², E. Kim ¹⁵³,
 Y.K. Kim ³⁹, N. Kimura ⁹⁵, A. Kirchhoff ⁵⁵, D. Kirchmeier ⁵⁰, C. Kirfel ²⁴, J. Kirk ¹³³,
 A.E. Kiryunin ¹⁰⁹, T. Kishimoto ¹⁵², D.P. Kisliuk ¹⁵⁴, C. Kitsaki ¹⁰, O. Kivernyk ²⁴,
 M. Klassen ^{63a}, C. Klein ³⁴, L. Klein ¹⁶⁵, M.H. Klein ¹⁰⁵, M. Klein ⁹¹, U. Klein ⁹¹,
 P. Klimek ³⁶, A. Klimentov ²⁹, F. Klimpel ¹⁰⁹, T. Klingl ²⁴, T. Klioutchnikova ³⁶,
 F.F. Klitzner ¹⁰⁸, P. Kluit ¹¹³, S. Kluth ¹⁰⁹, E. Kneringer ⁷⁸, T.M. Knight ¹⁵⁴, A. Knue ⁵⁴,
 D. Kobayashi ⁸⁸, R. Kobayashi ⁸⁶, M. Kocian ¹⁴², T. Kodama ¹⁵², P. Kodyš ¹³², D.M. Koeck ¹⁴⁵,
 P.T. Koenig ²⁴, T. Koffas ³⁴, N.M. Köhler ³⁶, M. Kolb ¹³⁴, I. Koletsou ⁴, T. Komarek ¹²¹,
 K. Köneke ⁵⁴, A.X.Y. Kong ¹, T. Kono ¹¹⁷, N. Konstantinidis ⁹⁵, B. Konya ⁹⁷,
 R. Kopeliansky ⁶⁷, S. Koperny ^{84a}, K. Korcyl ⁸⁵, K. Kordas ¹⁵¹, G. Koren ¹⁵⁰, A. Korn ⁹⁵,
 S. Korn ⁵⁵, I. Korolkov ¹³, N. Korotkova ³⁷, B. Kortman ¹¹³, O. Kortner ¹⁰⁹, S. Kortner ¹⁰⁹,
 W.H. Kostecka ¹¹⁴, V.V. Kostyukhin ^{140,37}, A. Kotsokechagia ⁶⁶, A. Kotwal ⁵¹, A. Koulouris ³⁶,
 A. Kourkoumeli-Charalampidi ^{72a,72b}, C. Kourkoumelis ⁹, E. Kourlitis ⁶, O. Kovanda ¹⁴⁵,
 R. Kowalewski ¹⁶⁴, W. Kozanecki ¹³⁴, A.S. Kozhin ³⁷, V.A. Kramarenko ³⁷, G. Kramberger ⁹²,
 P. Kramer ⁹⁹, M.W. Krasny ¹²⁶, A. Krasznahorkay ³⁶, J.A. Kremer ⁹⁹, J. Kretschmar ⁹¹,
 K. Kreul ¹⁸, P. Krieger ¹⁵⁴, F. Krieter ¹⁰⁸, S. Krishnamurthy ¹⁰², A. Krishnan ^{63b}, M. Krivos ¹³²,
 K. Krizka ^{17a}, K. Kroeninger ⁴⁹, H. Kroha ¹⁰⁹, J. Kroll ¹³⁰, J. Kroll ¹²⁷, K.S. Krowpman ¹⁰⁶,
 U. Kruchonak ³⁸, H. Krüger ²⁴, N. Krumnack ⁸⁰, M.C. Kruse ⁵¹, J.A. Krzysiak ⁸⁵, A. Kubota ¹⁵³,
 O. Kuchinskaia ³⁷, S. Kuday ^{3a}, D. Kuechler ⁴⁸, J.T. Kuechler ⁴⁸, S. Kuehn ³⁶, T. Kuhl ⁴⁸,
 V. Kukhtin ³⁸, Y. Kulchitsky ^{37,a}, S. Kuleshov ^{136d,136b}, M. Kumar ^{33g}, N. Kumari ¹⁰¹,
 M. Kuna ⁶⁰, A. Kupco ¹³⁰, T. Kupfer ⁴⁹, A. Kupich ³⁷, O. Kuprash ⁵⁴, H. Kurashige ⁸³,
 L.L. Kurchaninov ^{155a}, Y.A. Kurochkin ³⁷, A. Kurova ³⁷, E.S. Kuwertz ³⁶, M. Kuze ¹⁵³,
 A.K. Kvam ¹³⁷, J. Kvita ¹²¹, T. Kwan ¹⁰³, K.W. Kwok ^{64a}, C. Lacasta ¹⁶², F. Lacava ^{74a,74b},
 H. Lacker ¹⁸, D. Lacour ¹²⁶, N.N. Lad ⁹⁵, E. Ladygin ³⁸, B. Laforge ¹²⁶, T. Lagouri ^{136e},
 S. Lai ⁵⁵, I.K. Lakomic ^{84a}, N. Lalloue ⁶⁰, J.E. Lambert ¹¹⁹, S. Lammers ⁶⁷, W. Lampl ⁷,
 C. Lampoudis ¹⁵¹, A.N. Lancaster ¹¹⁴, E. Lançon ²⁹, U. Landgraf ⁵⁴, M.P.J. Landon ⁹³,
 V.S. Lang ⁵⁴, R.J. Langenberg ¹⁰², A.J. Lankford ¹⁵⁹, F. Lanni ²⁹, K. Lantzsch ²⁴, A. Lanza ^{72a},
 A. Lapertosa ^{57b,57a}, J.F. Laporte ¹³⁴, T. Lari ^{70a}, F. Lasagni Manghi ^{23b}, M. Lassnig ³⁶,
 V. Latonova ¹³⁰, T.S. Lau ^{64a}, A. Laudrain ⁹⁹, A. Laurier ³⁴, S.D. Lawlor ⁹⁴, Z. Lawrence ¹⁰⁰,
 M. Lazzaroni ^{70a,70b}, B. Le ¹⁰⁰, B. Leban ⁹², A. Lebedev ⁸⁰, M. LeBlanc ³⁶, T. LeCompte ⁶,
 F. Ledroit-Guillon ⁶⁰, A.C.A. Lee ⁹⁵, G.R. Lee ¹⁶, L. Lee ⁶¹, S.C. Lee ¹⁴⁷, S. Lee ^{47a,47b},
 L.L. Leeuw ^{33c}, B. Lefebvre ^{155a}, H.P. Lefebvre ⁹⁴, M. Lefebvre ¹⁶⁴, C. Leggett ^{17a},
 K. Lehmann ¹⁴¹, G. Lehmann Miotto ³⁶, W.A. Leight ¹⁰², A. Leisos ^{151,t}, M.A.L. Leite ^{81c},
 C.E. Leitgeb ⁴⁸, R. Leitner ¹³², K.J.C. Leney ⁴⁴, T. Lenz ²⁴, S. Leone ^{73a}, C. Leonidopoulos ⁵²,
 A. Leopold ¹⁴³, C. Leroy ¹⁰⁷, R. Les ¹⁰⁶, C.G. Lester ³², M. Levchenko ³⁷, J. Levêque ⁴,
 D. Levin ¹⁰⁵, L.J. Levinson ¹⁶⁸, D.J. Lewis ²⁰, B. Li ^{14b}, B. Li ^{62b}, C. Li ^{62a}, C-Q. Li ^{62c,62d},
 H. Li ^{62a}, H. Li ^{62b}, H. Li ^{14c}, H. Li ^{62b}, J. Li ^{62c}, K. Li ¹³⁷, L. Li ^{62c}, M. Li ^{14a,14d},
 Q.Y. Li ^{62a}, S. Li ^{62d,62c,d}, T. Li ^{62b}, X. Li ¹⁰³, Z. Li ^{62b}, Z. Li ¹²⁵, Z. Li ¹⁰³, Z. Li ⁹¹,
 Z. Liang ^{14a}, M. Liberatore ⁴⁸, B. Liberti ^{75a}, K. Lie ^{64c}, J. Lieber Marin ^{81b}, H. Lin ⁶⁵,
 K. Lin ¹⁰⁶, R.A. Linck ⁶⁷, R.E. Lindley ⁷, J.H. Lindon ², A. Linss ⁴⁸, E. Lipeles ¹²⁷,
 A. Lipniacka ¹⁶, T.M. Liss ^{161,af}, A. Lister ¹⁶³, J.D. Little ⁴, B. Liu ^{14a}, B.X. Liu ¹⁴¹,
 D. Liu ^{62d,62c}, J.B. Liu ^{62a}, J.K.K. Liu ³², K. Liu ^{62d,62c}, M. Liu ^{62a}, M.Y. Liu ^{62a}, P. Liu ^{14a},
 Q. Liu ^{62d,137,62c}, X. Liu ^{62a}, Y. Liu ⁴⁸, Y. Liu ^{14c,14d}, Y.L. Liu ¹⁰⁵, Y.W. Liu ^{62a},
 M. Livan ^{72a,72b}, J. Llorente Merino ¹⁴¹, S.L. Lloyd ⁹³, E.M. Lobodzinska ⁴⁸, P. Loch ⁷,
 S. Loffredo ^{75a,75b}, T. Lohse ¹⁸, K. Lohwasser ¹³⁸, M. Lokajicek ^{130,*}, J.D. Long ¹⁶¹,
 I. Longarini ^{74a,74b}, L. Longo ^{69a,69b}, R. Longo ¹⁶¹, I. Lopez Paz ³⁶, A. Lopez Solis ⁴⁸,

J. Lorenz ¹⁰⁸, N. Lorenzo Martinez ⁴, A.M. Lory ¹⁰⁸, A. Lösle ⁵⁴, X. Lou ^{47a,47b}, X. Lou ^{14a,14d}, A. Lounis ⁶⁶, J. Love ⁶, P.A. Love ⁹⁰, J.J. Lozano Bahilo ¹⁶², G. Lu ^{14a,14d}, M. Lu ⁷⁹, S. Lu ¹²⁷, Y.J. Lu ⁶⁵, H.J. Lubatti ¹³⁷, C. Luci ^{74a,74b}, F.L. Lucio Alves ^{14c}, A. Lucotte ⁶⁰, F. Luehring ⁶⁷, I. Luise ¹⁴⁴, O. Lukianchuk ⁶⁶, O. Lundberg ¹⁴³, B. Lund-Jensen ¹⁴³, N.A. Luongo ¹²², M.S. Lutz ¹⁵⁰, D. Lynn ²⁹, H. Lyons ⁹¹, R. Lysak ¹³⁰, E. Lytken ⁹⁷, F. Lyu ^{14a}, V. Lyubushkin ³⁸, T. Lyubushkina ³⁸, H. Ma ²⁹, L.L. Ma ^{62b}, Y. Ma ⁹⁵, D.M. Mac Donell ¹⁶⁴, G. Maccarrone ⁵³, J.C. MacDonald ¹³⁸, R. Madar ⁴⁰, W.F. Mader ⁵⁰, J. Maeda ⁸³, T. Maeno ²⁹, M. Maerker ⁵⁰, V. Magerl ⁵⁴, J. Magro ^{68a,68c}, D.J. Mahon ⁴¹, C. Maidantchik ^{81b}, A. Maio ^{129a,129b,129d}, K. Maj ^{84a}, O. Majersky ^{28a}, S. Majewski ¹²², N. Makovec ⁶⁶, V. Maksimovic ¹⁵, B. Malaescu ¹²⁶, Pa. Malecki ⁸⁵, V.P. Maleev ³⁷, F. Malek ⁶⁰, D. Malito ^{43b,43a}, U. Mallik ⁷⁹, C. Malone ³², S. Maltezos ¹⁰, S. Malyukov ³⁸, J. Mamuzic ¹¹⁹, G. Mancini ⁵³, J.P. Mandalia ⁹³, I. Mandić ⁹², L. Manhaes de Andrade Filho ^{81a}, I.M. Maniatis ¹⁵¹, M. Manisha ¹³⁴, J. Manjarres Ramos ⁵⁰, D.C. Mankad ¹⁶⁸, K.H. Mankinen ⁹⁷, A. Mann ¹⁰⁸, A. Manousos ⁷⁸, B. Mansoulie ¹³⁴, S. Manzoni ³⁶, A. Marantis ^{151,t}, G. Marchiori ⁵, M. Marcisovsky ¹³⁰, L. Marcoccia ^{75a,75b}, C. Marcon ⁹⁷, M. Marinescu ²⁰, M. Marjanovic ¹¹⁹, Z. Marshall ^{17a}, S. Marti-Garcia ¹⁶², T.A. Martin ¹⁶⁶, V.J. Martin ⁵², B. Martin dit Latour ¹⁶, L. Martinelli ^{74a,74b}, M. Martinez ^{13,u}, P. Martinez Agullo ¹⁶², V.I. Martinez Outschoorn ¹⁰², P. Martinez Suarez ¹³, S. Martin-Haugh ¹³³, V.S. Martoiu ^{27b}, A.C. Martyniuk ⁹⁵, A. Marzin ³⁶, S.R. Maschek ¹⁰⁹, L. Masetti ⁹⁹, T. Mashimo ¹⁵², J. Masik ¹⁰⁰, A.L. Maslennikov ³⁷, L. Massa ^{23b}, P. Massarotti ^{71a,71b}, P. Mastrandrea ^{73a,73b}, A. Mastroberardino ^{43b,43a}, T. Masubuchi ¹⁵², T. Mathisen ¹⁶⁰, A. Matic ¹⁰⁸, N. Matsuzawa ¹⁵², J. Maurer ^{27b}, B. Maček ⁹², D.A. Maximov ³⁷, R. Mazini ¹⁴⁷, I. Maznas ¹⁵¹, M. Mazza ¹⁰⁶, S.M. Mazza ¹³⁵, C. Mc Ginn ²⁹, J.P. Mc Gowan ¹⁰³, S.P. Mc Kee ¹⁰⁵, T.G. McCarthy ¹⁰⁹, W.P. McCormack ^{17a}, E.F. McDonald ¹⁰⁴, A.E. McDougall ¹¹³, J.A. Mcfayden ¹⁴⁵, G. Mchedlidze ^{148b}, R.P. Mckenzie ^{33g}, D.J. Mclaughlin ⁹⁵, K.D. McLean ¹⁶⁴, S.J. McMahon ¹³³, P.C. McNamara ¹⁰⁴, R.A. McPherson ^{164,x}, J.E. Mdhluli ^{33g}, S. Meehan ³⁶, T. Megy ⁴⁰, S. Mehlhase ¹⁰⁸, A. Mehta ⁹¹, B. Meirose ⁴⁵, D. Melini ¹⁴⁹, B.R. Mellado Garcia ^{33g}, A.H. Melo ⁵⁵, F. Meloni ⁴⁸, E.D. Mendes Gouveia ^{129a}, A.M. Mendes Jacques Da Costa ²⁰, H.Y. Meng ¹⁵⁴, L. Meng ⁹⁰, S. Menke ¹⁰⁹, M. Mentink ³⁶, E. Meoni ^{43b,43a}, C. Merlassino ¹²⁵, L. Merola ^{71a,71b}, C. Meroni ^{70a}, G. Merz ¹⁰⁵, O. Meshkov ³⁷, J.K.R. Meshreki ¹⁴⁰, J. Metcalfe ⁶, A.S. Mete ⁶, C. Meyer ⁶⁷, J-P. Meyer ¹³⁴, M. Michetti ¹⁸, R.P. Middleton ¹³³, L. Mijović ⁵², G. Mikenberg ¹⁶⁸, M. Mikestikova ¹³⁰, M. Mikuž ⁹², H. Mildner ¹³⁸, A. Milic ¹⁵⁴, C.D. Milke ⁴⁴, D.W. Miller ³⁹, L.S. Miller ³⁴, A. Milov ¹⁶⁸, D.A. Milstead ^{47a,47b}, T. Min ^{14c}, A.A. Minaenko ³⁷, I.A. Minashvili ^{148b}, L. Mince ⁵⁹, A.I. Mincer ¹¹⁶, B. Mindur ^{84a}, M. Mineev ³⁸, Y. Minegishi ¹⁵², Y. Mino ⁸⁶, L.M. Mir ¹³, M. Miralles Lopez ¹⁶², M. Mironova ¹²⁵, T. Mitani ¹⁶⁷, A. Mitra ¹⁶⁶, V.A. Mitsou ¹⁶², O. Miu ¹⁵⁴, P.S. Miyagawa ⁹³, Y. Miyazaki ⁸⁸, A. Mizukami ⁸², J.U. Mjörnmark ⁹⁷, T. Mkrtchyan ^{63a}, M. Mlynarikova ¹¹⁴, T. Moa ^{47a,47b}, S. Mobius ⁵⁵, K. Mochizuki ¹⁰⁷, P. Moder ⁴⁸, P. Mogg ¹⁰⁸, A.F. Mohammed ^{14a,14d}, S. Mohapatra ⁴¹, G. Mokgatitwane ^{33g}, B. Mondal ¹⁴⁰, S. Mondal ¹³¹, K. Mönig ⁴⁸, E. Monnier ¹⁰¹, L. Monsonis Romero ¹⁶², J. Montejo Berlingen ³⁶, M. Montella ¹¹⁸, F. Monticelli ⁸⁹, N. Morange ⁶⁶, A.L. Moreira De Carvalho ^{129a}, M. Moreno Llácer ¹⁶², C. Moreno Martinez ¹³, P. Morettini ^{57b}, S. Morgenstern ¹⁶⁶, M. Morii ⁶¹, M. Morinaga ¹⁵², V. Morisbak ¹²⁴, A.K. Morley ³⁶, F. Morodei ^{74a,74b}, L. Morvaj ³⁶, P. Moschovakos ³⁶, B. Moser ¹¹³, M. Mosidze ^{148b}, T. Moskalets ⁵⁴, P. Moskvitina ¹¹², J. Moss ^{31,n}, E.J.W. Moyses ¹⁰², S. Muanza ¹⁰¹, J. Mueller ¹²⁸, D. Muenstermann ⁹⁰, R. Müller ¹⁹, G.A. Mullier ⁹⁷, J.J. Mullin ¹²⁷, D.P. Mungo ^{70a,70b}, J.L. Munoz Martinez ¹³, F.J. Munoz Sanchez ¹⁰⁰, M. Murin ¹⁰⁰, W.J. Murray ^{166,133}, A. Murrone ^{70a,70b}, J.M. Muse ¹¹⁹, M. Muškinja ^{17a}, C. Mwewa ²⁹,

A.G. Myagkov [ID37,a](#), A.J. Myers [ID8](#), A.A. Myers [ID128](#), G. Myers [ID67](#), M. Myska [ID131](#), B.P. Nachman [ID17a](#),
 O. Nackenhorst [ID49](#), A. Nag [ID50](#), K. Nagai [ID125](#), K. Nagano [ID82](#), J.L. Nagle [ID29,ak](#), E. Nagy [ID101](#),
 A.M. Nairz [ID36](#), Y. Nakahama [ID82](#), K. Nakamura [ID82](#), H. Nanjo [ID123](#), R. Narayan [ID44](#),
 E.A. Narayanan [ID111](#), I. Naryshkin [ID37](#), M. Naseri [ID34](#), C. Nass [ID24](#), G. Navarro [ID22a](#),
 J. Navarro-Gonzalez [ID162](#), R. Nayak [ID150](#), P.Y. Nechaeva [ID37](#), F. Nechansky [ID48](#), T.J. Neep [ID20](#),
 A. Negri [ID72a,72b](#), M. Negrini [ID23b](#), C. Nellist [ID112](#), C. Nelson [ID103](#), K. Nelson [ID105](#), S. Nemecek [ID130](#),
 M. Nessi [ID36,g](#), M.S. Neubauer [ID161](#), F. Neuhaus [ID99](#), J. Neundorf [ID48](#), R. Newhouse [ID163](#),
 P.R. Newman [ID20](#), C.W. Ng [ID128](#), Y.S. Ng [ID18](#), Y.W.Y. Ng [ID159](#), B. Ngair [ID35e](#), H.D.N. Nguyen [ID107](#),
 R.B. Nickerson [ID125](#), R. Nicolaidou [ID134](#), J. Nielsen [ID135](#), M. Niemeyer [ID55](#), N. Nikiforou [ID36](#),
 V. Nikolaenko [ID37,a](#), I. Nikolic-Audit [ID126](#), K. Nikolopoulos [ID20](#), P. Nilsson [ID29](#), H.R. Nindhito [ID56](#),
 A. Nisati [ID74a](#), N. Nishu [ID2](#), R. Nisius [ID109](#), J-E. Nitschke [ID50](#), E.K. Nkadimeng [ID33g](#),
 S.J. Noacco Rosende [ID89](#), T. Nobe [ID152](#), D.L. Noel [ID32](#), Y. Noguchi [ID86](#), M.A. Nomura [ID29](#),
 M.B. Norfolk [ID138](#), R.R.B. Norisam [ID95](#), B.J. Norman [ID34](#), J. Novak [ID92](#), T. Novak [ID48](#),
 O. Novgorodova [ID50](#), L. Novotny [ID131](#), R. Novotny [ID111](#), L. Nozka [ID121](#), K. Ntekas [ID159](#), E. Nurse [ID95](#),
 F.G. Oakham [ID34,ah](#), J. Ocariz [ID126](#), A. Ochi [ID83](#), I. Ochoa [ID129a](#), S. Oda [ID88](#), S. Oerdek [ID160](#),
 A. Ogrodnik [ID84a](#), A. Oh [ID100](#), C.C. Ohm [ID143](#), H. Oide [ID153](#), R. Oishi [ID152](#), M.L. Ojeda [ID48](#),
 Y. Okazaki [ID86](#), M.W. O'Keefe [ID91](#), Y. Okumura [ID152](#), A. Olariu [ID27b](#), L.F. Oleiro Seabra [ID129a](#),
 S.A. Olivares Pino [ID136e](#), D. Oliveira Damazio [ID29](#), D. Oliveira Goncalves [ID81a](#), J.L. Oliver [ID159](#),
 M.J.R. Olsson [ID159](#), A. Olszewski [ID85](#), J. Olszowska [ID85,*](#), Ö.O. Öncel [ID54](#), D.C. O'Neil [ID141](#),
 A.P. O'Neill [ID19](#), A. Onofre [ID129a,129e](#), P.U.E. Onyisi [ID11](#), M.J. Oreglia [ID39](#), G.E. Orellana [ID89](#),
 D. Orestano [ID76a,76b](#), N. Orlando [ID13](#), R.S. Orr [ID154](#), V. O'Shea [ID59](#), R. Ospanov [ID62a](#),
 G. Otero y Garzon [ID30](#), H. Otono [ID88](#), P.S. Ott [ID63a](#), G.J. Ottino [ID17a](#), M. Ouchrif [ID35d](#),
 J. Ouellette [ID29,ak](#), F. Ould-Saada [ID124](#), M. Owen [ID59](#), R.E. Owen [ID133](#), K.Y. Oyulmaz [ID21a](#),
 V.E. Ozcan [ID21a](#), N. Ozturk [ID8](#), S. Ozturk [ID21d](#), J. Pacalt [ID121](#), H.A. Pacey [ID32](#), K. Pachal [ID51](#),
 A. Pacheco Pages [ID13](#), C. Padilla Aranda [ID13](#), G. Padovano [ID74a,74b](#), S. Pagan Griso [ID17a](#),
 G. Palacino [ID67](#), A. Palazzo [ID69a,69b](#), S. Palazzo [ID52](#), S. Palestini [ID36](#), M. Palka [ID84b](#), J. Pan [ID171](#),
 D.K. Panchal [ID11](#), C.E. Pandini [ID113](#), J.G. Panduro Vazquez [ID94](#), P. Pani [ID48](#), G. Panizzo [ID68a,68c](#),
 L. Paolozzi [ID56](#), C. Papadatos [ID107](#), S. Parajuli [ID44](#), A. Paramonov [ID6](#), C. Paraskevopoulos [ID10](#),
 D. Paredes Hernandez [ID64b](#), T.H. Park [ID154](#), M.A. Parker [ID32](#), F. Parodi [ID57b,57a](#), E.W. Parrish [ID114](#),
 V.A. Parrish [ID52](#), J.A. Parsons [ID41](#), U. Parzefall [ID54](#), B. Pascual Dias [ID107](#), L. Pascual Dominguez [ID150](#),
 V.R. Pascuzzi [ID17a](#), F. Pasquali [ID113](#), E. Pasqualucci [ID74a](#), S. Passaggio [ID57b](#), F. Pastore [ID94](#),
 P. Pasuwan [ID47a,47b](#), J.R. Pater [ID100](#), J. Patton [ID91](#), T. Pauly [ID36](#), J. Pearkes [ID142](#), M. Pedersen [ID124](#),
 R. Pedro [ID129a](#), S.V. Peleganchuk [ID37](#), O. Penc [ID130](#), C. Peng [ID64b](#), H. Peng [ID62a](#), M. Penzin [ID37](#),
 B.S. Peralva [ID81a](#), A.P. Pereira Peixoto [ID60](#), L. Pereira Sanchez [ID47a,47b](#), D.V. Perepelitsa [ID29,ak](#),
 E. Perez Codina [ID155a](#), M. Perganti [ID10](#), L. Perini [ID70a,70b,*](#), H. Pernegger [ID36](#), S. Perrella [ID36](#),
 A. Perrevoort [ID112](#), O. Perrin [ID40](#), K. Peters [ID48](#), R.F.Y. Peters [ID100](#), B.A. Petersen [ID36](#),
 T.C. Petersen [ID42](#), E. Petit [ID101](#), V. Petousis [ID131](#), C. Petridou [ID151](#), A. Petrukhin [ID140](#), M. Pettee [ID17a](#),
 N.E. Pettersson [ID36](#), A. Petukhov [ID37](#), K. Petukhova [ID132](#), A. Peyaud [ID134](#), R. Pezoa [ID136f](#),
 L. Pezzotti [ID36](#), G. Pezzullo [ID171](#), T. Pham [ID104](#), P.W. Phillips [ID133](#), M.W. Phipps [ID161](#),
 G. Piacquadio [ID144](#), E. Pianori [ID17a](#), F. Piazza [ID70a,70b](#), R. Piegaia [ID30](#), D. Pietreanu [ID27b](#),
 A.D. Pilkington [ID100](#), M. Pinamonti [ID68a,68c](#), J.L. Pinfeld [ID2](#), C. Pitman Donaldson [ID95](#), D.A. Pizzi [ID34](#),
 L. Pizzimento [ID75a,75b](#), A. Pizzini [ID113](#), M.-A. Pleier [ID29](#), V. Plesanovs [ID54](#), V. Pleskot [ID132](#),
 E. Plotnikova [ID38](#), G. Poddar [ID4](#), R. Poettgen [ID97](#), R. Poggi [ID56](#), L. Poggioli [ID126](#), I. Pogrebnyak [ID106](#),
 D. Pohl [ID24](#), I. Pokharel [ID55](#), S. Polacek [ID132](#), G. Polesello [ID72a](#), A. Poley [ID141,155a](#), R. Polifka [ID131](#),
 A. Polini [ID23b](#), C.S. Pollard [ID125](#), Z.B. Pollock [ID118](#), V. Polychronakos [ID29](#), D. Ponomarenko [ID37](#),
 L. Pontecorvo [ID36](#), S. Popa [ID27a](#), G.A. Popeneciu [ID27d](#), D.M. Portillo Quintero [ID155a](#), S. Pospisil [ID131](#),
 P. Postolache [ID27c](#), K. Potamianos [ID125](#), I.N. Potrap [ID38](#), C.J. Potter [ID32](#), H. Potti [ID1](#), T. Poulsen [ID48](#),

J. Poveda [ID](#)¹⁶², G. Pownall [ID](#)⁴⁸, M.E. Pozo Astigarraga [ID](#)³⁶, A. Prades Ibanez [ID](#)¹⁶², M.M. Prapa [ID](#)⁴⁶,
 J. Pretel [ID](#)⁵⁴, D. Price [ID](#)¹⁰⁰, M. Primavera [ID](#)^{69a}, M.A. Principe Martin [ID](#)⁹⁸, M.L. Proffitt [ID](#)¹³⁷,
 N. Proklova [ID](#)³⁷, K. Prokofiev [ID](#)^{64c}, G. Proto [ID](#)^{75a,75b}, S. Protopopescu [ID](#)²⁹, J. Proudfoot [ID](#)⁶,
 M. Przybycien [ID](#)^{84a}, J.E. Puddefoot [ID](#)¹³⁸, D. Pudzha [ID](#)³⁷, P. Puzo⁶⁶, D. Pyatiizbyantseva [ID](#)³⁷,
 J. Qian [ID](#)¹⁰⁵, Y. Qin [ID](#)¹⁰⁰, T. Qiu [ID](#)⁹³, A. Quadt [ID](#)⁵⁵, M. Queitsch-Maitland [ID](#)²⁴, G. Rabanal Bolanos [ID](#)⁶¹,
 D. Rafanoharana [ID](#)⁵⁴, F. Ragusa [ID](#)^{70a,70b}, J.L. Rainbolt [ID](#)³⁹, J.A. Raine [ID](#)⁵⁶, S. Rajagopalan [ID](#)²⁹,
 E. Ramakoti [ID](#)³⁷, K. Ran [ID](#)^{14a,14d}, V. Raskina [ID](#)¹²⁶, D.F. Rassloff [ID](#)^{63a}, S. Rave [ID](#)⁹⁹, B. Ravina [ID](#)⁵⁹,
 I. Ravinovich [ID](#)¹⁶⁸, M. Raymond [ID](#)³⁶, A.L. Read [ID](#)¹²⁴, N.P. Readioff [ID](#)¹³⁸, D.M. Rebutti [ID](#)^{72a,72b},
 G. Redlinger [ID](#)²⁹, K. Reeves [ID](#)⁴⁵, J.A. Reidelsturz [ID](#)¹⁷⁰, D. Reikher [ID](#)¹⁵⁰, A. Reiss⁹⁹, A. Rej [ID](#)¹⁴⁰,
 C. Rembser [ID](#)³⁶, A. Renardi [ID](#)⁴⁸, M. Renda [ID](#)^{27b}, M.B. Rendel¹⁰⁹, A.G. Rennie [ID](#)⁵⁹, S. Resconi [ID](#)^{70a},
 M. Ressegotti [ID](#)^{57b,57a}, E.D. Resseguie [ID](#)^{17a}, S. Rettie [ID](#)⁹⁵, B. Reynolds¹¹⁸, E. Reynolds [ID](#)^{17a},
 M. Rezaei Estabragh [ID](#)¹⁷⁰, O.L. Rezanova [ID](#)³⁷, P. Reznicek [ID](#)¹³², E. Ricci [ID](#)^{77a,77b}, R. Richter [ID](#)¹⁰⁹,
 S. Richter [ID](#)^{47a,47b}, E. Richter-Was [ID](#)^{84b}, M. Ridel [ID](#)¹²⁶, P. Rieck [ID](#)¹¹⁶, P. Riedler [ID](#)³⁶,
 M. Rijssenbeek [ID](#)¹⁴⁴, A. Rimoldi [ID](#)^{72a,72b}, M. Rimoldi [ID](#)⁴⁸, L. Rinaldi [ID](#)^{23b,23a}, T.T. Rinn [ID](#)¹⁶¹,
 M.P. Rinnagel [ID](#)¹⁰⁸, G. Ripellino [ID](#)¹⁴³, I. Riu [ID](#)¹³, P. Rivadeneira [ID](#)⁴⁸, J.C. Rivera Vergara [ID](#)¹⁶⁴,
 F. Rizatdinova [ID](#)¹²⁰, E. Rizvi [ID](#)⁹³, C. Rizzi [ID](#)⁵⁶, B.A. Roberts [ID](#)¹⁶⁶, B.R. Roberts [ID](#)^{17a},
 S.H. Robertson [ID](#)^{103,x}, M. Robin [ID](#)⁴⁸, D. Robinson [ID](#)³², C.M. Robles Gajardo^{136f},
 M. Robles Manzano [ID](#)⁹⁹, A. Robson [ID](#)⁵⁹, A. Rocchi [ID](#)^{75a,75b}, C. Roda [ID](#)^{73a,73b}, S. Rodriguez Bosca [ID](#)^{63a},
 Y. Rodriguez Garcia [ID](#)^{22a}, A. Rodriguez Rodriguez [ID](#)⁵⁴, A.M. Rodríguez Vera [ID](#)^{155b}, S. Roe³⁶,
 J.T. Roemer [ID](#)¹⁵⁹, A.R. Roepe-Gier [ID](#)¹¹⁹, J. Roggel [ID](#)¹⁷⁰, O. Røhne [ID](#)¹²⁴, R.A. Rojas [ID](#)¹⁶⁴,
 B. Roland [ID](#)⁵⁴, C.P.A. Roland [ID](#)⁶⁷, J. Roloff [ID](#)²⁹, A. Romaniouk [ID](#)³⁷, M. Romano [ID](#)^{23b},
 A.C. Romero Hernandez [ID](#)¹⁶¹, N. Rompotis [ID](#)⁹¹, L. Roos [ID](#)¹²⁶, S. Rosati [ID](#)^{74a}, B.J. Rosser [ID](#)³⁹,
 E. Rossi [ID](#)⁴, E. Rossi [ID](#)^{71a,71b}, L.P. Rossi [ID](#)^{57b}, L. Rossini [ID](#)⁴⁸, R. Rosten [ID](#)¹¹⁸, M. Rotaru [ID](#)^{27b},
 B. Rottler [ID](#)⁵⁴, D. Rousseau [ID](#)⁶⁶, D. Rousso [ID](#)³², G. Rovelli [ID](#)^{72a,72b}, A. Roy [ID](#)¹⁶¹, A. Rozanov [ID](#)¹⁰¹,
 Y. Rozen [ID](#)¹⁴⁹, X. Ruan [ID](#)^{33g}, A. Rubio Jimenez [ID](#)¹⁶², A.J. Ruby [ID](#)⁹¹, T.A. Ruggeri [ID](#)¹, F. Rühr [ID](#)⁵⁴,
 A. Ruiz-Martinez [ID](#)¹⁶², A. Rummler [ID](#)³⁶, Z. Rurikova [ID](#)⁵⁴, N.A. Rusakovich [ID](#)³⁸, H.L. Russell [ID](#)¹⁶⁴,
 J.P. Rutherford [ID](#)⁷, E.M. Rüttinger [ID](#)¹³⁸, K. Rybacki⁹⁰, M. Rybar [ID](#)¹³², E.B. Rye [ID](#)¹²⁴, A. Ryzhov [ID](#)³⁷,
 J.A. Sabater Iglesias [ID](#)⁵⁶, P. Sabatini [ID](#)¹⁶², L. Sabetta [ID](#)^{74a,74b}, H.F.-W. Sadrozinski [ID](#)¹³⁵,
 F. Safai Tehrani [ID](#)^{74a}, B. Safarzadeh Samani [ID](#)¹⁴⁵, M. Safdari [ID](#)¹⁴², S. Saha [ID](#)¹⁰³, M. Sahinsoy [ID](#)¹⁰⁹,
 M. Saimpert [ID](#)¹³⁴, M. Saito [ID](#)¹⁵², T. Saito [ID](#)¹⁵², D. Salamani [ID](#)³⁶, G. Salamanna [ID](#)^{76a,76b},
 A. Salnikov [ID](#)¹⁴², J. Salt [ID](#)¹⁶², A. Salvador Salas [ID](#)¹³, D. Salvatore [ID](#)^{43b,43a}, F. Salvatore [ID](#)¹⁴⁵,
 A. Salzburger [ID](#)³⁶, D. Sammel [ID](#)⁵⁴, D. Sampsonidis [ID](#)¹⁵¹, D. Sampsonidou [ID](#)^{62d,62c}, J. Sánchez [ID](#)¹⁶²,
 A. Sanchez Pineda [ID](#)⁴, V. Sanchez Sebastian [ID](#)¹⁶², H. Sandaker [ID](#)¹²⁴, C.O. Sander [ID](#)⁴⁸,
 J.A. Sandesara [ID](#)¹⁰², M. Sandhoff [ID](#)¹⁷⁰, C. Sandoval [ID](#)^{22b}, D.P.C. Sankey [ID](#)¹³³, A. Sansoni [ID](#)⁵³,
 C. Santoni [ID](#)⁴⁰, H. Santos [ID](#)^{129a,129b}, S.N. Santpur [ID](#)^{17a}, A. Santra [ID](#)¹⁶⁸, K.A. Saoucha [ID](#)¹³⁸,
 J.G. Saraiva [ID](#)^{129a,129d}, J. Sardain [ID](#)¹⁰¹, O. Sasaki [ID](#)⁸², K. Sato [ID](#)¹⁵⁶, C. Sauer^{63b}, F. Sauerburger [ID](#)⁵⁴,
 E. Sauvan [ID](#)⁴, P. Savard [ID](#)^{154,ah}, R. Sawada [ID](#)¹⁵², C. Sawyer [ID](#)¹³³, L. Sawyer [ID](#)⁹⁶, I. Sayago Galvan¹⁶²,
 C. Sbarra [ID](#)^{23b}, A. Sbrizzi [ID](#)^{23b,23a}, T. Scanlon [ID](#)⁹⁵, J. Schaarschmidt [ID](#)¹³⁷, P. Schacht [ID](#)¹⁰⁹,
 D. Schaefer [ID](#)³⁹, U. Schäfer [ID](#)⁹⁹, A.C. Schaffer [ID](#)⁶⁶, D. Schaile [ID](#)¹⁰⁸, R.D. Schamberger [ID](#)¹⁴⁴,
 E. Schanet [ID](#)¹⁰⁸, C. Scharf [ID](#)¹⁸, V.A. Schegelsky [ID](#)³⁷, D. Scheirich [ID](#)¹³², F. Schenck [ID](#)¹⁸,
 M. Schernau [ID](#)¹⁵⁹, C. Scheulen [ID](#)⁵⁵, C. Schiavi [ID](#)^{57b,57a}, Z.M. Schillaci [ID](#)²⁶, E.J. Schioppa [ID](#)^{69a,69b},
 M. Schioppa [ID](#)^{43b,43a}, B. Schlag [ID](#)⁹⁹, K.E. Schleicher [ID](#)⁵⁴, S. Schlenker [ID](#)³⁶, K. Schmieden [ID](#)⁹⁹,
 C. Schmitt [ID](#)⁹⁹, S. Schmitt [ID](#)⁴⁸, L. Schoeffel [ID](#)¹³⁴, A. Schoening [ID](#)^{63b}, P.G. Scholer [ID](#)⁵⁴, E. Schopf [ID](#)¹²⁵,
 M. Schott [ID](#)⁹⁹, J. Schovancova [ID](#)³⁶, S. Schramm [ID](#)⁵⁶, F. Schroeder [ID](#)¹⁷⁰, H.-C. Schultz-Coulon [ID](#)^{63a},
 M. Schumacher [ID](#)⁵⁴, B.A. Schumm [ID](#)¹³⁵, Ph. Schune [ID](#)¹³⁴, A. Schwartzman [ID](#)¹⁴², T.A. Schwarz [ID](#)¹⁰⁵,
 Ph. Schwemling [ID](#)¹³⁴, R. Schwienhorst [ID](#)¹⁰⁶, A. Sciandra [ID](#)¹³⁵, G. Sciolla [ID](#)²⁶, F. Scuri [ID](#)^{73a}, F. Scutti¹⁰⁴,
 C.D. Sebastiani [ID](#)⁹¹, K. Sedlaczek [ID](#)⁴⁹, P. Seema [ID](#)¹⁸, S.C. Seidel [ID](#)¹¹¹, A. Seiden [ID](#)¹³⁵,

B.D. Seidlitz ⁴¹, T. Seiss ³⁹, C. Seitz ⁴⁸, J.M. Seixas ^{81b}, G. Sekhniadze ^{71a}, S.J. Sekula ⁴⁴,
 L. Selem ⁴, N. Semprini-Cesari ^{23b,23a}, S. Sen ⁵¹, V. Senthilkumar ¹⁶², L. Serin ⁶⁶,
 L. Serkin ^{68a,68b}, M. Sessa ^{76a,76b}, H. Severini ¹¹⁹, S. Sevova ¹⁴², F. Sforza ^{57b,57a}, A. Sfyrla ⁵⁶,
 E. Shabalina ⁵⁵, R. Shaheen ¹⁴³, J.D. Shahinian ¹²⁷, N.W. Shaikh ^{47a,47b}, D. Shaked Renous ¹⁶⁸,
 L.Y. Shan ^{14a}, M. Shapiro ^{17a}, A. Sharma ³⁶, A.S. Sharma ¹⁶³, P. Sharma ⁷⁹, S. Sharma ⁴⁸,
 P.B. Shatalov ³⁷, K. Shaw ¹⁴⁵, S.M. Shaw ¹⁰⁰, P. Sherwood ⁹⁵, L. Shi ⁹⁵, C.O. Shimmin ¹⁷¹,
 Y. Shimogama ¹⁶⁷, J.D. Shinner ⁹⁴, I.P.J. Shipsey ¹²⁵, S. Shirabe ⁶⁰, M. Shiyakova ^{38,w},
 J. Shlomi ¹⁶⁸, M.J. Shochet ³⁹, J. Shojaii ¹⁰⁴, D.R. Shope ¹⁴³, S. Shrestha ¹¹⁸, E.M. Shrif ^{33g},
 M.J. Shroff ¹⁶⁴, P. Sicho ¹³⁰, A.M. Sickles ¹⁶¹, E. Sideras Haddad ^{33g}, O. Sidiropoulou ³⁶,
 A. Sidoti ^{23b}, F. Siegert ⁵⁰, Dj. Sijacki ¹⁵, R. Sikora ^{84a}, F. Sili ⁸⁹, J.M. Silva ²⁰,
 M.V. Silva Oliveira ³⁶, S.B. Silverstein ^{47a}, S. Simion ⁶⁶, R. Simoniello ³⁶, E.L. Simpson ⁵⁹,
 N.D. Simpson ⁹⁷, S. Simsek ^{21d}, S. Sindhu ⁵⁵, P. Sinervo ¹⁵⁴, V. Sinetckii ³⁷, S. Singh ¹⁴¹,
 S. Singh ¹⁵⁴, S. Sinha ⁴⁸, S. Sinha ^{33g}, M. Sioli ^{23b,23a}, I. Siral ¹²², S.Yu. Sivoklov ^{37,*},
 J. Sjölin ^{47a,47b}, A. Skaf ⁵⁵, E. Skorda ⁹⁷, P. Skubic ¹¹⁹, M. Slawinska ⁸⁵, V. Smakhtin ¹⁶⁸,
 B.H. Smart ¹³³, J. Smiesko ¹³², S.Yu. Smirnov ³⁷, Y. Smirnov ³⁷, L.N. Smirnova ^{37,a},
 O. Smirnova ⁹⁷, E.A. Smith ³⁹, H.A. Smith ¹²⁵, J.L. Smith ⁹¹, R. Smith ¹⁴², M. Smizanska ⁹⁰,
 K. Smolek ¹³¹, A. Smykiewicz ⁸⁵, A.A. Snesev ³⁷, H.L. Snoek ¹¹³, S. Snyder ²⁹,
 R. Sobie ^{164,x}, A. Soffer ¹⁵⁰, C.A. Solans Sanchez ³⁶, E.Yu. Soldatov ³⁷, U. Soldevila ¹⁶²,
 A.A. Solodkov ³⁷, S. Solomon ⁵⁴, A. Soloshenko ³⁸, K. Solovieva ⁵⁴, O.V. Solovyanov ³⁷,
 V. Solovyev ³⁷, P. Sommer ¹³⁸, A. Sonay ¹³, W.Y. Song ^{155b}, A. Sopczak ¹³¹, A.L. Soppio ⁹⁵,
 F. Sopkova ^{28b}, V. Sothilingam ^{63a}, S. Sottocornola ^{72a,72b}, R. Soualah ^{115b}, Z. Soumami ^{35e},
 D. South ⁴⁸, S. Spagnolo ^{69a,69b}, M. Spalla ¹⁰⁹, F. Spanò ⁹⁴, D. Sperlich ⁵⁴, G. Spigo ³⁶,
 M. Spina ¹⁴⁵, S. Spinali ⁹⁰, D.P. Spiteri ⁵⁹, M. Spousta ¹³², E.J. Staats ³⁴, A. Stabile ^{70a,70b},
 R. Stamen ^{63a}, M. Stamenkovic ¹¹³, A. Stampekis ²⁰, M. Standke ²⁴, E. Stanecka ⁸⁵,
 B. Stanislaus ^{17a}, M.M. Stanitzki ⁴⁸, M. Stankaityte ¹²⁵, B. Stapf ⁴⁸, E.A. Starchenko ³⁷,
 G.H. Stark ¹³⁵, J. Stark ^{101,aa}, D.M. Starko ^{155b}, P. Staroba ¹³⁰, P. Starovoitov ^{63a}, S. Stärz ¹⁰³,
 R. Staszewski ⁸⁵, G. Stavropoulos ⁴⁶, J. Steentoft ¹⁶⁰, P. Steinberg ²⁹, A.L. Steinhebel ¹²²,
 B. Stelzer ^{141,155a}, H.J. Stelzer ¹²⁸, O. Stelzer-Chilton ^{155a}, H. Stenzel ⁵⁸, T.J. Stevenson ¹⁴⁵,
 G.A. Stewart ³⁶, M.C. Stockton ³⁶, G. Stoicea ^{27b}, M. Stolarski ^{129a}, S. Stonjek ¹⁰⁹,
 A. Straessner ⁵⁰, J. Strandberg ¹⁴³, S. Strandberg ^{47a,47b}, M. Strauss ¹¹⁹, T. Strebler ¹⁰¹,
 P. Striznec ^{28b}, R. Ströhmer ¹⁶⁵, D.M. Strom ¹²², L.R. Strom ⁴⁸, R. Stroynowski ⁴⁴,
 A. Strubig ^{47a,47b}, S.A. Stucci ²⁹, B. Stugu ¹⁶, J. Stupak ¹¹⁹, N.A. Styles ⁴⁸, D. Su ¹⁴²,
 S. Su ^{62a}, W. Su ^{62d,137,62c}, X. Su ^{62a,66}, K. Sugizaki ¹⁵², V.V. Sulin ³⁷, M.J. Sullivan ⁹¹,
 D.M.S. Sultan ^{77a,77b}, L. Sultaniyeva ³⁷, S. Sultansoy ^{3b}, T. Sumida ⁸⁶, S. Sun ¹⁰⁵, S. Sun ¹⁶⁹,
 O. Sunneborn Gudnadottir ¹⁶⁰, M.R. Sutton ¹⁴⁵, M. Svatos ¹³⁰, M. Swiatlowski ^{155a},
 T. Swirski ¹⁶⁵, I. Sykora ^{28a}, M. Sykora ¹³², T. Sykora ¹³², D. Ta ⁹⁹, K. Tackmann ^{48,v},
 A. Taffard ¹⁵⁹, R. Tafirout ^{155a}, J.S. Tafoya Vargas ⁶⁶, R.H.M. Taibah ¹²⁶, R. Takashima ⁸⁷,
 K. Takeda ⁸³, E.P. Takeva ⁵², Y. Takubo ⁸², M. Talby ¹⁰¹, A.A. Talyshv ³⁷, K.C. Tam ^{64b},
 N.M. Tamir ¹⁵⁰, A. Tanaka ¹⁵², J. Tanaka ¹⁵², R. Tanaka ⁶⁶, M. Tanasini ^{57b,57a}, J. Tang ^{62c},
 Z. Tao ¹⁶³, S. Tapia Araya ⁸⁰, S. Tapprogge ⁹⁹, A. Tarek Abouelfadl Mohamed ¹⁰⁶, S. Tarem ¹⁴⁹,
 K. Tariq ^{62b}, G. Tarna ^{27b}, G.F. Tartarelli ^{70a}, P. Tas ¹³², M. Tasevsky ¹³⁰, E. Tassi ^{43b,43a},
 A.C. Tate ¹⁶¹, G. Tateno ¹⁵², Y. Tayalati ^{35e}, G.N. Taylor ¹⁰⁴, W. Taylor ^{155b}, H. Teagle ⁹¹,
 A.S. Tee ¹⁶⁹, R. Teixeira De Lima ¹⁴², P. Teixeira-Dias ⁹⁴, J.J. Teoh ¹⁵⁴, K. Terashi ¹⁵²,
 J. Terron ⁹⁸, S. Terzo ¹³, M. Testa ⁵³, R.J. Teuscher ^{154,x}, N. Themistokleous ⁵²,
 T. Thevenaux-Pelzer ¹⁸, O. Thielmann ¹⁷⁰, D.W. Thomas ⁹⁴, J.P. Thomas ²⁰, E.A. Thompson ⁴⁸,
 P.D. Thompson ²⁰, E. Thomson ¹²⁷, E.J. Thorpe ⁹³, Y. Tian ⁵⁵, V. Tikhomirov ^{37,a},
 Yu.A. Tikhonov ³⁷, S. Timoshenko ³⁷, E.X.L. Ting ¹, P. Tipton ¹⁷¹, S. Tisserant ¹⁰¹, S.H. Tlou ^{33g},

A. Tnourji ^{id40}, K. Todome ^{id23b,23a}, S. Todorova-Nova ^{id132}, S. Todt⁵⁰, M. Togawa ^{id82}, J. Tojo ^{id88},
 S. Tokár ^{id28a}, K. Tokushuku ^{id82}, R. Tombs ^{id32}, M. Tomoto ^{id82,110}, L. Tompkins ^{id142,p},
 P. Tornambe ^{id102}, E. Torrence ^{id122}, H. Torres ^{id50}, E. Torró Pastor ^{id162}, M. Toscani ^{id30}, C. Tosciri ^{id39},
 D.R. Tovey ^{id138}, A. Traeet¹⁶, I.S. Trandafir ^{id27b}, T. Trefzger ^{id165}, A. Tricoli ^{id29}, I.M. Trigger ^{id155a},
 S. Trincaz-Duvoid ^{id126}, D.A. Trischuk ^{id163}, B. Trocmé ^{id60}, A. Trofymov ^{id66}, C. Troncon ^{id70a},
 L. Truong ^{id33c}, M. Trzebinski ^{id85}, A. Trzupiek ^{id85}, F. Tsai ^{id144}, M. Tsai ^{id105}, A. Tsiamis ^{id151},
 P.V. Tsiareshka³⁷, A. Tsirigotis ^{id151,t}, V. Tsiskaridze ^{id144}, E.G. Tskhadadze^{148a}, M. Tsopoulou ^{id151},
 Y. Tsujikawa ^{id86}, I.I. Tsukerman ^{id37}, V. Tsulaia ^{id17a}, S. Tsuno ^{id82}, O. Tsur¹⁴⁹, D. Tsybychev ^{id144},
 Y. Tu ^{id64b}, A. Tudorache ^{id27b}, V. Tudorache ^{id27b}, A.N. Tuna ^{id36}, S. Turchikhin ^{id38}, I. Turk Cakir ^{id3a},
 R. Turra ^{id70a}, P.M. Tuts ^{id41}, S. Tzamarias ^{id151}, P. Tzanis ^{id10}, E. Tzovara ^{id99}, K. Uchida¹⁵²,
 F. Ukegawa ^{id156}, P.A. Ulloa Poblete ^{id136c}, G. Unal ^{id36}, M. Unal ^{id11}, A. Undrus ^{id29}, G. Unel ^{id159},
 K. Uno ^{id152}, J. Urban ^{id28b}, P. Urquijo ^{id104}, G. Usai ^{id8}, R. Ushioda ^{id153}, M. Usman ^{id107},
 Z. Uysal ^{id21b}, V. Vacek ^{id131}, B. Vachon ^{id103}, K.O.H. Vadla ^{id124}, T. Vafeiadis ^{id36}, C. Valderanis ^{id108},
 E. Valdes Santurio ^{id47a,47b}, M. Valente ^{id155a}, S. Valentinetti ^{id23b,23a}, A. Valero ^{id162}, A. Vallier ^{id101,aa},
 J.A. Valls Ferrer ^{id162}, T.R. Van Daalen ^{id137}, P. Van Gemmeren ^{id6}, S. Van Stroud ^{id95},
 I. Van Vulpen ^{id113}, M. Vanadia ^{id75a,75b}, W. Vandelli ^{id36}, M. Vandenbroucke ^{id134}, E.R. Vandewall ^{id120},
 D. Vannicola ^{id150}, L. Vannoli ^{id57b,57a}, R. Vari ^{id74a}, E.W. Varnes ^{id7}, C. Varni ^{id17a}, T. Varol ^{id147},
 D. Varouchas ^{id66}, L. Varriale ^{id162}, K.E. Varvell ^{id146}, M.E. Vasile ^{id27b}, L. Vaslin⁴⁰, G.A. Vasquez ^{id164},
 F. Vazeille ^{id40}, D. Vazquez Furelos ^{id13}, T. Vazquez Schroeder ^{id36}, J. Veatch ^{id31}, V. Vecchio ^{id100},
 M.J. Veen ^{id113}, I. Veliscek ^{id125}, L.M. Veloce ^{id154}, F. Veloso ^{id129a,129c}, S. Veneziano ^{id74a},
 A. Ventura ^{id69a,69b}, A. Verbytskyi ^{id109}, M. Verducci ^{id73a,73b}, C. Vergis ^{id24},
 M. Verissimo De Araujo ^{id81b}, W. Verkerke ^{id113}, J.C. Vermeulen ^{id113}, C. Vernieri ^{id142},
 P.J. Verschuuren ^{id94}, M. Vessella ^{id102}, M.L. Vesterbacka ^{id116}, M.C. Vetterli ^{id141,ah},
 A. Vgenopoulos ^{id151}, N. Viaux Maira ^{id136f}, T. Vickey ^{id138}, O.E. Vickey Boeriu ^{id138},
 G.H.A. Viehhauser ^{id125}, L. Vigani ^{id63b}, M. Villa ^{id23b,23a}, M. Villaplana Perez ^{id162}, E.M. Villhauer⁵²,
 E. Vilucchi ^{id53}, M.G. Vinciter ^{id34}, G.S. Virdee ^{id20}, A. Vishwakarma ^{id52}, C. Vittori ^{id23b,23a},
 I. Vivarelli ^{id145}, V. Vladimirov¹⁶⁶, E. Voevodina ^{id109}, F. Vogel ^{id108}, P. Vokac ^{id131}, J. Von Ahnen ^{id48},
 E. Von Toerne ^{id24}, B. Vormwald ^{id36}, V. Vorobel ^{id132}, K. Vorobev ^{id37}, M. Vos ^{id162},
 J.H. Vossebeld ^{id91}, M. Vozak ^{id113}, L. Vozdecky ^{id93}, N. Vranjes ^{id15}, M. Vranjes Milosavljevic ^{id15},
 M. Vreeswijk ^{id113}, R. Vuillermet ^{id36}, O. Vujanovic ^{id99}, I. Vukotic ^{id39}, S. Wada ^{id156}, C. Wagner¹⁰²,
 W. Wagner ^{id170}, S. Wahdan ^{id170}, H. Wahlberg ^{id89}, R. Wakasa ^{id156}, M. Wakida ^{id110},
 V.M. Walbrecht ^{id109}, J. Walder ^{id133}, R. Walker ^{id108}, W. Walkowiak ^{id140}, A.M. Wang ^{id61},
 A.Z. Wang ^{id169}, C. Wang ^{id62a}, C. Wang ^{id62c}, H. Wang ^{id17a}, J. Wang ^{id64a}, P. Wang ^{id44},
 R.-J. Wang ^{id99}, R. Wang ^{id61}, R. Wang ^{id6}, S.M. Wang ^{id147}, S. Wang ^{id62b}, T. Wang ^{id62a},
 W.T. Wang ^{id79}, W.X. Wang ^{id62a}, X. Wang ^{id14c}, X. Wang ^{id161}, X. Wang ^{id62c}, Y. Wang ^{id62d},
 Y. Wang ^{id14c}, Z. Wang ^{id105}, Z. Wang ^{id62d,51,62c}, Z. Wang ^{id105}, A. Warburton ^{id103}, R.J. Ward ^{id20},
 N. Warrack ^{id59}, A.T. Watson ^{id20}, M.F. Watson ^{id20}, G. Watts ^{id137}, B.M. Waugh ^{id95}, A.F. Webb ^{id11},
 C. Weber ^{id29}, M.S. Weber ^{id19}, S.A. Weber ^{id34}, S.M. Weber ^{id63a}, C. Wei ^{id62a}, Y. Wei ^{id125},
 A.R. Weidberg ^{id125}, J. Weingarten ^{id49}, M. Weirich ^{id99}, C. Weiser ^{id54}, C.J. Wells ^{id48}, T. Wenaus ^{id29},
 B. Wendland ^{id49}, T. Wengler ^{id36}, N.S. Wenke¹⁰⁹, N. Wermes ^{id24}, M. Wessels ^{id63a}, K. Whalen ^{id122},
 A.M. Wharton ^{id90}, A.S. White ^{id61}, A. White ^{id8}, M.J. White ^{id1}, D. Whiteson ^{id159},
 L. Wickremasinghe ^{id123}, W. Wiedenmann ^{id169}, C. Wiel ^{id50}, M. Wielers ^{id133}, N. Wieseotte⁹⁹,
 C. Wiglesworth ^{id42}, L.A.M. Wiik-Fuchs ^{id54}, D.J. Wilbern¹¹⁹, H.G. Wilkens ^{id36}, D.M. Williams ^{id41},
 H.H. Williams¹²⁷, S. Williams ^{id32}, S. Willocq ^{id102}, P.J. Windischhofer ^{id125}, F. Winklmeier ^{id122},
 B.T. Winter ^{id54}, M. Wittgen¹⁴², M. Wobisch ^{id96}, A. Wolf ^{id99}, R. Wölker ^{id125}, J. Wollrath¹⁵⁹,
 M.W. Wolter ^{id85}, H. Wolters ^{id129a,129c}, V.W.S. Wong ^{id163}, A.F. Wongel ^{id48}, S.D. Worm ^{id48},
 B.K. Wosiek ^{id85}, K.W. Woźniak ^{id85}, K. Wraight ^{id59}, J. Wu ^{id14a,14d}, M. Wu ^{id64a}, S.L. Wu ^{id169},

X. Wu ⁵⁶, Y. Wu ^{62a}, Z. Wu ^{134,62a}, J. Wuerzinger ¹²⁵, T.R. Wyatt ¹⁰⁰, B.M. Wynne ⁵², S. Xella ⁴², L. Xia ^{14c}, M. Xia ^{14b}, J. Xiang ^{64c}, X. Xiao ¹⁰⁵, M. Xie ^{62a}, X. Xie ^{62a}, I. Xiotidis ¹⁴⁵, D. Xu ^{14a}, H. Xu ^{62a}, H. Xu ^{62a}, L. Xu ^{62a}, R. Xu ¹²⁷, T. Xu ^{62a}, W. Xu ¹⁰⁵, Y. Xu ^{14b}, Z. Xu ^{62b}, Z. Xu ¹⁴², B. Yabsley ¹⁴⁶, S. Yacoob ^{33a}, N. Yamaguchi ⁸⁸, Y. Yamaguchi ¹⁵³, H. Yamauchi ¹⁵⁶, T. Yamazaki ^{17a}, Y. Yamazaki ⁸³, J. Yan ^{62c}, S. Yan ¹²⁵, Z. Yan ²⁵, H.J. Yang ^{62c,62d}, H.T. Yang ^{17a}, S. Yang ^{62a}, T. Yang ^{64c}, X. Yang ^{62a}, X. Yang ^{14a}, Y. Yang ⁴⁴, Z. Yang ^{62a,105}, W-M. Yao ^{17a}, Y.C. Yap ⁴⁸, H. Ye ^{14c}, J. Ye ⁴⁴, S. Ye ²⁹, X. Ye ^{62a}, I. Yeletsikh ³⁸, M.R. Yexley ⁹⁰, P. Yin ⁴¹, K. Yorita ¹⁶⁷, C.J.S. Young ⁵⁴, C. Young ¹⁴², M. Yuan ¹⁰⁵, R. Yuan ^{62b,j}, X. Yue ^{63a}, M. Zaazoua ^{35e}, B. Zabinski ⁸⁵, E. Zaid ⁵², T. Zakareishvili ^{148b}, N. Zakharchuk ³⁴, S. Zambito ⁵⁶, J. Zang ¹⁵², D. Zanzi ⁵⁴, O. Zaplatilek ¹³¹, S.V. Zeißner ⁴⁹, C. Zeitnitz ¹⁷⁰, J.C. Zeng ¹⁶¹, D.T. Zenger Jr ²⁶, O. Zenin ³⁷, T. Ženiš ^{28a}, S. Zenz ⁹³, S. Zerradi ^{35a}, D. Zerwas ⁶⁶, B. Zhang ^{14c}, D.F. Zhang ¹³⁸, G. Zhang ^{14b}, J. Zhang ⁶, K. Zhang ^{14a,14d}, L. Zhang ^{14c}, R. Zhang ¹⁶⁹, S. Zhang ¹⁰⁵, T. Zhang ¹⁵², X. Zhang ^{62c}, X. Zhang ^{62b}, Z. Zhang ⁶⁶, H. Zhao ¹³⁷, P. Zhao ⁵¹, T. Zhao ^{62b}, Y. Zhao ¹³⁵, Z. Zhao ^{62a}, A. Zhemchugov ³⁸, Z. Zheng ¹⁴², D. Zhong ¹⁶¹, B. Zhou ¹⁰⁵, C. Zhou ¹⁶⁹, H. Zhou ⁷, N. Zhou ^{62c}, Y. Zhou ⁷, C.G. Zhu ^{62b}, C. Zhu ^{14a,14d}, H.L. Zhu ^{62a}, H. Zhu ^{14a}, J. Zhu ¹⁰⁵, Y. Zhu ^{62a}, X. Zhuang ^{14a}, K. Zhukov ³⁷, V. Zhulanov ³⁷, N.I. Zimine ³⁸, J. Zinsser ^{63b}, M. Ziolkowski ¹⁴⁰, L. Živković ¹⁵, A. Zoccoli ^{23b,23a}, K. Zoch ⁵⁶, T.G. Zorbas ¹³⁸, O. Zormpa ⁴⁶, W. Zou ⁴¹, L. Zwalinski ³⁶.

¹Department of Physics, University of Adelaide, Adelaide; Australia.

²Department of Physics, University of Alberta, Edmonton AB; Canada.

³(^a)Department of Physics, Ankara University, Ankara; (^b)Division of Physics, TOBB University of Economics and Technology, Ankara; Türkiye.

⁴LAPP, Université Savoie Mont Blanc, CNRS/IN2P3, Annecy; France.

⁵APC, Université Paris Cité, CNRS/IN2P3, Paris; France.

⁶High Energy Physics Division, Argonne National Laboratory, Argonne IL; United States of America.

⁷Department of Physics, University of Arizona, Tucson AZ; United States of America.

⁸Department of Physics, University of Texas at Arlington, Arlington TX; United States of America.

⁹Physics Department, National and Kapodistrian University of Athens, Athens; Greece.

¹⁰Physics Department, National Technical University of Athens, Zografou; Greece.

¹¹Department of Physics, University of Texas at Austin, Austin TX; United States of America.

¹²Institute of Physics, Azerbaijan Academy of Sciences, Baku; Azerbaijan.

¹³Institut de Física d'Altes Energies (IFAE), Barcelona Institute of Science and Technology, Barcelona; Spain.

¹⁴(^a)Institute of High Energy Physics, Chinese Academy of Sciences, Beijing; (^b)Physics Department, Tsinghua University, Beijing; (^c)Department of Physics, Nanjing University, Nanjing; (^d)University of Chinese Academy of Science (UCAS), Beijing; China.

¹⁵Institute of Physics, University of Belgrade, Belgrade; Serbia.

¹⁶Department for Physics and Technology, University of Bergen, Bergen; Norway.

¹⁷(^a)Physics Division, Lawrence Berkeley National Laboratory, Berkeley CA; (^b)University of California, Berkeley CA; United States of America.

¹⁸Institut für Physik, Humboldt Universität zu Berlin, Berlin; Germany.

¹⁹Albert Einstein Center for Fundamental Physics and Laboratory for High Energy Physics, University of Bern, Bern; Switzerland.

²⁰School of Physics and Astronomy, University of Birmingham, Birmingham; United Kingdom.

²¹(^a)Department of Physics, Bogazici University, Istanbul; (^b)Department of Physics Engineering,

Gaziantep University, Gaziantep;^(c)Department of Physics, Istanbul University, Istanbul;^(d)Istinye University, Sariyer, Istanbul; Türkiye.

^{22(a)}Facultad de Ciencias y Centro de Investigaciones, Universidad Antonio Nariño,

Bogotá;^(b)Departamento de Física, Universidad Nacional de Colombia, Bogotá; Colombia.

^{23(a)}Dipartimento di Fisica e Astronomia A. Righi, Università di Bologna, Bologna;^(b)INFN Sezione di Bologna; Italy.

²⁴Physikalisches Institut, Universität Bonn, Bonn; Germany.

²⁵Department of Physics, Boston University, Boston MA; United States of America.

²⁶Department of Physics, Brandeis University, Waltham MA; United States of America.

^{27(a)}Transilvania University of Brasov, Brasov;^(b)Horia Hulubei National Institute of Physics and Nuclear Engineering, Bucharest;^(c)Department of Physics, Alexandru Ioan Cuza University of Iasi, Iasi;^(d)National Institute for Research and Development of Isotopic and Molecular Technologies, Physics Department, Cluj-Napoca;^(e)University Politehnica Bucharest, Bucharest;^(f)West University in Timisoara, Timisoara; Romania.

^{28(a)}Faculty of Mathematics, Physics and Informatics, Comenius University, Bratislava;^(b)Department of Subnuclear Physics, Institute of Experimental Physics of the Slovak Academy of Sciences, Kosice; Slovak Republic.

²⁹Physics Department, Brookhaven National Laboratory, Upton NY; United States of America.

³⁰Universidad de Buenos Aires, Facultad de Ciencias Exactas y Naturales, Departamento de Física, y CONICET, Instituto de Física de Buenos Aires (IFIBA), Buenos Aires; Argentina.

³¹California State University, CA; United States of America.

³²Cavendish Laboratory, University of Cambridge, Cambridge; United Kingdom.

^{33(a)}Department of Physics, University of Cape Town, Cape Town;^(b)iThemba Labs, Western

Cape;^(c)Department of Mechanical Engineering Science, University of Johannesburg,

Johannesburg;^(d)National Institute of Physics, University of the Philippines Diliman

(Philippines);^(e)University of South Africa, Department of Physics, Pretoria;^(f)University of Zululand,

KwaDlangezwa;^(g)School of Physics, University of the Witwatersrand, Johannesburg; South Africa.

³⁴Department of Physics, Carleton University, Ottawa ON; Canada.

^{35(a)}Faculté des Sciences Ain Chock, Réseau Universitaire de Physique des Hautes Energies - Université Hassan II, Casablanca;^(b)Faculté des Sciences, Université Ibn-Tofail, Kénitra;^(c)Faculté des Sciences Semlalia, Université Cadi Ayyad, LPHEA-Marrakech;^(d)LPMR, Faculté des Sciences, Université Mohamed Premier, Oujda;^(e)Faculté des sciences, Université Mohammed V, Rabat;^(f)Institute of Applied Physics, Mohammed VI Polytechnic University, Ben Guerir; Morocco.

³⁶CERN, Geneva; Switzerland.

³⁷Affiliated with an institute covered by a cooperation agreement with CERN.

³⁸Affiliated with an international laboratory covered by a cooperation agreement with CERN.

³⁹Enrico Fermi Institute, University of Chicago, Chicago IL; United States of America.

⁴⁰LPC, Université Clermont Auvergne, CNRS/IN2P3, Clermont-Ferrand; France.

⁴¹Nevis Laboratory, Columbia University, Irvington NY; United States of America.

⁴²Niels Bohr Institute, University of Copenhagen, Copenhagen; Denmark.

^{43(a)}Dipartimento di Fisica, Università della Calabria, Rende;^(b)INFN Gruppo Collegato di Cosenza, Laboratori Nazionali di Frascati; Italy.

⁴⁴Physics Department, Southern Methodist University, Dallas TX; United States of America.

⁴⁵Physics Department, University of Texas at Dallas, Richardson TX; United States of America.

⁴⁶National Centre for Scientific Research "Demokritos", Agia Paraskevi; Greece.

^{47(a)}Department of Physics, Stockholm University;^(b)Oskar Klein Centre, Stockholm; Sweden.

⁴⁸Deutsches Elektronen-Synchrotron DESY, Hamburg and Zeuthen; Germany.

- ⁴⁹Fakultät Physik , Technische Universität Dortmund, Dortmund; Germany.
- ⁵⁰Institut für Kern- und Teilchenphysik, Technische Universität Dresden, Dresden; Germany.
- ⁵¹Department of Physics, Duke University, Durham NC; United States of America.
- ⁵²SUPA - School of Physics and Astronomy, University of Edinburgh, Edinburgh; United Kingdom.
- ⁵³INFN e Laboratori Nazionali di Frascati, Frascati; Italy.
- ⁵⁴Physikalisches Institut, Albert-Ludwigs-Universität Freiburg, Freiburg; Germany.
- ⁵⁵II. Physikalisches Institut, Georg-August-Universität Göttingen, Göttingen; Germany.
- ⁵⁶Département de Physique Nucléaire et Corpusculaire, Université de Genève, Genève; Switzerland.
- ⁵⁷(^a)Dipartimento di Fisica, Università di Genova, Genova;(^b) INFN Sezione di Genova; Italy.
- ⁵⁸II. Physikalisches Institut, Justus-Liebig-Universität Giessen, Giessen; Germany.
- ⁵⁹SUPA - School of Physics and Astronomy, University of Glasgow, Glasgow; United Kingdom.
- ⁶⁰LPSC, Université Grenoble Alpes, CNRS/IN2P3, Grenoble INP, Grenoble; France.
- ⁶¹Laboratory for Particle Physics and Cosmology, Harvard University, Cambridge MA; United States of America.
- ⁶²(^a)Department of Modern Physics and State Key Laboratory of Particle Detection and Electronics, University of Science and Technology of China, Hefei;(^b)Institute of Frontier and Interdisciplinary Science and Key Laboratory of Particle Physics and Particle Irradiation (MOE), Shandong University, Qingdao;(^c)School of Physics and Astronomy, Shanghai Jiao Tong University, Key Laboratory for Particle Astrophysics and Cosmology (MOE), SKLPPC, Shanghai;(^d)Tsun-Dao Lee Institute, Shanghai; China.
- ⁶³(^a)Kirchhoff-Institut für Physik, Ruprecht-Karls-Universität Heidelberg, Heidelberg;(^b)Physikalisches Institut, Ruprecht-Karls-Universität Heidelberg, Heidelberg; Germany.
- ⁶⁴(^a)Department of Physics, Chinese University of Hong Kong, Shatin, N.T., Hong Kong;(^b)Department of Physics, University of Hong Kong, Hong Kong;(^c)Department of Physics and Institute for Advanced Study, Hong Kong University of Science and Technology, Clear Water Bay, Kowloon, Hong Kong; China.
- ⁶⁵Department of Physics, National Tsing Hua University, Hsinchu; Taiwan.
- ⁶⁶IJCLab, Université Paris-Saclay, CNRS/IN2P3, 91405, Orsay; France.
- ⁶⁷Department of Physics, Indiana University, Bloomington IN; United States of America.
- ⁶⁸(^a)INFN Gruppo Collegato di Udine, Sezione di Trieste, Udine;(^b)ICTP, Trieste;(^c)Dipartimento Politecnico di Ingegneria e Architettura, Università di Udine, Udine; Italy.
- ⁶⁹(^a)INFN Sezione di Lecce;(^b)Dipartimento di Matematica e Fisica, Università del Salento, Lecce; Italy.
- ⁷⁰(^a)INFN Sezione di Milano;(^b)Dipartimento di Fisica, Università di Milano, Milano; Italy.
- ⁷¹(^a)INFN Sezione di Napoli;(^b)Dipartimento di Fisica, Università di Napoli, Napoli; Italy.
- ⁷²(^a)INFN Sezione di Pavia;(^b)Dipartimento di Fisica, Università di Pavia, Pavia; Italy.
- ⁷³(^a)INFN Sezione di Pisa;(^b)Dipartimento di Fisica E. Fermi, Università di Pisa, Pisa; Italy.
- ⁷⁴(^a)INFN Sezione di Roma;(^b)Dipartimento di Fisica, Sapienza Università di Roma, Roma; Italy.
- ⁷⁵(^a)INFN Sezione di Roma Tor Vergata;(^b)Dipartimento di Fisica, Università di Roma Tor Vergata, Roma; Italy.
- ⁷⁶(^a)INFN Sezione di Roma Tre;(^b)Dipartimento di Matematica e Fisica, Università Roma Tre, Roma; Italy.
- ⁷⁷(^a)INFN-TIFPA;(^b)Università degli Studi di Trento, Trento; Italy.
- ⁷⁸Universität Innsbruck, Department of Astro and Particle Physics, Innsbruck; Austria.
- ⁷⁹University of Iowa, Iowa City IA; United States of America.
- ⁸⁰Department of Physics and Astronomy, Iowa State University, Ames IA; United States of America.
- ⁸¹(^a)Departamento de Engenharia Elétrica, Universidade Federal de Juiz de Fora (UFJF), Juiz de Fora;(^b)Universidade Federal do Rio De Janeiro COPPE/EE/IF, Rio de Janeiro;(^c)Instituto de Física, Universidade de São Paulo, São Paulo;(^d)Rio de Janeiro State University, Rio de Janeiro; Brazil.
- ⁸²KEK, High Energy Accelerator Research Organization, Tsukuba; Japan.

- ⁸³Graduate School of Science, Kobe University, Kobe; Japan.
- ⁸⁴(*a*) AGH University of Krakow, Faculty of Physics and Applied Computer Science, Krakow; (*b*) Marian Smoluchowski Institute of Physics, Jagiellonian University, Krakow; Poland.
- ⁸⁵Institute of Nuclear Physics Polish Academy of Sciences, Krakow; Poland.
- ⁸⁶Faculty of Science, Kyoto University, Kyoto; Japan.
- ⁸⁷Kyoto University of Education, Kyoto; Japan.
- ⁸⁸Research Center for Advanced Particle Physics and Department of Physics, Kyushu University, Fukuoka ; Japan.
- ⁸⁹Instituto de Física La Plata, Universidad Nacional de La Plata and CONICET, La Plata; Argentina.
- ⁹⁰Physics Department, Lancaster University, Lancaster; United Kingdom.
- ⁹¹Oliver Lodge Laboratory, University of Liverpool, Liverpool; United Kingdom.
- ⁹²Department of Experimental Particle Physics, Jožef Stefan Institute and Department of Physics, University of Ljubljana, Ljubljana; Slovenia.
- ⁹³School of Physics and Astronomy, Queen Mary University of London, London; United Kingdom.
- ⁹⁴Department of Physics, Royal Holloway University of London, Egham; United Kingdom.
- ⁹⁵Department of Physics and Astronomy, University College London, London; United Kingdom.
- ⁹⁶Louisiana Tech University, Ruston LA; United States of America.
- ⁹⁷Fysiska institutionen, Lunds universitet, Lund; Sweden.
- ⁹⁸Departamento de Física Teórica C-15 and CIAFF, Universidad Autónoma de Madrid, Madrid; Spain.
- ⁹⁹Institut für Physik, Universität Mainz, Mainz; Germany.
- ¹⁰⁰School of Physics and Astronomy, University of Manchester, Manchester; United Kingdom.
- ¹⁰¹CPPM, Aix-Marseille Université, CNRS/IN2P3, Marseille; France.
- ¹⁰²Department of Physics, University of Massachusetts, Amherst MA; United States of America.
- ¹⁰³Department of Physics, McGill University, Montreal QC; Canada.
- ¹⁰⁴School of Physics, University of Melbourne, Victoria; Australia.
- ¹⁰⁵Department of Physics, University of Michigan, Ann Arbor MI; United States of America.
- ¹⁰⁶Department of Physics and Astronomy, Michigan State University, East Lansing MI; United States of America.
- ¹⁰⁷Group of Particle Physics, University of Montreal, Montreal QC; Canada.
- ¹⁰⁸Fakultät für Physik, Ludwig-Maximilians-Universität München, München; Germany.
- ¹⁰⁹Max-Planck-Institut für Physik (Werner-Heisenberg-Institut), München; Germany.
- ¹¹⁰Graduate School of Science and Kobayashi-Maskawa Institute, Nagoya University, Nagoya; Japan.
- ¹¹¹Department of Physics and Astronomy, University of New Mexico, Albuquerque NM; United States of America.
- ¹¹²Institute for Mathematics, Astrophysics and Particle Physics, Radboud University/Nikhef, Nijmegen; Netherlands.
- ¹¹³Nikhef National Institute for Subatomic Physics and University of Amsterdam, Amsterdam; Netherlands.
- ¹¹⁴Department of Physics, Northern Illinois University, DeKalb IL; United States of America.
- ¹¹⁵(*a*) New York University Abu Dhabi, Abu Dhabi; (*b*) University of Sharjah, Sharjah; United Arab Emirates.
- ¹¹⁶Department of Physics, New York University, New York NY; United States of America.
- ¹¹⁷Ochanomizu University, Otsuka, Bunkyo-ku, Tokyo; Japan.
- ¹¹⁸Ohio State University, Columbus OH; United States of America.
- ¹¹⁹Homer L. Dodge Department of Physics and Astronomy, University of Oklahoma, Norman OK; United States of America.
- ¹²⁰Department of Physics, Oklahoma State University, Stillwater OK; United States of America.

- ¹²¹Palacký University, Joint Laboratory of Optics, Olomouc; Czech Republic.
- ¹²²Institute for Fundamental Science, University of Oregon, Eugene, OR; United States of America.
- ¹²³Graduate School of Science, Osaka University, Osaka; Japan.
- ¹²⁴Department of Physics, University of Oslo, Oslo; Norway.
- ¹²⁵Department of Physics, Oxford University, Oxford; United Kingdom.
- ¹²⁶LPNHE, Sorbonne Université, Université Paris Cité, CNRS/IN2P3, Paris; France.
- ¹²⁷Department of Physics, University of Pennsylvania, Philadelphia PA; United States of America.
- ¹²⁸Department of Physics and Astronomy, University of Pittsburgh, Pittsburgh PA; United States of America.
- ¹²⁹(^a) Laboratório de Instrumentação e Física Experimental de Partículas - LIP, Lisboa; (^b) Departamento de Física, Faculdade de Ciências, Universidade de Lisboa, Lisboa; (^c) Departamento de Física, Universidade de Coimbra, Coimbra; (^d) Centro de Física Nuclear da Universidade de Lisboa, Lisboa; (^e) Departamento de Física, Universidade do Minho, Braga; (^f) Departamento de Física Teórica y del Cosmos, Universidad de Granada, Granada (Spain); (^g) Departamento de Física, Instituto Superior Técnico, Universidade de Lisboa, Lisboa; Portugal.
- ¹³⁰Institute of Physics of the Czech Academy of Sciences, Prague; Czech Republic.
- ¹³¹Czech Technical University in Prague, Prague; Czech Republic.
- ¹³²Charles University, Faculty of Mathematics and Physics, Prague; Czech Republic.
- ¹³³Particle Physics Department, Rutherford Appleton Laboratory, Didcot; United Kingdom.
- ¹³⁴IRFU, CEA, Université Paris-Saclay, Gif-sur-Yvette; France.
- ¹³⁵Santa Cruz Institute for Particle Physics, University of California Santa Cruz, Santa Cruz CA; United States of America.
- ¹³⁶(^a) Departamento de Física, Pontificia Universidad Católica de Chile, Santiago; (^b) Millennium Institute for Subatomic physics at high energy frontier (SAPHIR), Santiago; (^c) Instituto de Investigación Multidisciplinario en Ciencia y Tecnología, y Departamento de Física, Universidad de La Serena; (^d) Universidad Andres Bello, Department of Physics, Santiago; (^e) Instituto de Alta Investigación, Universidad de Tarapacá, Arica; (^f) Departamento de Física, Universidad Técnica Federico Santa María, Valparaíso; Chile.
- ¹³⁷Department of Physics, University of Washington, Seattle WA; United States of America.
- ¹³⁸Department of Physics and Astronomy, University of Sheffield, Sheffield; United Kingdom.
- ¹³⁹Department of Physics, Shinshu University, Nagano; Japan.
- ¹⁴⁰Department Physik, Universität Siegen, Siegen; Germany.
- ¹⁴¹Department of Physics, Simon Fraser University, Burnaby BC; Canada.
- ¹⁴²SLAC National Accelerator Laboratory, Stanford CA; United States of America.
- ¹⁴³Department of Physics, Royal Institute of Technology, Stockholm; Sweden.
- ¹⁴⁴Departments of Physics and Astronomy, Stony Brook University, Stony Brook NY; United States of America.
- ¹⁴⁵Department of Physics and Astronomy, University of Sussex, Brighton; United Kingdom.
- ¹⁴⁶School of Physics, University of Sydney, Sydney; Australia.
- ¹⁴⁷Institute of Physics, Academia Sinica, Taipei; Taiwan.
- ¹⁴⁸(^a) E. Andronikashvili Institute of Physics, Iv. Javakhishvili Tbilisi State University, Tbilisi; (^b) High Energy Physics Institute, Tbilisi State University, Tbilisi; (^c) University of Georgia, Tbilisi; Georgia.
- ¹⁴⁹Department of Physics, Technion, Israel Institute of Technology, Haifa; Israel.
- ¹⁵⁰Raymond and Beverly Sackler School of Physics and Astronomy, Tel Aviv University, Tel Aviv; Israel.
- ¹⁵¹Department of Physics, Aristotle University of Thessaloniki, Thessaloniki; Greece.
- ¹⁵²International Center for Elementary Particle Physics and Department of Physics, University of Tokyo, Tokyo; Japan.

- ¹⁵³Department of Physics, Tokyo Institute of Technology, Tokyo; Japan.
- ¹⁵⁴Department of Physics, University of Toronto, Toronto ON; Canada.
- ¹⁵⁵^(a)TRIUMF, Vancouver BC; ^(b)Department of Physics and Astronomy, York University, Toronto ON; Canada.
- ¹⁵⁶Division of Physics and Tomonaga Center for the History of the Universe, Faculty of Pure and Applied Sciences, University of Tsukuba, Tsukuba; Japan.
- ¹⁵⁷Department of Physics and Astronomy, Tufts University, Medford MA; United States of America.
- ¹⁵⁸United Arab Emirates University, Al Ain; United Arab Emirates.
- ¹⁵⁹Department of Physics and Astronomy, University of California Irvine, Irvine CA; United States of America.
- ¹⁶⁰Department of Physics and Astronomy, University of Uppsala, Uppsala; Sweden.
- ¹⁶¹Department of Physics, University of Illinois, Urbana IL; United States of America.
- ¹⁶²Instituto de Física Corpuscular (IFIC), Centro Mixto Universidad de Valencia - CSIC, Valencia; Spain.
- ¹⁶³Department of Physics, University of British Columbia, Vancouver BC; Canada.
- ¹⁶⁴Department of Physics and Astronomy, University of Victoria, Victoria BC; Canada.
- ¹⁶⁵Fakultät für Physik und Astronomie, Julius-Maximilians-Universität Würzburg, Würzburg; Germany.
- ¹⁶⁶Department of Physics, University of Warwick, Coventry; United Kingdom.
- ¹⁶⁷Waseda University, Tokyo; Japan.
- ¹⁶⁸Department of Particle Physics and Astrophysics, Weizmann Institute of Science, Rehovot; Israel.
- ¹⁶⁹Department of Physics, University of Wisconsin, Madison WI; United States of America.
- ¹⁷⁰Fakultät für Mathematik und Naturwissenschaften, Fachgruppe Physik, Bergische Universität Wuppertal, Wuppertal; Germany.
- ¹⁷¹Department of Physics, Yale University, New Haven CT; United States of America.
- ^a Also Affiliated with an institute covered by a cooperation agreement with CERN.
- ^b Also at Borough of Manhattan Community College, City University of New York, New York NY; United States of America.
- ^c Also at Bruno Kessler Foundation, Trento; Italy.
- ^d Also at Center for High Energy Physics, Peking University; China.
- ^e Also at Centro Studi e Ricerche Enrico Fermi; Italy.
- ^f Also at CERN, Geneva; Switzerland.
- ^g Also at Département de Physique Nucléaire et Corpusculaire, Université de Genève, Genève; Switzerland.
- ^h Also at Departament de Física de la Universitat Autònoma de Barcelona, Barcelona; Spain.
- ⁱ Also at Department of Financial and Management Engineering, University of the Aegean, Chios; Greece.
- ^j Also at Department of Physics and Astronomy, Michigan State University, East Lansing MI; United States of America.
- ^k Also at Department of Physics and Astronomy, University of Louisville, Louisville, KY; United States of America.
- ^l Also at Department of Physics, Ben Gurion University of the Negev, Beer Sheva; Israel.
- ^m Also at Department of Physics, California State University, East Bay; United States of America.
- ⁿ Also at Department of Physics, California State University, Sacramento; United States of America.
- ^o Also at Department of Physics, King's College London, London; United Kingdom.
- ^p Also at Department of Physics, Stanford University, Stanford CA; United States of America.
- ^q Also at Department of Physics, University of Fribourg, Fribourg; Switzerland.
- ^r Also at Department of Physics, University of Thessaly; Greece.
- ^s Also at Department of Physics, Westmont College, Santa Barbara; United States of America.
- ^t Also at Hellenic Open University, Patras; Greece.

- ^u Also at Institutio Catalana de Recerca i Estudis Avancats, ICREA, Barcelona; Spain.
- ^v Also at Institut für Experimentalphysik, Universität Hamburg, Hamburg; Germany.
- ^w Also at Institute for Nuclear Research and Nuclear Energy (INRNE) of the Bulgarian Academy of Sciences, Sofia; Bulgaria.
- ^x Also at Institute of Particle Physics (IPP); Canada.
- ^y Also at Institute of Physics, Azerbaijan Academy of Sciences, Baku; Azerbaijan.
- ^z Also at Institute of Theoretical Physics, Ilia State University, Tbilisi; Georgia.
- ^{aa} Also at L2IT, Université de Toulouse, CNRS/IN2P3, UPS, Toulouse; France.
- ^{ab} Also at Lawrence Livermore National Laboratory, Livermore; United States of America.
- ^{ac} Also at National Institute of Physics, University of the Philippines Diliman (Philippines); Philippines.
- ^{ad} Also at Physics Department, An-Najah National University, Nablus; Palestine.
- ^{ae} Also at Physikalisches Institut, Albert-Ludwigs-Universität Freiburg, Freiburg; Germany.
- ^{af} Also at The City College of New York, New York NY; United States of America.
- ^{ag} Also at The Collaborative Innovation Center of Quantum Matter (CICQM), Beijing; China.
- ^{ah} Also at TRIUMF, Vancouver BC; Canada.
- ^{ai} Also at Università di Napoli Parthenope, Napoli; Italy.
- ^{aj} Also at University of Chinese Academy of Sciences (UCAS), Beijing; China.
- ^{ak} Also at University of Colorado Boulder, Department of Physics, Colorado; United States of America.
- ^{al} Also at Yeditepe University, Physics Department, Istanbul; Türkiye.
- * Deceased